ABSTRACT

LEBRASSE, MARIE CLAUDEMAY CINDY. The Influence of Tide-Induced Water circulation on Dissolved Organic Matter Dynamics and Export from Bald Head Creek estuary, NC

Dissolved organic matter (DOM) is an important component of the flux of carbon (C) from land to sea. In coastal environments, such as tidal creeks draining salt marshes, significant knowledge gaps remain regarding the quantity and quality of the DOM that tidally exchanges between salt marshes and their adjacent estuaries or coastal waters. Uncertainty in quantifying these fluxes lies in the challenge of modeling these complex and dynamic environments. DOM export in response to tide-induced water circulation was studied in Bald Head Creek, a tributary to the Cape Fear River estuary in eastern North Carolina, using field investigations, laboratory measurements, and numerical modeling. Water samples were collected at three locations along the creek (upstream, midway and near the creek mouth) over four tidal cycles between March and August 2016 for analysis of dissolved organic carbon (DOC) concentration and light absorption by chromophoric DOM (CDOM). These measurements showed that DOM characteristics differed substantially over the tidal cycle during all four months, with a similar pattern of higher CDOM and DOC concentration at low tide compared to high tide at all three sites, suggesting greater export of carbon from the marsh to the estuary during ebb tide. DOC fluxes were computed using a numerical hydrodynamic model, based on the strong linear inverse relationships between CDOM, DOC concentration, and salinity from field observations. Model predictions estimate an annual net export of DOC at 54 g C m^{-2} y^{-1} from the marsh into the adjacent estuary, within the range of values reported from the South Atlantic Bight (SAB) in Georgia and North Carolina (25-135

g C m^{-2} y^{-1}) but much lower than the reported value of 328 g C m^{-2} y^{-1} in North Inlet Estuary, South Carolina, suggesting even more heterogeneity in marsh C export across estuaries. Overall, results suggest that estuarine OM dynamics in tidal creeks are strongly controlled by the circulation of water and by tidal pumping, which leaches DOM from salt marshes and exports it to adjacent waters at magnitudes comparable to other marshes in the SAB. This work demonstrates the need to quantify the importance of these tidal wetland system in the ocean's coastal C cycle.

The Influence of Tide-induced Water Circulation on Dissolved Organic Matter Dynamics and Export from Bald Head Creek estuary, NC.

by
Marie Claudemay Cindy Lebrasse

A thesis submitted to the Graduate Faculty of
North Carolina State University
in partial fulfillment of the
requirements for the degree of
Master of Science

Marine, Earth and Atmospheric Sciences

Raleigh, North Carolina

2017

APPROVED BY:

_____	_____
Dr Christopher L. Osburn Committee Chair	Dr Ruoying He

_____
Dr DelWayne Bohnenstiehl

DEDICATION

To my husband David for his endless love and support in helping me achieve my goals and to my parents, who always believed in me and never let me down.

BIOGRAPHY

I was born and raised on Mauritius island, a tropical, paradise island on the East coast of Africa in the Indian Ocean, where I received my Bachelor's degree in Marine Science and Technology from the University of Mauritius in May 2012. After graduating, I worked as an intern in a poultry industry in the quality department for five months and volunteered at the Mauritius Marine Conservation Society, which focuses on the protection of cetaceans and sea turtles in Mauritian waters. Following this, I joined the Mauritius Oceanography Institute as an Associate Research Scientist where I worked for two years in the chemical oceanography department before coming to the US on a Fulbright scholarship to pursue my Masters at North Carolina State University.

ACKNOWLEDGMENTS

I would like to express my warmest thanks to my advisor, Dr. Chris Osburn, for his continuous assistance, critical suggestions and helpful guidance throughout those two years. I also thank my thesis committee, Dr. Roy He and Dr. Del Bohnenstiehl, for their guidance and support in helping me complete my research.

My deepest gratitude goes towards my husband David for being understanding, caring and supportive throughout the years and always encouraging me to push myself further. I am also thankful to my parents who supported me and who always did, raising me the best way possible. I am also grateful to the Fulbright program for giving me the opportunity of a lifetime to study in the US.

I am also thankful to the Bald Head Island Conservancy staff: Poul Lindegaard, Will Benfield and Amy Eldridge, for their assistance and logistical support during field work. Thanks to Dr. Bohnenstiehl and his graduate student, my friend Sam Levy, for helping in the deployment of the USV. Special thanks to Dr. Nabi Allahdadi, from the Ocean Observing and Modeling Group at NC State, for his time, patience, teaching and encouragement in completing the modeling part of my work, which was very challenging. Thank you to Dr Joseph Zhang, Fei Ye and Zhengui Wang from the Virginia Institute of Marine Sciences and Dr. Gary Howell from the IT help desk at NC State for their technical support. I would like to express my warmest thanks to the past and present members of the Osburn Lab Group, for their help and support but also most importantly, their friendship.

Last but not least, my eternal gratitude goes towards the Almighty for giving me the strength, courage and determination to accomplish this work. Thank you God.

TABLE OF CONTENTS

LIST OF TABLES

LIST OF FIGURES

INTRODUCTION

Dissolved organic matter (DOM) is the dissolved fraction of the organic matter (OM) pool, operationally defined as organic matter (OM) that passes through a 0.45 μm filter. It is well established that it plays an important role in biogeochemical cycles in aquatic ecosystems, influencing the nutrient availability, carbon dynamics, phytoplankton activity and ecosystem productivity (Tzortziou *et al.,* 2008; Downing *et al.,* 2009). DOM forms the basis for bacterial heterotrophic activity, which is crucial for the regeneration of inorganic nutrients (Hansell and Carlson, 2002; Søndergaard and Thomas, 2004).

The DOM pool can be investigated by examining the light-absorbing component of DOM termed chromophoric DOM (CDOM) (Coble, 2007; Dittmar and Stubbins, 2014), whose spectroscopic properties play a central role in understanding DOM sources (Stedmon and Markager, 2001; Dixon *et al.,* 2014), molecular size (Helms *et al.,* 2008) and serve as a proxy for dissolved organic carbon (DOC) concentrations, a globally important pool of carbon (Fichot and Benner, 2011; Downing *et al.,* 2009). Though CDOM spectroscopic properties only measure a portion of the DOM pool, their relatively quick and non-destructive measurements reveal both quantitative and qualitative information about the whole DOM pool (Nelson and Siegel, 2013). In coastal waters, CDOM is mainly a mixture of humic and fulvic acids coming from terrestrial sources, via river runoff (Chaichitehrani *et al.,* 2014), which are largely responsible for the optical properties of most natural waters (Stedmon and Markager, 2003; Helms *et al.,* 2008). Employed as a semiconservative water mass tracer, CDOM also has been used as an important indicator of water mass mixing and as a water quality index (Blough and Del Vecchio, 2002; Coble *et al*., 2004). CDOM has a

significant effect on the biological activity of aquatic ecosystems since it controls light attenuation within the water column and high CDOM absorption can remove potentially damaging ultraviolet radiation and effect primary productivity by reducing penetration of photosynthetically active radiation (PAR) (Harvey *et al.*, 2015). Estuaries are highly dynamic and productive ecosystems connecting terrestrial river environments to the ocean. Being a transition zone between terrestrial and oceanic systems, estuaries not only have among the highest organic carbon (OC) loading, with terrestrial OC flux estimated at ~460 Tg C $year^{-1}$, but they also have tremendously high rates of primary productivity (average net primary productivity (NPP): 1275 g C m^{-2} $year^{-1}$, range: 400–2,250 g C m^{-2} y^{-1}) (Hopkinson, 1988). Additionally, estuaries receive large amounts of allochthonous (from outside the system) and autochthonous (from within the system) OM and nutrients. Allochthonous inputs include riverine OM from rivers and surrounding watersheds, of which DOC is a major component (60%) (Raymond and Bauer, 2001), while internal autochthonous DOC comes mainly from estuarine phytoplankton (Peterson *et al*., 1994; Bouillon *et al*., 2012) and marshes (Raymond and Bauer, 2001). These inputs make estuaries key areas of DOM cycling due to dynamic physical and biological activities, thereby influencing DOM distribution, transformation and degradation (Bauer and Bianchi, 2011; Aiken, 2014). Most estuaries exhibit high internal spatial and temporal heterogeneity in carbon processing and fluxes, which makes it difficult to quantify an estuary's net carbon balance (Bauer *et al*., 2013). Therefore, an understanding of the overall OM cycling in estuaries is critical to be able to constrain local carbon budgets but also to assess the role of estuaries in regulating carbon fluxes to the oceans.

The coastal ecosystem that surrounds an estuary will directly impact its DOM composition and quality due to differences in DOM sources and sinks (Boyd and Osburn, 2004; Bauer and Bianchi, 2011). One common type of coastal ecosystem in the mid- to high-latitudes is tidal salt marshes, which are intertidal ecosystems populated by a variety of primary producers such as macroalgae, diatoms and cyanobacteria, but physically dominated by vascular plants (Chmura, 2009). Tidal salt marshes are hotspots of OM transformation and exchange with their adjacent estuary (Tzortziou *et al.,* 2011) and have been ranked as one of the most productive ecosystems on Earth (Cai 2011; Fagherazzi *et al.,* 2013; Osburn *et al.,* 2015). In recent years, considerable attention has been focused on the buried carbon in the sediments of salt marshes, termed 'blue carbon'. This blue carbon is a significant carbon sink, storing approximately 4.8–87.2 Tg C $year^{-1}$ globally (Chmura *et al.* 2003; Duarte *et al.* 2005; Fagherazzi *et al.,* 2013) and carbon burial rates in salt marshes are among the highest globally (Fig. 1). This carbon is thought to be exported hydrologically to adjacent estuaries based on the outwelling hypothesis (Teal, 1962).

Salt marshes bury carbon at a rate ~55 times faster than tropical rainforests and can store this carbon for millennia compared to rainforests which can only store carbon for decades (Macreadie *et al*., 2013). As much as they bury carbon at faster rates than terrestrial ecosystems, salt marshes also are being lost at faster rates than terrestrial ecosystems, 1-2% yearly compared to ~0.5% yearly for terrestrial ecosystems (Duarte *et al*., 2008). Despite being one of the most powerful carbon sinks on Earth, salt marshes have been subject to rapid global decline (Duarte *et al*., 2008), mostly due to changes in land use (Mcleod *et al*., 2011) but also more recently to sea level rise (SLR). Salt marshes act as a filter and trap

laterally-imported carbon, that gets buried into the sediments and contributes to the carbon stocks in the marsh. However, disturbances caused by changes in land use and SLR can reduce this trapping capacity and cause the salt marsh to shift from a net carbon sink to a source of carbon to the atmosphere and to the continental shelf (Mcleod *et al.*, 2011; Hopkinson *et al*., 2012; Macreadie *et al*., 2013).

Coastal ecosystems are highly heterogeneous in time and space and current C export estimates across this land-ocean interface still have large uncertainties (Cai 2011; Wang *et al.*, 2016); Carbon fluxes and export have historically been hard to quantify because of their variability with respect to hydrology and geomorphology (Tobias and Neubaeur, 2009; Cai 2011; Wang *et al*., 2016) and the balance between net organic carbon production (autotrophy) and consumption (heterotrophy) in coastal ecosystems remain poorly quantified (Bauer *et al*., 2013). DOM dynamics in estuarine systems are often driven by important physical variables including salinity (Stedmon and Markager, 2003), estuarine water circulation, river and groundwater discharge, and tidal flooding (Clark *et al.,* 2008; Osburn *et al.,* 2015). Tidal movements, for instance, whose associated currents advect saline water along the estuary and enhance mixing (Becker *et al*., 2010), play a central role in the lateral exchange of material between a salt marsh and its adjacent estuary, where salt marshes outwell OC via tidal exchange (Guo *et al.,* 2009). The effect of such export on estuarine biogeochemistry however remains poorly resolved, with only a few studies providing flux estimates (Wang *et al*., 2016). For example, at flood tide, disturbance of the marsh platform causes resuspension of sediments and this carbon is pumped into the water, while bidirectional flow results in the mixing of marsh plants' DOM with estuarine DOM, resulting

in significant exchange with adjacent coastal waters (Osburn *et al.*, 2015). This carbon is then transported offshore with the outgoing tide. DOM from marshes has been estimated to be exported at a rate of 15-328 g C m^{-2} yr^{-1}, mostly during ebb tide and DOC concentration and fluxes have been shown to vary over tidal cycles (Tzortziou *et al.*, 2008; Tobias and Neubauer, 2009; Osburn *et al.*, 2015). Still, constraining this C exchange in the coastal setting has been challenging, mostly due to the difficulty in scaling up relatively few observational studies (Cai 2011, Bauer *et al*., 2013). Therefore, it would be desirable to find an approach that would fill in those gaps and better constrain C exchange for more accurate estimates.

"Blue" carbon is mostly stored in coastal ecosystems within the soil, the living biomass aboveground (leaves, branches, stems) and belowground (roots) and within the non-living biomass (such as litter and dead wood) (Mcleod *et al*., 2011). In tidal salt marshes, most carbon is stored in the living belowground biomass and soil as OM and contributes to >98% of the carbon stock of tidal salt marshes (Chmura *et al.*, 2003). As the tides flood the marsh platform, OM from these belowground biomass and soils is leached into the adjacent water, and this water is then carried away at ebb tide so the best way to study and quantify this carbon is through CDOM spectroscopic properties of this outgoing water. Based on the spectral properties of CDOM, including absorption coefficient (a_λ) at 254 nm and spectral slope ratio of the shorter wavelength region ($S_{275\text{-}295}$) to that of the longer wavelength region ($S_{350\text{-}400}$), it is possible to quantify and characterize the CDOM pool, which makes up ~ 60% of the DOC pool (Coble *et al*., 2007). The strong linkage between these optical properties and salinity have been widely studied, particularly in coastal ecosystems, and they have been

shown to typically vary with salinity by conservative mixing, where a constituent varies linearly with mixing of two water masses (Stedmon and Markager 2003; Helms *et al.,* 2008; Bauer and Bianchi, 2011). Salinity is an important conservative constituent of water, especially in aquatic systems like estuaries, where there is mixing of saline water with fresh water. The way a constituent behaves can be assessed by examining its relationship with salinity, where non-conservative behavior would indicate a net removal or addition of this constituent throughout the salinity gradient (Stedmon and Markager, 2003).

Multiple approaches have been attempted to improve lateral DOM flux estimates from estuaries to continental shelves such as estuarine mass balance of river and wetland inputs, the volume of the tidal prism and DOM concentrations (Osburn *et al*., 2015), estuarine CO_2 degassing, marsh and estuarine net ecosystem productivities (NEP) (Bauer *et al.*, 2013) as well as the use of satellite ocean color to determine CDOM distribution (Chaichitehrani *et al*., 2014). Although the use of satellite ocean color data through remote sensing to monitor CDOM has been reported in various studies, this method is hampered by cloud coverage and sun glint effects, affecting imagery quality (Chaichitehrani *et al*., 2014). Outputs from numerical circulation models, like currents and salinity, can be derived at high temporal and spatial resolution (Chaichitehrahni *et al*., 2014). A strong inverse linear relationship between CDOM absorption coefficient and salinity has been observed in various coastal waters and estuaries (Table 1), suggesting a simple dilution process between two water masses (Chaichitehrani *et al*., 2014). This strong linkage suggests that salinity could be used as a proxy to determine CDOM from simulated salinity, hence the application of a numerical circulation model. Numerical hydrodynamic models give a more predictive

understanding of how coastal ecosystems respond to human impacts and climate threats (Bauer *et al*., 2013) than just mass balance alone or scaled up estimates and can mechanistically incorporate factors that control C dynamics, such as inputs and residence times of OM and nutrients (Bauer *et al*., 2013), hence the rationale behind the use of a numerical model to better constrain C exchange (Wang *et al*., 2016).

Uncertainties in quantifying DOM fluxes and export in tidal salt marshes lie in the challenge of modeling these complex and dynamic environments. In this regard, the main aim of this study was to investigate the role of tide-induced water circulation on spatial and seasonal variation in DOM quantity and quality in Bald Head Creek (BHC), a tributary to the Cape Fear River (CFR) estuary in eastern North Carolina, and to quantify carbon exchange between a salt marsh and its adjacent estuary in terms of DOC export and fluxes using a hydrodynamic circulation model along with discrete sampling. The main objectives were to measure CDOM a_{254} and DOC concentrations ([DOC]) at three creek locations (upper creek, middle creek and lower creek) over tidal and seasonal cycles, determine the sources of DOM to BHC from stable isotopes measurements, to map the bathymetry of BHC's channel utilizing NC State's unmanned surface vehicle (USV), to map the water circulation along the creek using a cross-scale hydrodynamic model and compute DOC fluxes and export by combining field measurements of [DOC] with model predictions of [DOC] and current velocities. It is of central importance to understand the factors that regulate DOC dynamics and export between a salt marsh and its adjacent estuary but also how this export affects the ocean and global C budgets (Bauer *et al*., 2013). This is particularly important in the face of increasing pressures and alterations by climate and anthropogenic changes. The outcome of

this study is important for estuarine biogeochemistry, providing key insights on how estuarine DOM dynamics are affected or modified by the circulation of water, especially for tidal creeks where tidal pumping can dominate lateral fluxes of DOM to adjacent waters.

MATERIALS AND METHODS

Study site and sampling

Bald Head Island is located at the mouth of the Cape Fear River, North Carolina, USA (33.86°N, 77.99°W) and is bounded by the Atlantic Ocean on the south and east and approximately 1.5 km^2 of tidal salt marshes in the north (Sherill *et al.*, 2010) (Fig. 2). Bald Head Creek is an estuary that flows through the island and drains extensive salt marsh into the estuarine Cape Fear River, on the west of the island. The estuarine Cape Fear River receives freshwater from North Carolina's largest and most industrialized watershed via the Cape Fear River and two ''black-water'' streams, the Black and Northeast Cape Fear Rivers, which originate in swamps high in organic matter (Becker *et al*., 2010). The Cape Fear River estuary is characterized by a relatively large, open mouth which allows tidal currents to propagate well into the system and into its adjacent creeks such as Bald Head Creek. These characteristics result in the Cape Fear River Estuary being partially mixed to well mixed and sharing hydrodynamic properties of tidally energetic systems similar to the Hudson River (Becker *et al*., 2010). The vegetation on the marsh platform is mostly dominated by saltmarsh cordgrass (*Spartina alterniflora*) and black needlerush (*Juncus roemerianus*), with a transitional fringe of saltgrass (*Distichlis spicata*), sea ox-eye (*Borrichia frutescens*), and seacoast marshelder (*Iva imbricate*). These plants were more abundant at the upper part of the creek, near the head of the creek compared to the mouth of the estuary (Sherill *et al.*, 2010; Cooper and Satterthwaite, 1964).

Elevations of the marsh platform range from about 0 to 0.5 m NAVD88 (meters, relative to the North American Vertical Datum of 1988). Tides in the estuary are semi-

diurnal, with water levels typically ranging from 0 m at low tide to ~1.6 m at high tide (relative to the mean low low water (MLLW) datum). Three main sites along Bald Head Creek were sampled for this work (Table 2). The first site (Site 1) is located near the mouth of the creek where the CFR estuary converges with the Atlantic Ocean (Onslow Bay) near the Village of Bald Head Island. Site 2 is located in the middle of the creek, and Site 3 is located near the head of the creek.

The Bald Head Island Conservancy (BHIC) staff members also have collected weekly samples from the three sites since 2014 for water quality purposes and weekly sampling is ongoing. Sampling of BHC occurred in March, May, June and August 2016. Samples were collected every 4 hours over 24 hours capturing an entire tidal cycle. Four such tidal cycles were sampled in total.

The USV, equipped with an Edgetech 6205 bathymetric sonar, was deployed during the August 2016 sampling trip during periods of high-tide. The vehicle was operated autonomously, following a survey route designed to provide coverage within the deeper portions of the channel close to the mouth of the creek, near Site 1 and Site 2. The USV was not deployed near Site 3 due to the narrowness and shallowness of the channel near the head of the creek. Bathymetry data were corrected for tides, cleaned and edited in HYPACK's MB-MAX ® program and exported as sounding (x,y,z) points. The USV bathymetry were merged with the ground and bathymetric point classes extracted from a bathymetric LIDAR survey conducted by NOAA in the fall of 2014 following Hurricane Sandy. The LIDAR data were flown at low tide; they constrain the elevation of the marsh platform and depth of the channel within the upper, shallower reaches of the creek. Combined bathymetric and LIDAR

data were gridded using MB-system (Caress *et al*., 2010) to produce a 1 x 1 m resolution digital elevation model of the creek and marsh platform (Fig. 3).

Unfiltered surface water samples were collected at each site during each sampling. Samples were collected in cleaned (detergent-washed and thoroughly rinsed with Milli-Q water) 1000 ml brown high-density polyethylene bottles and samples were stored on ice until return to the BHIC laboratory for processing. Weekly sampling from 2014 onward was not processed immediately; samples were frozen until transport to the NC State University home laboratory and stored frozen for a period of up to 1 year.

Sample preparation and optical DOM Analysis

In the BHIC laboratory, samples were filtered through pre-combusted (500°C for 5 h) Whatman GF/F filters (pore size 0.7 μm) using gentle vacuum within 24 hours of collection. Before filtration of the samples, each filter was pre-rinsed with 150 ml Milli-Q water. The filtrate was considered the dissolved fraction and divided into a 60-ml polycarbonate bottle, for optics (CDOM) and a 40-ml borosilicate glass vial (detergent-washed and thoroughly rinsed with Milli-Q water, then baked at 500°C for 5 h) for DOC concentration and stable isotope analyses. The CDOM samples were kept refrigerated at 4°C until analysis, generally within 48 hours. The BHIC staff processed and filtered the weekly water samples following the same protocol. The samples were frozen and then thawed to room temperature before analysis at NC State University.

Absorbance on the filtered DOM samples were measured on a Varian Cary 300UV spectrophotometer in 1 cm quartz cells at wavelengths ranging from 200 to 800 nm and blank

corrected with Milli-Q water. Napierian absorption coefficients (*a*) were computed in m^{-1} using the following equation:

$$a(\lambda) = \frac{A(\lambda_{sample} - \lambda_{blank})}{L} \times 2.303 \quad (1)$$

where *a* is the absorption coefficient, λ is the wavelength in nanometers, *A* is the absorbance (optical density) of the sample or blank, measured on the spectrophotometer, and *L* is the pathlength of the quartz cell, in meters (Osburn and Morris, 2003). UV-visible absorption spectra for CDOM increase exponentially with decreasing wavelength. Several spectral parameters have been defined to extract information about CDOM properties from these spectra (Helms *et al.,* 2008). One of these parameters is the absorption coefficient at 254 nm (a_{254}), which serves as a proxy for DOC concentration, owing to their high correlation, with higher a_{254} values being representative of higher DOC concentrations. The slope ratio (S_R) of spectral slope fit over a shorter wavelength region ($S_{275\text{-}295}$) to that of a longer wavelength region ($S_{350\text{-}400}$) has been shown to be inversely correlated to molecular weight (MW) of DOM. As MW increases, S_R decreases because of stronger light absorption by high-molecular-weight (HMW) CDOM at longer wavelengths (Helms *et al.,* 2008). Another parameter, $SUVA_{254}$, defined as the ratio of specific UV absorbance at 254 nm (decadic absorbance) measured in inverse meters (m^{-1}) to DOC concentration measured in milligrams per liter (mg C L^{-1}), was shown to correlate strongly with DOM aromaticity (Weishaar *et al.,* 2003), which is indicative of DOM quality.

DOC and Stable Isotopes Analyses

DOC analysis was conducted on a modified OI Analytical Aurora Model 1030 TOC analyzer, using the high temperature combustion method, coupled to a Delta V Plus isotope ratio mass spectrometer (IRMS) for $\delta^{13}C$ analysis. Prior to analysis, the samples were acidified to pH 2 with 85% phosphoric acid and sparged using ultra-high purity Argon gas for twenty minutes to remove any dissolved inorganic carbon. Reference CO_2 was run through the system before analysis until a good standard deviation (<0.05) was observed. Before analysis of samples, twelve blanks (Milli-Q) were analyzed followed by a calibration curve. The calibration curve consisted of six caffeine standards (IAEA-600), ranging from 1 to 40 mg C L^{-1}, and two sucrose standards (IAEA Sucrose C6) ranging from 2 to 5 mg C L^{-1} obtained from the International Atomic Energy Agency (IAEA). Based on the Vienna Pee Dee Belemnite (VPDB), the caffeine standards had isotope values of $\delta^{13}C_{VPDB}$ = -27.77 ± 0.04 ‰ while the sucrose standards had isotope values of $\delta^{13}C_{VPDB}$ = -10.80 ± 0.03 ‰. Using the high temperature combustion technique as described in Lalonde *et al*. (2014), a volume of sample was injected and vaporized onto the head of a heated (680˚C) combustion column, which was purged by constant flow of high purity oxygen carrier gas. The vaporized sample was then converted to CO_2 through a 5% platinum oxide catalyst. Water vapor was removed from the carrier gas stream by condensation in a drain chamber, by a selectively permeable Nafion membrane as well as copper chips. The dried gas stream was then passed through a non-dispersive infrared detector that detects and measures the CO_2 absorption, following which the detector signal was forwarded to a data gathering system to process and determine concentration. After quantification measurement, the CO_2 is captured from the oxygen gas stream into a molecular sieve trap, and then heated to desorb the CO_2 into a stream of

ultrapure He and introduced into the IRMS for stable isotope measurement (Lalonde *et al*., 2014). For isotope ratio analyses on the IRMS, the standard convention for expressing stable isotope values is the delta notation 'δ' where the ratio (*R)* of ^{13}C to ^{12}C for an unknown sample is calibrated against a known standard:

$$\delta^{13}\text{C}\ (‰) = \left[\left(\frac{R_{\text{sample}}}{R_{\text{standard}}} - 1\right) \times 1000\right] \quad (2)$$

The values are in parts per thousand and expressed as 'per mil' (‰) (Osburn and St Jean, 2007). When the heavy isotope is more abundant than the standard, a sample is considered enriched, resulting in a more positive $\delta^{13}C$ value. In contrast, a sample is considered depleted when the heavy isotope is less abundant than the standard, resulting in more negative $\delta^{13}C$ values. From previous studies, a range of $\delta^{13}C$-DOC values have been established in estuaries to determine DOM sources and to differentiate between autochthonous and allochthonous inputs (Deines, 1980; Fry and Sherr, 1984; Raymond and Bauer, 2001a;) (Table 3).

Unstructured Mesh-grid Generation

An unstructured mesh, or finite element mesh, is a network of triangle or quadrilateral elements built up from nodes and capable of resolving complex geometry. This constitutes the basis for hydraulic analysis of water bodies such as estuaries. For Bald Head Creek, mesh-grid generation was performed using the Surface-water Modeling System (SMS, Aquaveo, LLC, Provo, UT), which is used to create, visualize, manipulate and analyze numerical data representing surface water (Aquaveo, LLC 2016).

Feature arcs, which are sequences of line segments representing linear features such as channel edges, were generated to define the boundaries for the mesh using a 1 m

resolution digital elevation model (DEM) (Fig. 3). The DEM was obtained by merging bathymetric data from the USV's Edgetech 6205 sonar, collected during a survey in Bald Head Creek in August 2016, with the National Oceanic and Atmospheric Agency (NOAA) bathymetric LIDAR data collected in 2014 following hurricane Sandy, representing both land and water. At the end of the mesh generation process, the bathymetry from the DEM was interpolated to the mesh and the mesh was saved for use in the water circulation model.

Water Circulation Model Description

Circulation in Bald Head Creek was mapped using the cross-scale hydrodynamic model SCHISM (Semi-implicit Cross-scale Hydroscience Integrated System Model). SCHISM is an open-source, 3D community-supported model based on unstructured grids for hydrodynamics and ecosystem dynamics. It is a derivative product built from the original SELFE (v3.1dc; Zhang and Baptista 2008) and distributed with an open-source Apache v2 license, with many enhancements and upgrades including new extensions to large-scale eddying regime and a seamless cross-scale capability from creek to ocean (Zhang *et al*. 2016). SCHISM uses a highly efficient and accurate semi-implicit finite-element/finite-volume method with Eulerian-Lagrangian algorithm to solve the Reynolds-Averaged Navier-Stokes (RANS) equation (3-6) with transport of heat, salts and tracers with Boussinesq approximation (in either hydrostatic and non-hydrostatic form), to address a wide range of physical and biological processes. Mass conservation is enforced with the finite-volume transport algorithm and it also incorporates wetting and drying of tidal flats (Zhang *et al*., 2016). A semi-implicit method, like the one integrated in SCHISM, is one that allows the stable integration of the transport equations with a much larger time step than would

otherwise be possible, hence saving computational time. The way in which this is achieved is to treat certain terms as means over times (t-Δt) and (t+ Δt) rather than at time t to obtain a coupled set of equations. In the case of SCHISM, the viscosity term is treated implicitly while the Coriolis term is treated explicitly.

Momentum equation:

$$\frac{\partial \boldsymbol{u}}{\partial t} = \frac{\partial}{\partial z}\left(\nu \frac{\partial \boldsymbol{u}}{\partial z}\right) - g\nabla\eta + \mathbf{F} \quad (3)$$

Continuity equation:

$$\frac{\partial \eta}{\partial t} + \nabla . \int_{-h}^{\eta} \boldsymbol{u} dz = 0, \quad (4)$$

$$\nabla . \boldsymbol{u} + \frac{\partial w}{\partial z} = 0 \quad (5)$$

Transport equations:

$$\frac{\partial C}{\partial t} + \nabla . (\boldsymbol{u} C) + \frac{\partial w C}{\partial z} = \frac{\partial}{\partial z}\left(\kappa \frac{\partial C}{\partial z}\right) + F_h + Q \quad (6)$$

The different variables in Equation 3-6 are defined in Table 4.

With its highly flexible network, this model has proven to be efficient in a wide range of applications from creeks to deep oceans, in general circulation (Zhang *et al*., 2015) and biogeochemistry (Rodrigues *et al*., 2009). Standard model outputs from numerical models like SCHISM include water levels, salinity, temperature, and horizontal velocity based on the initial and boundary conditions enforced before running the model. Boundary conditions are a set of constraints that define the behavior of functions on the spatial boundary of the domain, that is its area of definition, while initial conditions define the behavior of functions with respect to time. With its high efficiency, SCHISM has proven to be a reliable numerical

model. Salinity, as a conservative tracer, can be used to track freshwater masses and study CDOM distribution in estuaries (Del Vecchio and Blough, 2006). A strong inverse linear relationship between CDOM absorption coefficient and salinity has been observed in various coastal waters and estuaries (Table 1). Additionally, a high positive relationship between CDOM and DOC has been reported in previous studies (Green and Blough, 1994; Ferrari *et al.*, 1996; Vodacek *et al*., 1997), indicating that these two parameters are controlled by mixing of the riverine end-member with the seawater end-member (Coble, 2007) resulting in a conservative behavior. Therefore, using the salinity output from the model as a proxy for CDOM a_{254} values based on their strong inverse linear relationship, the model-simulated salinity was validated against field measurements of salinity and translated into CDOM a_{254} values. Moreover, using the strong positive relationship between CDOM a_{254} and [DOC], model-derived CDOM a_{254} values were validated against field measurements and translated into [DOC].

The Model Set-up and forcing

The model grid consists of 94,482 triangular elements and 47,811 nodes in the horizontal grid and one depth level in the vertical grid, since a 2D surface simulation was performed. At the open boundary on the Cape Fear River, time series of water level (from NOAA tides and currents, station ID 8658901, last accessed in Dec 2016) were interpolated to the model for water level boundary forcing in NAVD88 to match the DEM's datum. No appropriate ocean observing station with hourly salinity datasets was available at the mouth of Bald Head Creek for application to the model boundary forcing. However, the closest monitoring station to the creek, with hourly salinity values for the simulation period, was

obtained from the University of North Carolina, Wilmington's Coastal Ocean Research and Monitoring Program buoy SUN2 (www.cormp.org). The buoy is located at 33.8373 ° N and 78.4768 ° W and collects wind speed, wind gust, wind direction, salinity, air temperature, air pressure, humidity and water temperature data. SUN2 buoy is located approximately 45 km from BHC. This distance was not ideal but unavoidable and we anticipated some error will be introduced in our model outputs from using salinity measurements made at this distance from BHC. Weekly historical data collected by the Bald Head Island Conservancy since 2013 was also available near the boundary. Therefore, the salinity boundary condition was estimated by applying a monthly correlation coefficient, calculated from data collected at the same time on the same day from SUN2 and the historical dataset, to SUN2 hourly salinity dataset for each of the four sampling months (March, May, June and August). Each month had a different correlation coefficient. These data were then interpolated to the model for salinity boundary forcing.

Model Initialization and parameters

To run a model on SCHISM, several mandatory input files are required and samples of these input files are found in Appendix A. Once all input files have been set with the correct parameters, the model was run on NC State's Henry2 cluster via their high-performance computer (HPC). Henry2 is a Linux cluster constructed from IBM blade servers, which are stored in blade chassis that hold fourteen blades. The job was initialized with 8 cores, with a maximum run time of 300 minutes. A constant bottom roughness of 0.001 mm and a horizontal eddy viscosity coefficient of 0.025 were used for model initialization. A time step of 120 s was used in the simulation. A point source with freshwater discharge of 5 m^3 s^{-1} and

salinity 0 at node 4499 was turned on in the model to account for freshwater input from groundwater upstream. The sampling dates for this study were March 11th, May 12th, June 23rd, and August 3rd, 2016 and sampling was performed over a 24-h period but the numerical model simulation was conducted for a 5-day period for each month in GMT, including a two-day spin-up to allow for thermodynamic adjustment in the model. The model was run from March 9th to March 13th, 2016, May 10th to May 14th, 2016, June 21st to June 25th, 2016 and August 1st to August 4th, 2016.

DOC Flux and Export Calculations

DOC flux and export numbers were computed from the model's horizontal velocity and water level output and the area of cross-section close to the mouth of the creek using the MATLAB computing environment (Mathworks, Inc., Natick, MA). A 420-m cross-section was defined across the creek and marsh area based on the model unstructured mesh grid. The starting point was northwest (NW_x=222836 m, NW_y=3753041 m) and the cross-section was drawn over a 420-m distance at an angle of 22 degrees south east with a 0.5 m distance between each node, making the cross-section 840 points long (Fig. 4a). The cross-section of interest, just across the creek, used for flux calculations was 147 m wide and the channel depth of the cross-section at each time step across the 147 m was calculated as the difference, in meters, between the bathymetry and the water level (Fig. 4b). The scatteredinterp function was used to interpolate bathymetry while the predictor function was used to calculate DOC, the u component and the v component of the velocity over the entire 420 m cross-sectional profile. These parameters were then calculated over the cross-section of interest, which is 147 m wide. The area of the cross-section was calculated by multiplying the channel depth at

each of the points along the 147-m width by the 0.5 m distance between each point. Then, the unit vector normal to the cross-section was calculated to estimate current velocity (m s^{-1}) based on the u and v component of the horizontal velocity. Water flux, in cubic meters per second (m^3s^{-1}), was then computed by multiplying the cross-sectional area (m^2) by the current velocity. By multiplying the water flux (m^3s^{-1}) by DOC concentration (g m^3), DOC flux per second was computed and converted to hourly DOC flux. The total marsh area was estimated using the meshgrid function in MATLAB, which approximated to 4,249,153 m^2. DOC export measurements were then computed by dividing DOC flux by the maximum flooded marsh area as estimated by taking the ratio of the number of nodes flooded over the total number of nodes multiplied by the total marsh area.

Statistical Analysis

Statistical criteria such as the root mean square error (RMSE), bias and correlation coefficient (R^2) were used to assess the model's performance in matchup comparisons between model-derived estimates and *in situ* measurements. Equations for these statistical parameters are defined in Table 5. The MATLAB computing environment (Mathworks, Inc., Natick, MA) and SigmaPlot (Systat software Inc.) were used for data processing, graphical illustrations and visualization of the model outputs. Descriptive statistics were also performed in SigmaPlot. In general results were not normally distributed; therefore, the non-parametric Kruskal-Wallis rank sum test was used to compute differences for one-way ANOVA between station and season. Significant differences between stations were calculated using the Tukey HSD (Honestly Significant Difference) test.

RESULTS

Tidal variability in DOM quantity and quality along BHC

Through all four tidal cycles, a similar pattern was observed, with decreasing CDOM a_{254} values at flood tide, lowest values at high tide, and higher a_{254} values observed at ebb tide, reaching a maximum at low tide (Fig. 5). Additionally, overall higher values were observed at Site 3 compared to Sites 1 and 2 during all four months, with the highest recorded CDOM absorption coefficient value (56.38 m^{-1}) in March (Fig. 5a). The lowest CDOM value (7.81 m^{-1}) was recorded at Site 1 in August (Fig. 4d). Site 2 exhibited a_{254} values that were higher than Site 1 and but lower than Site 3 during all four tidal cycles (Table 6). Tidal exchange of CDOM a_{254} was evident during all four months sampled and followed similar tidal DOM exchange observed in other marshes and their adjacent estuaries (Osburn *et al.*, 2015; Tzortziou *et al.*, 2008; Tzortziou *et al.*, 2011).

Variation in [DOC] over four tidal cycles was also investigated (Fig. 6) and was consistent with CDOM a_{254} values. DOC concentration reached higher values at low tide and as water started to flow into the creek during flood tide, then [DOC] gradually decreased, reaching minimum concentrations at high tide. DOC concentration gradually increased again as water started draining off the marsh platform into BHC at ebb tide. Overall higher DOC concentrations were recorded at Site 3, frequently being more than two-fold higher than [DOC] at Site 1, throughout all four tidal cycles, consistent with a similar observed trend in a_{254}. Both the lowest (1.58 mg C L^{-1}) and the highest (5.77 mg C L^{-1}) [DOC] were recorded in June (Fig. 6c) at Sites 1 and 3 respectively. Consistent with the tidal variation in a_{254} in BHC, [DOC] at Site 2 was higher than at Site 1 but lower than at Site 3 (Table 6). Again,

tidal exchange in [DOC] between the marsh and BHC was evident during all four months sampled.

S_R, which is a qualitative measurement of CDOM optical properties inversely correlated to the molecular weight of DOM, did not vary as much throughout the tidal cycles at Site 2 and 3 but was more variable at Site 1 (Fig. 7). In March, the S_R values ranged between 0.86 and 0.92 at Site 2 and between 0.89 and 0.93 at Site 3 while the range for Site 1 was between 0.87 and 1.06. Except for May, most of the variability in S_R occurred at Site 1, which showed the greatest amount of DOM quality change compared to Sites 2 and 3, with a substantial difference between the values at high tide and low tide. May did not show much variability in S_R values at all three locations throughout the tidal cycle compared to the three other months, with values ranging between 0.92 and 1.01 (Fig. 7b). August showed the greatest variability in S_R values throughout the tidal cycle at all three locations, with the highest variability at Site 1 where values ranged between 0.95 and 1.25 (Fig. 7d). Additionally, the highest S_R value (1.25) was recorded in August at Site 1 and a significant difference ($P<0.05$) was observed between Sites 1 and 3 and Sites 2 and 3 during that tidal cycle.

Tidal variability in $SUVA_{254}$, which is a measure of DOM aromaticity, was also investigated in BHC to assess changes in DOM quality, specifically its aromatic content. Our results showed an inverse relationship in $SUVA_{254}$ with the tidal cycle, increasing at ebb tide and decreasing at flood tide (Fig. 8). However, the range of $SUVA_{254}$ values displayed little variation over the tidal cycle, much like the low variability in S_R values. In March, the range of $SUVA_{254}$ values at Site 1 was between 2.85 and 5.40 L mg C^{-1} m^{-1} while both the largest

range (between 3.30 and 6.56 L mg C^{-1} m^{-1}) and the highest $SUVA_{254}$ value (6.56 L mg C^{-1} m^{-1}) over the four tidal cycles studied were recorded at Site 2 (Fig. 8a). $SUVA_{254}$ values normally range between 0 and 4 L mg C^{-1} m^{-1}, as reported in previous studies in similar systems (Chen *et al*., 2013; Phong *et al*., 2014; Cawley *et al*., 2014). $SUVA_{254}$ values that are greater than 4 L mg C^{-1} m^{-1} tend to suggest a source of iron to the system (Weishaar *et al*., 2003; Poulin *et al*., 2014), possibly coming from groundwater or from humic-rich waters with a substantial terrestrial influence supplying the iron. A significant difference in $SUVA_{254}$ values was only observed in August ($P = 0.005$; $F(2,18) = 7.24$,). Post hoc comparisons revealed a significant difference in $SUVA_{254}$ values between Site 1 and Site 3 ($P<0.05$).

Tidal variability in δ^{13}C-DOC values was also investigated in BHC (Fig. 9). In May, considerable variability was observed at all three sites, with Site 1 displaying the largest variability (between -25.9‰ and -24.5‰). A pattern of increasing δ^{13}C-DOC values at ebb tide at Sites 1, 2 and 3 after the first high tide and a decrease in δ^{13}C-DOC values at flood tide after the first low tide, except for Site 1 where δ^{13}C-DOC values increased, was observed in May. During the second high tide, more enriched δ^{13}C-DOC values were observed at Sites 2 and 3 (-24.7‰ and -24.1‰ respectively) while a more depleted δ^{13}C-DOC value (-25.0‰) was observed at Site 1. In June and August, there was a general lack of variation in δ^{13}C-DOC values at Site 3 over the tidal cycle, except at the first ebb tide in June, where an enrichment in δ^{13}C-DOC value from -24.1‰ to -23.5‰ was noted. Both Sites 1 and 2 in June and August exhibited the same pattern as in May, with an increase in δ^{13}C-DOC values

at the first ebb tide and a decrease in δ^{13}C-DOC values at the first flood tide. However, this pattern was not consistent throughout the tidal cycle for all the three months.

Spatial and temporal trends in DOM quantity and quality in BHC

Spatial trends in DOM quantity and quality

Spatial differences in [DOC] along BHC were visualized using boxplots for the three sampling sites over the four sampling months (Fig. 10). The average and standard deviation of these values are summarized in Table 4. A clear trend of increasing [DOC] was observed from Site 1 near the creek mouth to Site 3 in the upper reach of BHC (Fig. 10). Except for the month of June, overall higher mean [DOC] were recorded at Site 3 compared to Sites 1 and 2, frequently being more than two-fold higher than DOC concentrations at Site 1 (Table 6). The lowest mean DOC concentration (2.49±0.85 mg C L^{-1}) was recorded at Site 1 in March while the highest mean DOC concentration (4.89±0.71 mg C L^{-1}) was recorded in May at Site 3. May also stood out as the month with the highest mean [DOC] at all three locations along the creek, compared to March, June and August (Table 6). A significant difference was observed in March ($F(2,15) = 7.12$, $P=0.007$), May ($F(2,18) = 7.30$, $P=0.005$) and June ($F(2,18) = 6.29$, $P=0.008$) but no significant difference was observed in August. Post hoc comparisons indicated a significant difference ($P<0.05$) in [DOC] between Site 1 and Site 3. Spatial trends in S_R and $SUVA_{254}$ values were also investigated (Table 6). In March, a higher mean S_R value of 0.96±0.08 was observed at Site 1 compared to a mean S_R value of 0.90±0.02 at Site 3. Site 2 registered a mean S_R value (0.89±0.02) lower than both Sites 1 and 3 (Table 5). In May, both Sites 1 and 2 had a mean S_R value (0.97±0.03 and 0.97±0.02 respectively) higher than Site 3 (0.94±0.02). Similar to March and May, June and August

registered a higher mean S_R value at Site 1 (1.03±0.09 and 1.13±0.11 respectively) compared to Sites 2 and 3, which had slightly lower mean S_R values (Table 5). Overall, little variation was observed in the mean S_R values between Sites 1, 2 and 3 but Sites 2 and 3 generally exhibited lower S_R values than Site 1.

Consistent with the spatial variability in S_R values, higher mean $SUVA_{254}$ values were recorded at Site 3 compared to Sites 1 and 2, except for May, where a slightly higher mean $SUVA_{254}$ value was recorded at Site 2 (3.82±0.28 L mg C^{-1} m^{-1}) compared to Site 3 (3.75±0.13 L mg C^{-1} m^{-1}) (Table 6). March registered the highest mean $SUVA_{254}$ values at all three sites compared to the three other months, with a mean $SUVA_{254}$ value of 5.38±0.31 L mg C^{-1} m^{-1} at Site 3, 5.06±1.06 L mg C^{-1} m^{-1} at Site 2 and 4.08±1.11 L mg C^{-1} m^{-1} at Site 1. An overall decreasing spatial trend in mean $SUVA_{254}$ values as we moved downstream from Site 3 to Site 1 was observed during all four sampling months (Table 5).

δ^{13}C-DOC values can be used to identify the sources of DOM in aquatic ecosystems, compared to DOM optical properties, which correspond to only a portion of the total DOM. From previous studies, a range of δ^{13}C-DOC values have been established in estuaries to determine DOM sources and to differentiate between autochthonous and allochthonous inputs (Fry and Sherr, 1984; Neubauer, 2000; Raymond and Bauer, 2001a; McCallister *et al*, 2004) (Table 3). Salt marsh plants, for instance, normally consist of both C3 plants (e.g *Juncus spp*) and C4 plants (e.g *Spartina spp*), which are differentiated by their photosynthetic pathways. This difference results in more enriched δ^{13}C-DOC values produced from C4 plants (-15 to -12‰) and more depleted δ^{13}C-DOC values produced from C3 plants (-32 to -21‰). Isotopic fractionation based on fractionation through photosynthetic pathways govern

these ranges in isotopic values for C3 and C4 plants (Bianchi, 2011). The range of isotopic values for C3 plants result from the fractionation between photosynthetic carbon ($\delta^{13}C$=-27‰) and atmospheric or dissolved carbon ($\delta^{13}C$=-7‰) (Bianchi, 2011). In contrast, the range of values for C4 plants result from a much smaller isotopic fractionation during C4 fixation, making C4 plants more enriched than C3 plants (O'Leary, 1992).

End-member mixing models of stable isotope values have also been widely used to determine sources of DOM in estuaries (Raymond and Bauer, 2001a,b; Gordon and Goni, 2003; McCallister *et al*., 2004). In this study, a two end-member mixing model in which a more enriched isotopic signal from the Onslow Bay region of the coastal Atlantic Ocean near North Carolina ($\delta^{13}C$=-22.64‰) was used along with a more depleted Cape Fear River (CFR) end-member ($\delta^{13}C$=-27.15‰) to determine their relative abundance throughout BHC estuary (Fig. 11). The end members and a 50-50 mixture of the end members are indicated as dashed lines in each panel of Figure 9. Except for the month of May, the $\delta^{13}C$-DOC values showed a general lack of variation, with no clear separation between the three different locations. Mean values of -24.15, -24.21, and -24.09‰ at Sites 1, 2, and 3, respectively, were recorded in June (Fig. 11b) and mean values of -24.1, -24.07, and -24.02‰ at Sites 1, 2, and 3 respectively were recorded in August (Fig. 11c). June values were more enriched than the values recorded in May. From the end-member mixing model, it appeared that the $\delta^{13}C$-DOC values for June and August corresponded to contributions from the coastal Atlantic Ocean and 50% of each of the Atlantic Ocean and the CFR signal (-24.85‰). No significant difference was found in $\delta^{13}C$-DOC between the three different sites except for the month of May, where a significant difference ($P<0.01$) was observed in $\delta^{13}C$-DOC between Site 1 and

Site 3. No significant difference in δ^{13}C-DOC was observed between Sites 1 and 2 and Sites 2 and 3.

More depleted δ^{13}C-DOC values were recorded at Sites 1 and 2 (Mean=-25.4‰ and -25.2‰ respectively) in May, compared to Site 3 which had a more enriched value (Mean = -24.6‰) (Fig. 11a). According to the two end-member mixing model, it appeared that the more depleted δ^{13}C-DOC values at Sites 1 and 2 in May correspond to contributions from the more depleted CFR and 50% of each of the Atlantic Ocean and the CFR signal. The more depleted values tend to suggest a mix between freshwater or terrigenous δ^{13}C-DOC values and marine δ^{13}C-DOC values while the more enriched values could suggest a mix between both freshwater and marine δ^{13}C-DOC values with leachates from salt marsh plants such as *Spartina* (-15 to -12‰) or marsh OM (Raymond and Bauer, 2001a;b).

Temporal trends in CDOM quantity and quality in BHC

To further explore the characteristics of CDOM properties in BHC over time, differences in the amounts and quality of DOM over the four sampling months were visualized in boxplots of a_{254}, $SUVA_{254,}$ S_R and δ^{13}C-DOC respectively (Fig. 12) values. A seasonal difference was observed between spring (March and May) and summer (June and August), with higher CDOM a_{254}, higher $SUVA_{254,}$ lower S_R and more depleted δ^{13}C-DOC observed during the spring. BHC in March had a mean CDOM a_{254} value of 37.6±14.1 m^{-1} and a mean $SUVA_{254}$ value of 4.84±1.02 L mg C^{-1} m^{-1}, which were the highest among the four months. Consistent with the increased aromaticity, BHC in March also had the lowest mean S_R (0.92±0.06), indicative of HMW DOM. An increasing trend in S_R from March to August was observed, consistent with the decrease in $SUVA_{254}$ values (Fig. 12). In May, the

mean a_{254}, and $SUVA_{254}$ values of BHC were smaller than in March but larger than June and August (Table 7). A mean S_R value of 0.96±0.03 was recorded in BHC May while BHC in June registered a mean S_R value of 1.00±0.06. Analysis of the temporal variation in δ^{13}C-DOC values showed a more depleted signal in BHC in May (-25.1±0.63) compared to June and August, which both displayed more enriched mean δ^{13}C-DOC values (-24.2±0.44 and -24.1±0.34 respectively) (Fig. 12). The lowest mean a_{254}, and $SUVA_{254}$ values in BHC were recorded in August, along with the highest mean S_R value (Table 7). The overall trend was that a decrease in a_{254} values in BHC from March to August was accompanied by a decrease in $SUVA_{254}$ values as well as an increase in both S_R and δ^{13}C-DOC values. Next, the average discharge from the CFR ten days before sampling was investigated to determine if discharge was responsible for the differences in a_{254}, $SUVA_{254}$, S_R and δ^{13}C-DOC between spring and summer. Higher mean discharge was recorded in spring (March and May) compared to summer (June and August), with a nearly seven-fold difference between the discharge value in March and August (Table 7). The high discharge in March and May corresponded to the high mean a_{254} and $SUVA_{254}$ values as well as the low S_R measured during these two months, compared to the values recorded in June and August. The high discharge recorded in May also corresponded to the more depleted δ^{13}C-DOC value during that month. Similarly, analysis of the time series of a_{254} (Fig. 13) collected approximately weekly since 2014 also shows that during the spring, there is increased CDOM a_{254} at all the three sites, probably resulting from high flow from the CFR estuary in the spring.

Temporal trends in CDOM sources along BHC

The relationship between a^*_{375}, the ratio of a_{375} (m^{-1}) to [DOC] (mg C L^{-1}) termed specific absorption coefficient, and the spectral slope, *S*, was investigated in BHC over the four sampling months to identify the different CDOM pools affecting DOM dynamics in the creek (Fig. 14). In this case, the different pools are the CFR (*S*= 15.0 μm^{-1}, a^*_{375}= 2.14 $m^2 g^{-1}$ C) and Onslow Bay, coastal Atlantic Ocean (*S*= 11.6 μm^{-1}, a^*_{375}= 0.08 $m^2 g^{-1}$ C) near North Carolina. In general, a^*_{375} showed a curvilinear decline with increasing *S* values, as shown for other systems (Stedmon *et al*., 2000; Stedmon and Markager, 2001; Kowalczuk *et al*., 2006; Anderson and Stedmon, 2007) (Fig. 14). The a^*_{375} values in March were substantially higher than the other months, with a maximum value of 3.15 $m^2 g^{-1}$ C and a mean value of 2.14 ± 0.48 $m^2 g^{-1}$ C (Table 8). Corresponding *S* values in March also were substantially lower than the other months, the lowest value being 14.2 μm^{-1}. The mean value for *S* and a^*_{375} in March corresponded to the values from the CFR. The lowest a^*_{375} value (0.56 $m^2 g^{-1}$ C) was recorded in June. May also appeared to have slightly higher a^*_{375} values than did June and August (Fig. 14), indicating a seasonal difference between spring (March and May) and summer (June and August). March values were close to the freshwater, CFR influence while May, June and August had lower mean a^*_{375} values and approximately the same high mean *S* values (Table 8). These values did not correspond to the Onslow Bay value, which had both a lower a^*_{375} and *S* value (*S*= 11.6 μm^{-1}, a^*_{375}= 0.08 $m^2 g^{-1}$ C). Overall, the *S* values for the four months ranged between 14 and 19 μm^{-1}, similar to the range of 15 to 19 μm^{-1} reported in coastal waters in other studies (Stedmon and Markager, 2001; Del Vecchio and Blough, 2004; Granskog 2012). This trend in a^*_{375} and *S* throughout the four months, with large a^*_{375} and small *S* values recorded in March while May, June and August were clustered

together at low a^*_{375} value and higher *S* values, were consistent with the decreasing patterns observed in $SUVA_{254}$, increasing S_R values and increasing δ^{13}C-DOC values.

CDOM, DOC concentration and salinity relationships

To develop a numerical model that uses salinity as a tracer for CDOM, which itself will be a proxy for DOC concentration, conservative behavior between CDOM, DOC and salinity is necessary. Based on measurements collected over four tidal cycles in BHC in March, May, June and August, CDOM a_{254} values varied spatially at the three locations along the salinity gradient (Fig. 15). Mixing lines were created by performing linear regressions on the data for each month. CDOM a_{254} values decreased linearly with increasing salinity towards the mouth of the creek (Site 1) for all four datasets except for May 2016, indicating a conservative behavior with respect to salinity. In March, a few points above the regression line at Sites 1 and 2 could suggest input from the marsh. In May, a decrease in CDOM a_{254} with increasing salinity was observed at Site 1 (Fig. 15b), but most of the CDOM a_{254} values at Sites 2 and 3 were clustered around salinity ranging between 25 and 27.9, thereby disrupting a linear inverse relationship. Most of the points at Site 2 were found below the regression line, while a few points at Site 3 were above the regression line. June and August exhibited a wide range of variability in CDOM a_{254} along the salinity gradient at all the three sites in BHC, resulting in generally conservative mixing of CDOM.

Seasonality can induce variability in CDOM optical properties and [DOC], not only influencing biogeochemical cycles but also affecting the relationship between these two parameters and salinity. In this regard, the relationship between CDOM, [DOC] and salinity was investigated between spring (March and May) and summer (June and August) to assess

seasonality in the data. Figure 16a shows that the inverse linear relationship between a_{254} and salinity varied seasonally, with a stronger correlation observed in summer as compared to spring (Table 9). A much narrower salinity range (between 28.9 and 35.0) also was observed in June, compared to the three other months. Consistent with the CDOM-salinity relationship, [DOC] also decreased linearly with increasing salinity throughout all four months, with a stronger correlation observed in March and August (Table 8, Fig. 16b). Overall, the seasonal relationships between a_{254} and salinity (Table 8, Fig. 16a) as well as [DOC] and salinity (Table 9, Fig. 16b) showed robust linear inverse correlations for both spring and summer, except for the month of May where a significant weaker correlation was observed.

To assess the seasonal relationship between CDOM and [DOC], a_{254} values were regressed against [DOC] for spring and summer (Fig. 16c). Results showed a strong positive linear relationship between both parameters for both seasons, indicative of a conservative behavior and indicating that a_{254} served as a good proxy for [DOC]. Additionally, during March, BHC appeared to have more CDOM per unit DOC than did May, June or August, all of which were similar. Regression analyses resulted in high R^2 values for both seasons (Table 9), with the highest correlation found during August (R^2 =0.95). This strong positive relationship between CDOM a_{254} and [DOC] for all four months sampled suggests that both CDOM a_{254} and [DOC] behaved conservatively. These results indicate that the main condition to derive CDOM a_{254} and [DOC] from simulated salinity has been met. Hence, salinity was used as a proxy to derive CDOM a_{254} and [DOC] from simulated salinity using the SCHISM numerical model.

Numerical modeling of Bald Head Creek for carbon flux calculations

Validation of model-simulated salinity, CDOM and [DOC]

The main condition for estimating CDOM and [DOC] from model-simulated salinity is a robust relationship between CDOM, [DOC] and salinity. Equations based on the strong CDOM-salinity relationship and on the robust relationship between a_{254} and [DOC] were applied to model-simulated salinity values to first derive CDOM, and in turn derive [DOC] from simulated CDOM (Figs. 18 and 19). Other simulated parameters from the model included water levels, which are plotted in Appendix B. Model performance was assessed using the statistical quantities root mean square error (RMSE), bias function and correlation coefficient (R^2) (Tehrani *et al*., 2013) (Table 5).

Figure 17 illustrates the match-up comparisons between field measurements and simulated salinity values for the three different locations along BHC, across the four months sampled. A satisfactory trend was observed between in situ salinity and model-simulated salinity for March, with the values distributed closely along the 1:1 line (Fig. 17a). Based on the statistical analysis, the model performed well in estimating salinity along the creek for March with a relatively high R^2 (0.60), low RMSE (4.38) and low bias (-0.87). The match-up comparisons in May indicated a less satisfactory trend as indicated by a low R^2 (0.01). Although some points fell close to the 1:1 line, many points for Site 1deviated by as much as 20% (Fig. 17b). Match-up comparisons for June indicated a better match between observed and simulated salinities along the creek than in May, with a low RMSE (1.97) and a low bias (-0.52), though still not as good as for March (Fig. 17c). In August, the model overestimated salinity values as indicated by most of the data being scattered above the 1:1 line and

producing a correlation with an R^2 of only 0.44 (Fig. 17d). The RMSE (3.49) and bias (1.56) were higher in August than the three other months.

The validation match-up comparison between in situ and model-derived a_{254} in March (R^2=0.62, RMSE=13.2, Bias=4.72) again indicated that the model performed better in March than in May, which had a lower R^2 (0.12) and Bias (-0.84) (Fig. 18). The data during both months was distributed along the 1:1 line, with a_{254} values at Site 1 showing the largest deviations from the 1:1 line. In June, the Bias was the highest of the four months with most of the data deviating from the 1:1 line, except for a few samples from each of the three sites (Fig. 18c). The match-up comparisons between in situ and model-derived a_{254} values in August indicated that the model underestimated the a_{254} values, with most of the data lying on or below the 1:1 line (Fig. 18d). While having a higher R^2 (0.45) than June (R^2=0.16), August however had a lower RMSE (6.95) and a lower and negative Bias (-2.82), which means that model-derived a_{254} values were smaller than in-situ a_{254} values. Overall, in agreement with the field measurements except for May, the model performed well in simulating higher CDOM a_{254} values at Site 3 and lower CDOM a_{254} values at Site 1, despite variability in the simulated a_{254} values during each month.

Similarly, DOC concentration was derived from simulated CDOM a_{254} values based on the CDOM-DOC relationship during the four sampling months (Fig. 19). Consistent with the model performance in predicting salinities and CDOM a_{254}, predictions of [DOC] in March showed close agreement to in situ [DOC], with the data uniformly distributed along the 1:1 line (Fig. 19a). Additionally, statistical analysis showed satisfactory performance of the model with a relatively high R^2 (0.64), low RMSE (0.81) and low Bias (0.30). Statistical

analysis in May produced an $R^2 = 0.16$, a low RMSE (0.82) and a low Bias (-0.05), with [DOC] at Site 1 showing the largest deviations from the 1:1 line. (Fig. 19b). Similar to model simulations of a_{254} values, the match-up comparisons in June between in situ and simulated [DOC] illustrates estimations of [DOC] with R^2=0.2, RMSE=1.25 and Bias=-0.51 (Fig. 19c), where again, the Bias was the highest of the four months with most of the data deviating from the 1:1 line, except for a few samples from Sites 1 and 2. August [DOC] predictions had an R^2 of 0.41, higher than in May and June, a low RMSE (0.74) and a low, negative Bias (-0.29) (Fig. 19d). This low, negative Bias along with large deviations from the 1:1 line at all three sites indicated that most of the DOC predictions were underestimated for August. However, consistent with in-situ measurements, overall higher [DOC] were predicted at Site 3 while lower [DOC] were predicted at Site 1 except for May, despite variability in [DOC] during each month.

Figure 20 shows maps of water level, salinity and [DOC] obtained from the numerical modeling of BHC for the month of March at low tide. It can be observed that at low tide, salinity was lower near Site 3 (upstream) and [DOC] was higher, consistent with field measurements. Higher salinities were recorded near the mouth of the creek, where the creek converges into the CFR (Fig. 20b). A similar pattern of lower salinity at Site 3 and higher salinity near the mouth of the creek was observed in May, June and August as well at low tide. Consistent with field measurements of [DOC] during all four months at low tide, higher [DOC] was observed inside the creek, where during ebb tide, water draining off the marsh platform picked up marsh DOC and exported it to the adjacent creek waters (Fig. 20c). Overall higher [DOC] was observed around Site 3 (upstream) during all four months.

Figure 21 shows maps of water level, salinity and [DOC] obtained from the numerical modeling of BHC for March at high tide. As the marsh platform was flooded, there was an increase in salinity as the water flowed upstream towards Site 3, which was characterized by lower salinity (Fig. 21b). Again, higher [DOC] was observed at high tide upstream while lower [DOC] was observed around Site 1 (downstream) and Site 2 (middle stream) (Fig. 21c).

Dissolved organic carbon fluxes and export

DOC fluxes were computed near the mouth of the creek, to compare fluxes between the four sampling months. Using the model-derived horizontal velocity and DOC concentration, daily DOC flux for each month was computed as described in the Methods section on DOC flux and export calculations.

Tidal variability in hourly DOC fluxes for the four months sampled was investigated to assess the magnitudes in fluxes between ebb and flood tide (Fig. 22). Negative values mean export from the marsh into the CFR while positive values mean import to, or uptake by (or degradation in), the marsh. During all four months, a similar pattern of increased DOC flux (more negative) at ebb tide and decreased DOC flux (more positive) at flood tide was observed following the tidal cycle (Fig. 22). Both the maximum DOC flux (-11.9×10^5 g C hr^{-1}) and the minimum DOC flux (19.4×10^5 g C hr^{-1}) in BHC among the four tidal cycles sampled were recorded in March at ebb tide and flood tide respectively, while the net daily DOC flux for that month was 9.01×10^4 g C hr^{-1} (Fig. 22a). BHC in May had a maximum DOC flux of -10.7×10^5 g C hr^{-1} at ebb tide while the minimum DOC flux during this tidal cycle was 14.5×10^5 g C hr^{-1}. In June, BHC had a maximum DOC flux of -5.94×10^5 g C hr^{-1}

while in August, BHC had a maximum DOC flux of -7.35×10^5 g C hr^{-1}, both recorded at ebb tide (Fig. 22c and 22d). Overall, the highest hourly DOC flux out of the marsh was estimated in March while the lowest hourly DOC flux out of the marsh was estimated in June.

Tidal variability in hourly DOC export was also investigated to assess the difference between ebb and flood tide (Fig. 23). Hourly export values were computed by dividing the hourly DOC flux by the maximum flooded marsh area as calculated in the methods sections (See DOC flux and export calculations in Methods). Consistent with the trend in hourly DOC fluxes in BHC during the four months sampled, a similar pattern of increasing DOC export from the marsh (where export occurs below the dashed line in Fig. 23a) at ebb tide was observed while the marsh appeared to be importing DOC at flood tide as shown by the decreased DOC export values (values become more positive) during the four tidal cycles sampled (Fig. 23). A maximum hourly DOC export of -0.31 g C m^{-2} hr^{-1} at ebb tide was estimated in March and was the highest estimated hourly DOC export among the four months (Fig. 23a). Uptake by the marsh was also highest during March with a DOC import of 0.51 g C m^{-2} hr^{-1} at flood tide.

Daily DOC fluxes were also computed for each month by summing the hourly fluxes over 24 hours (Table 10). BHC during all four months displayed a net daily DOC flux out of the marsh to the CFR as indicated by the negative values estimated, with an increase in net DOC flux from March to August. The highest daily DOC flux from the marsh to the CFR was estimated in August (-1.53×10^6 g C day^{-1}) while the lowest daily DOC flux was estimated in March (-9.01×10^4 g C day^{-1}) (Table 10). In June, the net DOC flux was higher (-3.81×10^5 g C day^{-1}) than in May (-2.99×10^5 g C day^{-1}) (Table 10). Daily DOC export for

each of the sampling month was also estimated by summing the hourly export values (Table 10). Consistent with the trend in daily DOC flux, BHC appeared to be exporting DOC during all four months, with an increase in daily DOC export from March to August (Table 10). The highest daily DOC export value of -0.40 g C m^{-2} day^{-1} was estimated in August while the lowest daily DOC export was estimated in March (-0.02 g C m^{-2} day^{-1}). The estimated mean daily DOC export from BHC (computed as the average of daily DOC export for the four months) was -0.15 g C m^{-2} day^{-1} (Table 10). The uncertainty in these estimates was calculated as per the equation in Appendix D, where BHC's DOC export estimate had an uncertainty of ±0.0.003 g C m^{-2} day^{-1} in March, ±0.017 g C m^{-2} day^{-1} in May, ±0.039 g C m^{-2} day^{-1} in June and ±0.11 g C m^{-2} day^{-1} in August.

DISCUSSION

Inundation of the marsh platform causes lateral DOC inputs to BHC.

The aim of this study was to determine how water circulation influenced the quantity and quality of DOM along BHC, in which water circulation is mainly tide-dominated, and to compute estimates of the DOC export from this tidal creek system. Tidal salt marshes have long been recognized among the most productive ecosystems on Earth but also as important sources of DOM, contributing to the carbon budgets of their adjacent coastal waters (Peterson *et al*., 1994; Gardner *et al*., 2005; Tzortziou *et al*., 2011). In agreement with these studies, we found that the tidal marshes surrounding BHC are indeed important sources of DOM to the adjacent estuary, over the tidal cycles and seasonally. Changes in the quantity and quality of DOM over tidal cycles as evidenced by analysis of a_{254}, DOC concentration, $SUVA_{254}$ and S_R, reflect similar observations as in previous studies carried out along freshwater to estuarine gradients (Tzortziou *et al*., 2008; Tzortziou *et al*., 2011; Osburn *et al*., 2015,), suggesting similar biogeochemical controls influencing the source and fate of DOM across different estuaries.

As expected based on tidal variability of a_{254} and [DOC] from previous studies (Tzortziou *et al*., 2008; Osburn *et al*., 2015), more DOM is exported at ebb tide, reaching a maximum concentration at low tide, while the lowest concentration is observed at high tide (Fig. 5). These results suggest that at ebb tide, DOM is leached from the salt marsh into the water, resulting in lateral export of DOM to the adjacent creek, hence increasing the creek water's DOM concentration. The decreasing concentration at flood tide, reaching a minimum at high tide, could simply be attributed to dilution from tidal inundation.

Additionally, a_{254} and [DOC] at low tide were nearly two to three-fold higher than the values at high tide, along the creek and across the four months (Figs. 5 and 6). These results support the assertion that DOM is leached from the marsh into the water, during inundation, and increases the creek water DOM concentration as the outgoing tide drains off the marsh platform. This also corroborates with studies in the Chesapeake Bay by Tzortziou *et al*., (2008) which revealed that water draining off the Kirkpatrick marshes at ebb tide had an approximately two-fold higher [DOC] than water entering the marsh during flood tide. The two-fold to three-fold difference in CDOM and [DOC] over the tidal cycle was also observed in other U.S salt marshes in Southern California and Eastern North Carolina (Clark *et al*., 2008; Osburn *et al*., 2015). Differences in CDOM and [DOC] could be attributed to tidal pumping of DOM as the marsh platform is flooded, and transport of leached DOM from the marsh at ebb tide is consistent with the so-called "outwelling hypothesis" (Teal 1962). The outwelling hypothesis implies that salt marshes export DOM and nutrients to BHC and surrounding coastal waters, thereby emphasizing the role that tide-induced water circulation plays in such connected coastal systems.

Further analysis of CDOM quality based on measurements of S_R and $SUVA_{254}$ over tidal cycles showed that water draining off the marshes at ebb tide was enriched in higher molecular weight (HMW), aromatic-rich DOM, as evidenced by their relatively invariant low S_R values and high $SUVA_{254}$, compared to water imported to the marsh at flood tide (Figs. 7 and 8). These results are congruent with previous studies which found that tidal marshes were a source of HMW and aromatic-rich DOM to adjacent coastal waters (Tzortziou *et al*., 2008; Tzortziou *et al*., 2011). The increased S_R values and decreased $SUVA_{254}$ observed at

Site 1 could be directly related to salinity, suggesting a decrease in MW and aromaticity of DOM towards higher salinities due to the influence of coastal Atlantic Ocean water from Onslow Bay. Site 1, being closer to the mouth, experienced greater variability in S_R due to this greater tidal influence. The greatest variability in S_R in August at Site 1 could be attributed to increased salinity during that month, where the salinity ranged between 30.3 and 34.8 near the mouth of the creek. Summer months have been found to be associated with increased solar radiation, so another possibility could be the progressive photochemical bleaching of CDOM as it transits downstream, resulting in LMW and less aromatic DOM near the mouth of BHC (Helms *et al*., 2008; Stedmon and Nelson, 2014). Overall, shifts in the quality of marsh-derived CDOM as it is transported downstream to the mouth are most likely due to mixing with the seawater end-member, photodegradation and to a lesser extent microbial alteration or production (Boyd and Osburn, 2004; Helms *et al*., 2008).

A one-way ANOVA was conducted on S_R and $SUVA_{254}$ results to determine statistical differences in DOM quality between the sites. Results showed a statistically significant difference ($P<0.05$) in S_R and $SUVA_{254}$ between Site 1 (lower creek) and Site 3 (upper creek) in August. This difference could again be attributed to the high salinities observed at Site 1 during that month, where the salinity ranged between 30.3 and 34.8 near the mouth of the creek. Helms *et al*. (2008) showed that there was a shift from HMW to LMW DOM both with irradiation from sunlight and increase in salinity across the freshwater-marine continuum. These results support the assertion that DOM quality is directly affected by an increase in salinity, brought about by tidal circulation in the creek. These observations also suggest that

the marshes surrounding BHC are a major source of HMW, aromatic-rich CDOM to the adjacent estuary through tidal flushing.

Based on the spatial differences in [DOC] from Site 1 (lower creek) to Site 3 (upper creek) (Fig. 10), upstream marsh sources, including marsh plants and soil leachates, could be the major sources of DOM to BHC. Overall higher mean [DOC] toward the marsh end-member (Site 3) and a decrease in [DOC] towards the mouth indicated that most of the DOM loading to the estuary was from upstream marsh sources (Table 6). The decrease in concentration as DOM transits through the estuary downstream could also be attributed to mixing of high concentration, marsh-derived DOM with low concentration marine-derived DOM. Another possible explanation would be the breakdown of freshly-produced marsh DOM through processes such as photochemical degradation or microbial alteration (Boyd and Osburn, 2004).

Tidal marshes have been shown to substantially affect carbon dynamics in adjacent estuaries by acting as sources, sinks or transformers of the carbon that is transported in the water exchanged between the marsh and estuary (Kowalczuk *et al*. 2009; Guo *et al*., 2011; Tzortziou *et al*., 2011). The statistically significant difference ($P<0.05$) in [DOC] between Site 1 and Site 3 during March, May and June indicated that the same mechanisms responsible for transformation of DOM as it transits downstream are driving this difference in [DOC] between Site 1 and Site 3 across these three months.

Seasonal differences in DOM quantity and quality as evidenced by the analysis of a_{254}, $SUVA_{254,}$ and S_R over spring and summer (Fig. 12) further reinforced the importance of terrestrial (marsh-derived) carbon sources to BHC. These results showed that the highest

average a_{254} with the highest average aromaticity was observed during the spring months (March and May), which coincided with the highest freshwater discharge from the CFR (Table 7). Both the high a_{254} and $SUVA_{254}$ values as well as the low S_R values in the spring could be explained by increased inputs of terrigenous DOM from increased freshwater inputs. These increased inputs of terrigenous DOM via increased flow from the CFR could also explain the more depleted terrestrial δ^{13}C-DOC signal recorded in May (Table 7). This strong signature of terrestrial DOM in the spring compared to summer, characterized by high discharge, corresponds to findings in Peierls and Paerl (2010), which revealed that DOC inputs and concentrations in the Neuse River Estuary correlated with seasonal patterns of discharge.

Similarly, Chen and Gardner (2004) found that CDOM was generally higher during high flow conditions in the Mississippi and Atchafalaya River plumes in the spring, probably due to the greater leaching from their adjacent productive wetlands during periods of high flow. In another study in Narragansett Bay, the highest average CDOM absorptions occurred during the spring and were strongly correlated (R^2=0.88) with freshwater discharge from the Narragansett Basin watershed, which is a combination of twelve rivers and streams (Keith *et al*., 2002). Figure 12 and Table 7 lend support to this idea of freshwater discharge from the CFR heavily influencing DOM quantity and quality in BHC during the spring. Freshwater discharge and tidal forcing result in the turbulent mixing of fresh and salt water, which can drive abrupt changes in DOM dynamics along BHC (Hedges and Keil, 1999).

From May to August, the mean $SUVA_{254}$ values were in the range of 0-4 L mg C^{-1} m^{-1} reported in previous studies in similar systems (Table 7) (Chen *et al*., 2013; Phong *et al*.,

2014; Cawley *et al*., 2014) but in this study, unusually higher values were observed in March, with a mean $SUVA_{254}$ value of 4.84±1.02 L mg C^{-1} m^{-1}. These enriched $SUVA_{254}$ values in March, greater than 4 L mg C^{-1} m^{-1}, could again be attributed to the increased freshwater discharge in March and hence a greater influence from the CFR, whose $SUVA_{254}$ value is 4.76 L mg C^{-1} m^{-1}. Higher $SUVA_{254}$ values could also indicate a source of iron to the system, coming from iron-enriched sediments from the CFR (Weishaar *et al*., 2003; Poulin *et al*., 2014) while higher [DOC] from iron-enriched marsh sediment and soils could likely contribute to iron in the system as well. These variations in $SUVA_{254}$ values indicated compositional differences in DOM, with high discharge resulting in an increase in aromatic carbon content contributed by terrigenous substances (Yoon and Raymond, 2012).

To further investigate a seasonal variation in DOM sources to BHC, the relationship between a^*_{375} and *S* were plotted along with the values from the CFR and Onslow Bay in the Atlantic Ocean over the four months to identify to which extent these two CDOM pools were affecting DOM dynamics in the creek, along with other sources. Our results show that BHC in March was under the influence of a different source of DOM compared to the three other months (Fig. 14). Our results show that BHC in March was to some extent influenced by inputs from the CFR as evidenced by a mean *S* value of 15.1±0.48 μm^{-1} and a mean a^*_{375} value of 2.14±0.48 m^2 g^{-1} C which were similar to values from the CFR (*S*= 15.0 μm^{-1}, a*375= 2.14 m^2 g^{-1} C). These results suggest that the creek waters in March was characterized by more freshwater, terrestrial CDOM, possibly due to higher freshwater discharge during that month introducing terrigenous material to the creek (Markager and Vincent, 2000; Stedmon and Markager, 2001; Anderson and Stedmon, 2007) (Table 5).

Additionally, Stedmon *et al*. (2000) showed that low *S* values could also be attributed to higher fractions of humic, terrestrial and HMW CDOM sources, which again agrees with the increased freshwater discharge in March.

As most of the samples from May, June and August exhibited *S* values ranging between 15.5 to 17 μm^{-1} and lower a^*_{375} values compared to March, it means that similar processes were acting on CDOM during those months. From Table 8, May, June and August had a mean *S* value of 16.3 ± 0.51, 16.4 ± 0.40, and 16.4 ± 0.39 μm^{-1} respectively, which was similar to the *S* value of the Onslow Bay region of the Atlantic Ocean (*S*= 16.0 μm^{-1}) but they had larger mean a^*_{375} values (Table 6) than the Onslow Bay region (a^*_{375}= 0.08 m^2 g^{-1} C). *Keith et al*. (2002) reported that in Narragansett Bay, increased *S* values were thought to arise from the transformation of terrestrially-derived CDOM and (or) the replacement of this terrestrially-derived CDOM by CDOM produced in situ. In the case of tidal marshes such as BHC, internal inputs are mainly dominated by C3 or C4 marsh plants (Chmura and Aharon, 1995). These results suggest that in May, June and August, the creek's DOM consisted of a mixture of both the CFR and the Atlantic Ocean waters but also substantial inputs from the marsh as evidenced by the majority of the data during these months deviating from the curvilinear trend, similar to what was observed in Stedmon and Markager (2001). The deviations of the data in Stedmon and Markager (2001) were attributed to the mixing of coastal waters with waters from the North Sea.

These observations, based on CDOM spectroscopic properties and [DOC], suggest that marsh export of CDOM to BHC exhibits considerable variation in time and space in terms of concentration and composition over short, tidal timescales which substantially

affects estuarine carbon cycling. On a seasonal basis, the observed differences in CDOM optical properties throughout the year was mostly driven by freshwater river discharge from the CFR, as evidenced by increased a_{254} in the spring from the time series analysis of the weekly samples (Fig. 13)

Salt marsh inputs and terrigenous DOM as the main DOM sources to BHC

Estuaries such as BHC may receive DOM from a variety of sources, both imported from outside the system (e.g. marine inputs, terrigenous inputs), and produced within the estuarine system (e.g. marsh plants inputs, estuarine phytoplankton) (Bouillon *et al.*, 2012). To distinguish between these sources of DOM to BHC, each of which has a unique biochemical and isotopic characteristic, stable carbon isotopes (δ^{13}C-DOC) were utilized to look at the tidal, spatial and seasonal trend along the creek. The δ^{13}C values of organic matter have proven to be a very useful tracer for DOC in estuaries and tidal marshes (Peterson *et al*., 1994; Chmura and Aharon, 1995; Cifuentes and Eldridge, 1998; Raymond and Bauer, 2001a,b), where the different sources of DOM in such dynamic systems typically have different but sometimes overlapping stable isotope signatures (Bouillon *et al*., 2012). In estuaries and tidal marshes, a gradual transition may exist from a C3-dominated plant community to a C4-dominated plant community, in parallel to the change in salinity along the freshwater-marine continuum (Chmura and Aharon, 1995). In this study, the δ^{13}C-DOC values fall between the range of values expected for different sources as described in Table 3., which makes up a wide range of overlapping sources.

Consistent with the variability in S_R and $SUVA_{254}$ values over the tidal cycles studied, analysis of δ^{13}C-DOC values revealed that when waters coming from the CFR (δ^{13}C=-27.15)

and the Atlantic Ocean Onslow Bay region ($\delta^{13}C$=-22.64) flooded the marsh, it resulted in the dilution of the more enriched *Spartina* signal ($\delta^{13}C$=-15 to -12‰) in the marsh, as evidenced by the depleted values recorded in May, June and August at flood tide at all three sites (Fig. 9). However, at ebb tide, as the waters from BHC drained off the marsh platform, they picked up the enriched marsh material coming from the marsh plants and soil leachates, resulting in a more enriched $\delta^{13}C$-DOC values at ebb tide. These results are consistent with the observed patterns in S_R and in $SUVA_{254}$ values at ebb tide, where the marsh was found to be a source of HMW, more aromatic-rich DOM but also more isotopically-enriched DOM. The relatively invariant, more enriched $\delta^{13}C$-DOC values at Site 3 compared to Sites 1 and 2 are congruent with the variability in a_{254} and [DOC] over the tidal cycles, where higher DOM concentration were observed upstream. Further, these results suggest the pattern in the $\delta^{13}C$-DOC values are attributable to marsh sources of DOM rather than phytoplankton, which would have lower aromaticity and molecular weight.

Analysis of spatial variations (Fig. 11) indicated that, except for May, no clear separation in $\delta^{13}C$-DOC values existed between the three locations along BHC with values averaging -24‰. Based on the two end-member mixing model and the different potential sources of DOM to estuaries outlined in Table 3, the relatively invariant $\delta^{13}C$-DOC values implied that the entire system was dominated by a balance between external contributions from the coastal Atlantic Ocean and the CFR and internal contributions from salt marsh plants, resulting in a uniform distribution and a narrower range of values (Fig. 11). Salt marsh plants in BHC consist of both C3 plants (*Juncus roemerianus*) and C4 plants (e.g *Spartina alterniflora*), with more enriched $\delta^{13}C$-DOC values for C4 plants (-15 to -12‰) and

more depleted δ^{13}-DOC values for C3 plants (-32 to -21‰). Our results show that the C3 plants *Juncus roemerianus* appeared to exert a greater influence on the δ^{13}C-DOC values of BHC. Based on studies by Raymond and Bauer (2001b) in a similar system as BHC, it was found that the upper, low-salinity reaches of the York River Estuary was mostly influenced by tidal marshes while the middle and lower York were mostly influenced by estuarine phytoplankton, resulting from increased light availability and high flushing rates in the high salinity reaches of the estuary. Contrastingly, our results did not follow the same pattern and displayed a lack of variation in δ^{13}C-DOC from Site 3 to Site 1, moving downstream towards the mouth. Bouillon *et al*. (2012) reported that a relatively uniform linear trend means that the end-members' stable isotope signatures are identical. This could be explained by a balance in the mixing of internal inputs of DOC from marsh plants and phytoplankton production (more enriched δ^{13}C-DOC) with tidally imported carbon sources (more depleted δ^{13}C-DOC) brought about by the mixing of the Atlantic Ocean coastal waters and the CFR. Rapid tidal flushing could also explain this lack of variation in the DOM sources along the creek (Peterson *et al*., 1994). In another study by Middelburg and Herman (2007), it was reported that in tide-dominated estuaries where extensive processing and mixing of DOM along the salinity gradient occurs, there is a less pronounced gradient and a narrower range in isotope signatures, which is congruent with our results in tide-dominated BHC.

The slightly depleted δ^{13}C-DOC values in May at Sites 1 and 2 indicated a greater influence from the CFR waters flooding the marsh, which matched the more depleted CFR (δ^{13}C=-27.15‰) signal in the two end-member mixing model (Bouillon *et al*., 2012) (Fig. 11). This could be explained by the increased freshwater discharge from the CFR in May,

contributing to a more depleted, freshwater isotopic signal at Sites 1 and 2. This corroborates with findings from Raymond and Bauer (2001b) that during periods of moderate to high flow, riverine DOC entering the York River Estuary had a terrestrial or freshwater isotopic signature.

Neubauer *et al*. (2000) stated that salt marshes located in the low-salinity, upper York river estuary experience significant OM decomposition and that DOC cycling there is strongly influenced by marsh DOC input and OM turnover. This statement agrees with our results for May at Site 3, where analysis of [DOC], S_R and $SUVA_{254}$ revealed that the upstream marsh was a major source of DOM (Fig. 9) but also a source of HMW, aromatic-rich DOM to the adjacent waters, hence resulting in more enriched δ^{13}C-DOC at Site 3 that we can attribute to C4 plant (*Spartina*) dominated sources of DOM and not to phytoplankton. This dynamic would also explain the significant difference ($P < 0.01$) between Site 1 and Site 3 during that month, where the upper creek (Site 3) was more influenced by marsh DOM inputs while the middle and lower creek (Sites 2 and 1 respectively) were more influenced by terrestrial, freshwater inputs from the CFR.

Seasonal variations in δ^{13}-DOC values were consistent with the seasonal variations observed in a_{254}, S_R and $SUVA_{254}$ values, where a more depleted δ^{13}C-DOC value in May corresponded to a higher a_{254} and $SUVA_{254}$ value and a lower S_R value during that month (Fig. 12). These results during the spring coincided with the highest freshwater discharge from the CFR (Table 7). The highest average a_{254} along with the highest average aromaticity, higher MW and more depleted δ^{13}C-DOC signal observed in May could be explained by increased inputs of terrigenous DOM from increased freshwater inputs resulting from the

higher flow from the CFR during that month. Contrastingly in periods of low flow during June and August (Table 7), a more enriched δ^{13}C-DOC signal was observed, consistent with higher mean S_R values and lower $SUVA_{254}$ values during these two months, pointing to a greater influence from the marsh than the CFR during these two months.

CDOM results examining the relationships between a^*_{375} and *S* values also collectively supported our δ^{13}C-DOC results (Fig. 14). BHC in March had a lower mean *S* value and a higher mean a^*_{375} value (Table 8), which corresponded to the same a^*_{375} and *S* value as the CFR. These results pointed to a greater influence from the CFR compared to the Onslow Bay region, outpacing inputs from the marsh during that month. Contrastingly in May, June and August, higher mean *S* values and lower mean a^*_{375} values were observed, together with relatively invariant, more enriched δ^{13}C-DOC values, pointing to a balance between internal inputs from salt marsh plants and external inputs from mixing of the CFR.

The CDOM-DOC-salinity conservative relationship in BHC sets the stage for its numerical modeling

The conservative behavior of CDOM and DOC were analyzed through the correlations between CDOM, DOC and salinity, which is the main condition to be able to derive CDOM and DOC from the model's salinity, and consequently compute DOC fluxes (Figs. 15 and 16, Table 9). Our results are consistent with similar conservative behavior observed in other estuaries (Table 1). The strong inverse relationship exhibited between CDOM, DOC and salinity indicates that the upper creek, marsh-derived DOC was conserved during mixing of freshwater end member with marine end member waters. The elevated export of CDOM per unit DOC observed in BHC in March was possibly due to outwelled

CDOM-laden waters from the productive adjacent salt marsh in the spring as a result of high freshwater discharge during that period. Studies in the lower Atchafalaya River plume suggested that elevated CDOM and DOC likely occurred as a result of interactions between discharge from the Atchafalaya River and their adjacent extensive and productive salt marshes (Tehrani *et al*., 2013).

The non-conservative behavior of CDOM and DOC at Sites 2 and 3 and the associated decoupling in the conservative relationship between CDOM, DOC and salinity in May pointed to an additional source to BHC (Figs. 16a and 16b). Historical precipitation data for 2016 shows that on the sampling dates for May, 12th and 13th, 0.56 and 0.24 inches of rain were recorded respectively (usclimatedata.com). This local precipitation event could be another source of freshwater to the creek, but could have also increased the release of marsh-derived DOM through the associated run-off during this event. This precipitation event in addition to the high freshwater discharge from the CFR could explain the low salinity range recorded during sampling for that month. Joshi *et al*. (2017) reported that the non-conservative behavior of CDOM in the coastal waters of Apalachicola Bay likely occurred due to increased DOM inputs from different terrestrial sources at the freshwater end-members.

Carbon export from BHC exceeds export from major US rivers

It is essential to understand how carbon fluxes between tidal wetlands such as BHC and their connected oceans affect the global carbon (C) cycle and budget. However, carbon fluxes and export between tidal marshes and their adjacent estuaries have historically been hard to quantify because of their variability with respect to hydrology and geomorphology,

and current C export estimates across this land-ocean interface still have large uncertainties (Tobias and Neubauer, 2009; Cai 2011; Wang *et al*., 2016). These uncertainties resulted in significant knowledge gaps in the quantity and quality of carbon fluxes from tidal wetlands, which is central to the issue of blue carbon loss to coastal waters (Bauer *et al*., 2013). However, the use of a numerical hydrodynamic model like SCHISM in this study allowed for a better representation of the system by constraining the boundaries of the tidal marsh using an unstructured mesh grid for more accurate DOC flux estimates but also a better understanding of the carbon cycle in these dynamic systems which are hotspots for OM transformation and exchange with their adjacent estuaries. This approach also resolved DOC export from marshes on a more realistic temporal scale (from tidal to seasonal cycles), and as such provided a more robust estimate than in previous studies (Tzortziou *et al*., 2008; Osburn *et al*., 2015).

Assessment of the model performance indicated that a better estimate of salinity, CDOM and DOC was obtained in March compared to the three other months in BHC, exhibiting the highest accuracy in salinity and CDOM retrievals for this month. This result could be attributed to the generally higher flow observed in the spring, which the model has been able to reproduce well, but also to a stronger coefficient in calculating salinity for the model's boundary conditions. The match-up comparison between in situ and model-derived salinity in August showed an overestimation of salinity, resulting in an underestimation of CDOM, which could mainly be explained by errors and uncertainties in the boundary conditions (Figs. 17d and 18d). A more robust salinity dataset would have likely produced better estimates for May, June and August. The lack of an appropriate observing station

recording salinity data at the boundary and the uncertainties associated with the coefficients computed to obtain an hourly salinity dataset based on the data from UNCW's buoy SUN2 likely introduced discrepancies in the results. Likewise, strong over- and underestimation of CDOM values in May, June and August, as shown by match-up comparisons between in situ a_{254} and model-derived a_{254} as well as statistical analysis, indicated that the model exhibited low accuracy in CDOM simulations for those months. Again, these discrepancies in CDOM estimation from salinity were related to uncertainties in the boundary conditions since CDOM and salinity are tightly coupled. Consistent with the salinity and CDOM simulations, the under- and overestimation of [DOC] in May, June and August not only reflect errors and uncertainties associated with the regression used in deriving [DOC] from CDOM but also from uncertainties in the boundary conditions at the mouth of BHC. The setting-up of an appropriate observing and monitoring station at the mouth of BHC, collecting hourly salinity data, could improve these disparities and produce better estimates. Still the model performed well in developing [DOC] maps for BHC, with higher concentrations in the upper creek (near Site 3) and lower concentrations in the lower creek (near Site 1) (Figs. 20c and 21c), indicating that using a numerical model's salinity output as a tracer for CDOM and [DOC] is possible in systems like BHC estuary, provided a robust dataset for boundary conditions is available.

Finally, daily DOC flux and export and net annual DOC export for BHC were estimated from the model. Consistent with the tidal variability in [DOC] during all four months where increased [DOC] was recorded at ebb tide, BHC was shown to export DOC out of the marsh to the CFR and net fluxes and export were found to be higher at ebb tide

(Figs. 22 and 23). Since the four months sampled revealed a net export from the marsh to the CFR, these results support the assertion that the marshes surrounding BHC estuary indeed export DOC in the outgoing tide as reported in previous studies (Tzortziou *et al*., 2008; Tobias and Neubauer, 2009). These results for DOC flux and export over the tidal cycles are also congruent with the tidal variability in [DOC] where higher concentrations were observed at ebb tide in June and August (Fig. 6).

For comparison with reported estimates of DOC export in the literature from various marshes, net annual DOC export was computed by multiplying the mean daily DOC export by 365 days. Model predictions estimated an annual net DOC export of 54 g C m^2 yr^{-1} from the marsh into the adjacent estuary, within the reported range of 15-328 g C m^2 yr^{-1} of DOC exports from other marshes in recent studies (Tzortziou *et al*., 2008; Tobias and Neubauer, 2009; Osburn *et al*., 2015). BHC had a greater export than other creeks studied on the Upper Texas coast (20 g C m^2 yr^{-1}) and on the U.S. east coast such as in the Rhode River estuary (32 g C m^2 yr^{-1}) and in Carter Creek in Virginia (25 g C m^2 yr^{-1}) (Table 11). However, this net annual DOC export of 54 g C m^2 yr^{-1} was lower than the export values on the US west coast such as on Brown's island in San Francisco (235 g C m^2 yr^{-1}) and on the Gulf coast such as in Apalachicola Bay, Louisiana (97 g C m^2 yr^{1}), suggesting even more heterogeneity in marsh C export across estuaries (Table 11). In the South Atlantic Bight (SAB) region, which extends from North Carolina to Florida, our reported net annual DOC export of 54 g C m^{-2} y^{-1} was much lower than the reported range of DOC export in estuaries of North Carolina, South Carolina and Georgia (128-328 g C m^{-2} y^{-1}) but was within the reported range of DOC export in estuaries on the U.S east coast (25-328 g C m^{-2} y^{-1}) (Table 11).

Despite the uncertainties and assumptions in the modeling process, this approach for evaluating DOC fluxes and export from a salt marsh to its adjacent estuary could lead to a broader understanding of estuarine biogeochemistry, especially in the face of SLR, blue carbon loss and the general loss of coastal salt marshes. Globally, the rate of SLR in southeastern U.S. has been found to be approximately 2.5 mm yr^{-1} while the vertical accretion rates of tidal marshes in the same region ranged approximately between 4 to 6 mm yr^{-1} (Craft, 2007). These observations indicate that in general tidal marshes in southeastern U.S have been able to keep pace with SLR but could become less resilient with the increasing pressures from coastal build-up and climate change.

An OC accumulation rate of 40 g C m^{-2} y^{-1} was reported in salt marshes along three estuaries in Georgia (Loomis and Craft, 2010). Interpolating this value for BHC relative to its DOC export of 54 g C m^2 yr^{-1}, this suggest that for now blue carbon in the system could be lost at approximately the same rate as it is buried but the loss of blue carbon could potentially exceed the amount stored with increasing pressures from coastal build-up, SLR and climate change. The quantity of C stored in coastal vegetated ecosystems such as tidal marshes like BHC makes them the most C-rich ecosystems on Earth but also plays a major role in regulating climate change by sequestering atmospheric CO_2. BHC is a relatively pristine environment, and its DOC export rate seems to be comparable to its OC accumulation rate. However, for systems that are more urbanized and actively eroding, it is highly anticipated that their DOC export rate would be higher than BHC and would exceed the OC burial rate, having major consequences in terms of loss of blue carbon. The increased human- and climate-driven threats to such systems will likely exacerbate this blue carbon loss,

consequently impacting the carbon storage capacity of such valuable ecosystems. Additionally, DOC export from tidal marshes to their adjacent estuaries has an effect on estuarine microbial metabolism, nutrient cycling and UV light penetration of the water column (Zepp, 2007). These processes are likely to be affected by an increased DOC export to estuaries, which may impact remineralization and productivity in these estuarine waters, consequently impacting the coastal C cycle.

Additionally, BHC's estimated annual DOC export was nearly 10-fold greater than the mean export of 15 major U.S rivers (Spencer *et al*., 2013). Among those 15 rivers, 5 rivers (the Androscoggin, Penobscot, Edisto, Atchafalaya, and Mobile) were found to exhibit the highest DOC exports ranging between 2.4 g C m^2 yr^{-1} and 7.7 g C m^2 yr^{-1}, which was attributed to the extensive wetlands surrounding their watersheds (Table 11) (Spencer *et al*., 2013). Similarly, BHC drains its surrounding extensive marsh but despite its smaller area compared to the rivers mentioned above, has a disproportionately greater estimated DOC export than those 5 rivers combined. This implies that despite their small watersheds the extensive and productive salt marshes surrounding saline tidal creeks are quantitatively significant sources of DOC to coastal waters, supporting observations that DOC export from tidal marshes play a central role in regional and global carbon budgets.

Comparing export from the salt marshes flanking BHC to other carbon export such as DIC, POC and CO_2 from similar intertidal salt marshes along the U.S southeastern coast, the annual DOC export from BHC was much lower than those reported values. An estimated DIC export of 156 g C m^2 yr^{-1} from the Sapelo Island marshes in Georgia was reported by Wang and Cai (2004). This marsh DIC export was comparable to the estimated marsh DIC

export of 197 g C m^2 yr^{-1} from tidal freshwater marshes in Virginia (Neubauer and Anderson, 2003). Both values exceed the reported DOC export of 54 g C m^2 yr^{-1} for this study by approximately 2-fold. Megonigal and Neubauer (2009) reported that compared to DIC, much less DOC is exported from tidal wetlands to estuaries, despite DOC being the most important form of C exported from these systems. Several other studies also suggest that there is substantial DIC export from tidal marshes to estuaries (Frankignoulle and Bourges, 1996; Cai and Wang, 1998; Wang *et al*., 2016). Studies by Cai (2011) and Kroeger *et al*. (2012) revealed that changes of DIC concentration over tidal cycles across all seasons were almost always larger than DOC concentration. These observations suggest that hydrology likely influences DIC and DOC fluxes in a similar way but it is expected that the DIC export from BHC could be higher than the DOC export. Scale-up exercises of the tidal marsh carbon budget in the U.S. east coast (tidal wetland area of 12, 300 km^2) by Wang *et al*. (2016) showed that 12% (130 g C m^2 yr^{-1}) of the total marsh NPP (1073 g C m^2 yr^{-1}) was exported as DOC compared to 39% (414 g C m^2 yr^{-1}) for DIC export. The DOC export value reported in Wang *et al*. (2016) exceeds our reported DOC export value by approximately 2-fold. Additionally, these observations suggest that about three times more DIC is exported compared to DOC and interpolating this ratio to BHC suggest that DIC export in BHC could be approximately 162 g C m^2 yr^{-1}. This estimated DIC export is comparable to the DIC export from the tidal marshes in Virginia (Neubauer and Anderson, 2003). Still from the same scale-up exercise in Wang *et al*. (2016), our estimated net annual DOC export of 54 g C m^2 yr^{-1} for BHC was comparable to the net annual POC export of 49 g C m^2 yr^{-1} reported, both of which were within the range of net annual POC export of 11-128 g C m^2 yr^{-1}

compiled from marsh-estuarine systems (Tobias and Neubauer, 2009). Interpolating these observations to BHC suggest that POC export could be approximately 50-54 g C m^2 yr^{-1} in BHC. CO_2 release from the marsh-dominated Sapelo Island in Georgia ranged between 256-306 g C m^2 yr^{-1}, which when interpolated to BHC, is much higher compared to the DOC export estimated for our study (Wang and Cai, 2004). Wang *et al*. (2016) reported a CO_2 export value of 358 g C m^2 yr^{-1}, three times higher than our reported DOC export. These observations suggest that in addition to this blue carbon that tidal marshes have stored for centuries being lost through tidal flushing in the estuary, a substantial amount could also be emitted to the atmosphere, becoming a source of greenhouse gas. Given the magnitude of these carbon exports in BHC, their impacts on the coastal carbon budget and carbon cycling could potentially be even greater,

Blue carbon sinks like tidal marshes cover only about 0.2% of the seafloor but account for approximately 50% of the total C buried in ocean sediments (Duarte *et al*., 2005). However, tidal marshes are being lost at a rate of 1-2% yearly and 25% of their historical global coverage has been lost (Duarte *et al*., 2008; Nelleman *et al*., 2009). The loss of blue carbon sinks such as tidal marshes not only represent a threat to biodiversity and coastal protection but also the loss of a natural carbon sink, affecting the capacity of the biosphere to remove anthropogenic CO_2 emissions (Nelleman *et al*., 2009). Additionally, as mentioned earlier, salt marshes can be vulnerable to SLR, being low lying coastal areas. It is estimated that in combination with human-induced threats, a 1-m rise in sea level could threaten up to half of the coastal wetlands (Nicholls *et al*., 1999). This would not only affect their carbon

storage capacity but increase the risk of erosion and flooding. As coastal build up and sea level rise both increase, additional pressures and stresses are being put on salt marsh habitats.

Besides being valuable blue carbon sinks, coastal ecosystems like tidal marshes also deliver important ecosystem goods and services to coastal communities. They are necessary to sustain the commercial interests of the multi-billion-dollar fishing industry, and in turn the livelihoods of various communities that depend upon its success. 70% of commercial fish depend on salt marshes; a 1999 estimate shows that this 70% represents $2.45 billion dollars to the U.S. GDP in fish alone (NOAA, 2000). The most important service they provide is coastline protection, where salt marshes act as a buffer against natural hazards like storms, hurricanes, and tsunamis (Nelleman *et al*., 2009).

Overall, this research demonstrates the need to quantify the importance of these tidal coastal wetland systems in the ocean's coastal carbon cycle and assess the extent to which rising sea levels could contribute to a major loss of carbon from one of the world's most important carbon storage and how coastal infrastructure development could potentially deflect tidal energy towards the unprotected estuaries on which many living organisms rely.

CONCLUSIONS

The major conclusions of this study are:

1. The main differences in DOM between ebb and flood tide were driven by tidal pumping, which flushes DOM out of the marsh surface sediments, resulting in lateral export of DOM to the adjacent estuary and substantially higher CDOM values during ebb tide than flood tide.
2. Overall higher [DOC] at Site 3 (upper creek) and a gradual decrease in [DOC] towards the mouth (Site 1) indicated that most of the DOM loading to BHC was from upstream marsh plants and soil leachates. The decrease in concentration as DOM transited downstream to Site 1 was attributed to mixing of high concentration, marsh-derived DOM with low concentration, marine-derived DOM, brought about by bidirectional flow from tides.
3. Analysis of CDOM quality based on S_R and $SUVA_{254}$ showed that the marsh was a source of HMW, aromatic-rich DOM to BHC through tidal flushing. Major shifts and the significant differences observed in DOM quality between Sites 1, 2 and 3 were attributed to mixing with the seawater end-member and inputs from the marsh.
4. Seasonal differences in DOM quantity and quality in BHC were mainly driven by freshwater discharge from the CFR. Differences between ebb and flood tide were most pronounced during the summer months, indicating seasonal variability based on flow of the Cape Fear River. Tidal pumping can dominate lateral fluxes of blue carbon as DOM to adjacent waters and vary seasonally with the dominant effect in this marsh occurring during the summer, or when river discharge is low.

5. The source of the DOM in BHC, as evidenced by the relatively invariant δ^{13}C-DOC values, was similar throughout the creek, pointing to a balance in the mixing of internal inputs of DOM from marsh plants and phytoplankton production with tidally imported carbon sources brought about by the mixing of the Atlantic Ocean coastal waters and the CFR.
6. Model predictions estimated an annual net export of DOC at 54 g C m^{-2} y^{-1} from the marsh into the adjacent estuary, greater than the export from other creeks studied on the Upper Texas coast (20 g C m^2 yr^{-1}) and on the US east coast such as in the Rhode River estuary (32 g C m^2 yr^{-1}), lower than the export values on the US west coast such as on Brown's island in San Francisco (235 g C m^2 yr^{-1}) and Gulf coast such as in Apalachicola Bay, Louisiana (97 g C m^2 yr^1), suggesting even more heterogeneity in marsh C export across estuaries. Overall, results suggest that estuarine OM dynamics in tidal creeks are strongly controlled by the circulation of water and by tidal pumping, which leaches DOM from salt marshes and exports it to adjacent waters, emphasizing the roles of such tidal creeks in the ocean's coastal C cycle.

Discrete sampling of surface water samples coupled with numerical modeling in this study provided a valuable tool to investigate the effect of physical processes such as tidal circulation on DOM dynamics and export with high spatial and temporal resolution in BHC. Accordingly, an approach was used to develop CDOM and [DOC] maps for the estuary using modeled salinity, where the main condition for implementing this approach was a conservative behavior between CDOM, DOC and salinity. The resulting CDOM-DOC-salinity relationships were applied to model-derived salinity to produce estimates of DOC

flux and export from BHC. Match-up comparisons between *in situ* measurements and model-derived measurements revealed that the model performed well in estimating CDOM a_{254} and [DOC] for March while disparities were observed in the three other months. These disparities were mainly attributed to uncertainties associated with the boundary conditions due to a lack of appropriate observing station at the mouth of BHC to acquire the high-resolution salinity required for model.

This study also intended to demonstrate that significant shifts in DOM quantity and quality can occur with space and time, within the system, which can be investigated through the analysis of DOM optical properties. While a variety of physical/chemical processes or biological drivers can induce differences in DOM quality, spatial and seasonal changes can also have an influence on DOM dynamics as shown by this study. Both CDOM a_{254} and [DOC] varied tidally and seasonally, with tidal pumping and freshwater discharge being the dominant forces driving these changes.

Our results indicate that tidal circulation in BHC exerts a large control on the variation in DOM quantity and quality, as evidenced by model predictions of DOC flux and export over tidal cycles. The net annual DOC export of 54 g C m^{-2} y^{-1} estimated for BHC was greater than the export from other creeks studied on the Upper Texas coast and on the U.S. east coast such as in the Rhode River estuary but lower than the export values on the US west coast such as on Brown's island in San Francisco, suggesting even more heterogeneity in marsh C export across estuaries. In the SAB region, our reported net annual DOC export of 54 g C m^{-2} y^{-1} was lower than the reported range of DOC export in North Carolina, South Carolina and Georgia (128-328 g C m^{-2} y^{-1}).

Additionally, our estimated DOC export of 54 g C m^{-2} y^{-1} exceeded DOC export from some of the major U.S rivers, which ranged between 2.4 g C m^2 yr^{-1} and 7.7 g C m^2 yr^{-1} (Spencer *et al*., 2013). Despite its relatively small tidal marsh area, BHC drains its surrounding productive marsh at magnitudes much larger than those rivers, which do have much larger total exports of OC than BHC, given their larger flows and watersheds. However, what our results do clearly highlight is the substantial contribution of such tidal marshes in aggregate to the ocean's coastal C budget and cycle. DOM flux derived from vascular plants and soils in tidal marshes thus represents an important term in coastal carbon budgets and thus is a dominant linkage between terrestrial and aquatic systems across the freshwater-marine continuum. Despite DOC being the most important form of C exported from such systems, interpolation from other studies suggested that DIC export from BHC could exceed DOC export by a factor of three. The magnitude of DOC export combined with other carbon exports such as DIC, POC and CO_2 export, based on computed values from other studies (Neubauer and Anderson, 2003; Wang and Cai, 2004; Tobias and Neubauer, 2009, Wang *et al*., 2016), make tidal marshes such as BHC a valuable component of the coastal C cycle. DOM typically constitutes the largest pool of detrital OC and DOC represents the most important intermediate in the global C cycle (Battin *et al*., 2008). Therefore, the production, loss and transport of DOC represent valuable terms in the C budget (Jaffé *et al*., 2008). Though the fate of blue carbon has been harder to quantify than its source, it is anticipated that once the blue carbon is exported from estuaries to continental shelves, it enters the C cycle of the open ocean and gets recycled. This C also gets buried into the sediments where around 80% OC burial in sediments is contributed by shelves (Bauer *et*

al., 2013). Additionally, 50% of the OC supplied to the deep ocean comes from continental shelves. In addition to burial in sediments, OC in continental shelves is transported to the open ocean through processes such as bioturbation or physical resuspension, where it gets remineralized by bacteria as it enters the coastal ocean C cycle (Bauer *et al*., 2013).

Bald Head Creek estuary is a relatively pristine environment, though Bald Head Island has been subject to considerable coastal build-up and development. However, with increasing human pressures, development and anthropogenic disturbances, these tidal wetlands are undergoing global decline, while associated climate change effects such as SLR constitute an additional threat to these valuable ecosystems. Coupling the modeling approach in this study with studies of photochemical and biological degradation of DOM in tidal creeks and estuaries could provide useful insights into their complex estuarine biogeochemistry, especially in the face of SLR, blue carbon loss and global decline in coastal wetlands (Tzortziou *et al*., 2011; Osburn *et al*., 2015).

Combining high-resolution tidal sampling with numerical modeling provided a key means of quantifying salt marsh DOM cycling and export. The marshes surrounding BHC are representative of the marshes of the Mid- and South Atlantic Bight, thus our results highlight the importance of marshes in exporting DOM to coastal waters. Our model predictions estimate that these tidal marshes are an important source of DOC to the adjacent estuary, and release HMW, aromatic-rich DOM into the estuary through tidal pumping. These results imply that tidal marsh outwelling of DOC through tidal flushing exerts a significant influence on estuarine biogeochemistry and the subsystems of the marsh-estuarine interface (Tzortziou *et al*., 2011).

Future directions

The advantage of using CDOM as a tracer for [DOC] is the relative simplicity and economy of the measurement. Since field measurement and analysis of [DOC] is time-consuming and expensive, CDOM serves as an inexpensive intermediary to estimate DOC and study the carbon cycle in coastal environments, with the possibility of examining preliminary data on the spot using ocean color sondes and sensors. CDOM contributes from 20% to 70% of the total DOC in coastal regions and serves a good proxy for DOC (Coble, 2007). On regional timescales, such as in estuaries like BHC, CDOM provides a simple measure to evaluate the distribution of freshwater components.

The approach followed in this study was based on available field measurements. However, as mentioned in the discussion section, the lack of an appropriate observing station at the mouth of the creek to collect hourly salinity data for use as the boundary conditions of the model resulted in some uncertainties and errors in the model simulations. For future studies at this site and similar tidal marshes which involve the use of a numerical hydrodynamic model, the setting-up of an observing and monitoring station to collect hourly data would be desirable to develop more robust correlations and algorithms to estimate CDOM and DOC and to gain more insight about DOC dynamics and the C cycle.

This study has demonstrated the importance of combining high resolution hydrologic measurements of CDOM absorption with numerical modeling to assess DOM biogeochemistry in a tidal marsh. Tidal circulation plays a significant role in draining the marsh platform and future work in tidal creeks similar to BHC could also focus on carbon exports such as DOC, DIC and POC during extreme weather events such as storms and

hurricanes, which are associated with storm surge. The erosive power of storm surge and strong winds associated with extreme weather events are highly anticipated to have large effects on the creek's water quality, potentially increasing carbon exports from salt marshes to their adjacent estuaries (Chen *et al*., 2009). These effects could also result in eutrophication and hypoxia events in the estuary, which would be an important ecological threat. Chen *et al*. (2011) showed that heavy precipitation and its associated run-off resulted in the increase of marsh-derived blue carbon release into Apalachicola Bay. In other settings, the rapid increase of terrestrially-derived DOM concentration and flux during rainfall events have been shown (Ward *et al*., 2012). The use of a hydrodynamic model could again serve as a valuable tool in assessing the effect of these extreme weather events on carbon exports. Together, this work demonstrates the need to quantify the importance of these tidal wetland systems in the ocean's coastal C cycle.

TABLES

Table 1. Correlation between CDOM and salinity for different estuaries.

Location	Absorption wavelength (nm)	R^2	Reference
Cape Fear River, USA	440	0.96	Kowalczuk *et al.*, 2003
Pearl River, China	355	0.88	Chen *et al.*, 2004
St Lawrence, Canada	440	0.99	Nieke *et al.*, 1997
Southern Baltic Sea	375	0.88	Kowalczuk *et al.*, 2006
Conwy, Wales	440	0.98	Bowers *et al.*, 2004
Everglades National Park, USA	254	0.72	Jaffé *et al.*, 2004
Bekanbeushi River, Japan	254	0.85	Maie *et al.*, 2014
Judan River, Malaysia	254	0.99	Maie *et al.*, 2014
Orinoco River, South America	300	0.88	Del Castillo *et al.*, 1999
Skidaway River	254	0.85	Bittar *et al.*, 2016
East Siberian Shelf	254	0.85	Pugach *et al.*, 2015

Table 2. Site description for the locations sampled in Bald Head Creek, eastern North Carolina.

Site	Description	Width of creek (m)	Distance from the sea (m)	Coordinates
1 (Lower creek)	near the mouth of the creek	110	3400	33.8757°N, -77.9981°W
2 (Middle creek)	in the middle of the creek	70	2360	33.8633°N, -77.9866°W
3 (Upper creek)	near the head of the creek	20	940	33.8587°N, -77.9729°W

Table 3. Published ranges of $\delta^{13}C$ values of potential sources of DOM to estuaries.

Source	**$\delta^{13}C$ (‰)**	**Reference**
C4 salt marsh plants (e.g. *Spartina spp.*)	-15 to -12	Fry and Sherr, 1984
C3 salt marsh plants (e.g. *Juncus spp.*)	-32 to -21	Deines, 1980
Marine/estuarine phytoplankton	-24 to -18	Fry and Sherr, 1984
Freshwater phytoplankton	-30 to -24	Anderson and Arthur, 1983
Bacteria	-27 to -12	Coffin *et al*., 1989
Marsh sediment OM	-26.4 to -22.3	Raymond and Bauer 2001a

Table 4. Summary of variables used in the Reynolds-Averaged Navier-Stokes equation.

Variable	Meaning
∇	$(\frac{\partial}{\partial x}, \frac{\partial}{\partial y})$
(x, y)	horizontal Cartesian coordinates.
z	vertical coordinate, positive upward
t	time
G (x, y, t)	Free-surface elevation
h (x, y)	Bathymetric depth
u (x, y, z, t)	horizontal velocity, with Cartesian components (u, v)
w	vertical velocity
F	other forcing terms in momentum (baroclinicity, horizontal viscosity, Coriolis, earth tidal potential, atmospheric pressure, radiation stress).
g	acceleration of gravity, in [m s^{-2}]
C	tracer concentration (e.g., salinity, temperature).
v	vertical eddy viscosity, in [m^2 s^{-1}]
κ	vertical eddy diffusivity in [m^2 s^{-1}]
F_h	horizontal diffusion
Q	mass source/sink

Table 5. Statistical parameters and their formula used in model performance assessment

Statistical Parameter	Formula
Root Mean Square Error	$\sqrt{\frac{1}{N}\sum_{i=1}^{N}(y_i - x_i)^2}$
Bias	$\frac{1}{N}\sum_{i=1}^{N}(y_i - x_i)$

Where y_i is model-derived values and x_i is field-measured values

Table 6. Comparisons of a_{254}, DOC, S_R and $SUVA_{254}$ values between Sites 1, 2 and 3 in Bald Head Creek during 2016.

Parameter	Month	Sites		
		1	**2**	**3**
a_{254} (m^{-1})	*March*	25.0±14.8	39.6±9.88	48.4±5.00
	May	30.1±10.5	36.5±4.20	42.2±5.45
	June	16.8±7.18	26.4±10.7	36.1±12.3
	August	15.4±7.1	21.5±6.35	28.0±8.31
DOC (mg C L^{-1})	*March*	2.49±0.85	3.43±0.68	3.91±0.36
	May	3.54±0.86	4.15±0.29	4.89±0.71
	June	2.73±0.82	3.85±1.2	3.28±1.06
	August	2.64±0.88	3.20±0.69	3.77±0.83
S_R	*March*	0.96±0.08	0.89±0.02	0.90±0.02
	May	0.97±0.03	0.97±0.02	0.94±0.02
	June	1.03±0.09	0.98±0.05	0.98±0.02
	August	1.13±0.11	1.00±0.05	1.02±0.06
$SUVA_{254}$ (L mg C^{-1} m^{-1})	*March*	4.08±1.11	5.06±1.06	5.38±0.31
	May	3.58±0.66	3.82±0.28	3.75±0.13
	June	2.61±0.54	2.89±0.51	3.28±0.55
	August	2.44±0.51	2.87±0.29	3.19±0.25

All values are presented as the Mean ± Standard deviation. (March: *N*=6; May-August: *N*=7)

Table 7. Comparisons of a_{254}, $SUVA_{254}$, S_R and δ^{13}-DOC values in Bald Head Creek during the spring and summer of 2016.

Month	Season	a_{254} (m^{-1})	$SUVA_{254}$ (L mg^{-1} m^{-1})	S_R	δ^{13}-DOC (‰)	Q (m^3s^{-1})
March	Spring	37.6±14.1	4.84±1.02	0.92±0.06	n/a	267
May		36.3±8.56	3.72±0.41	0.96±0.03	-25.1±0.63	146
June	Summer	26.4±12.7	2.93±0.58	1.00±0.06	-24.2±0.44	51
August		21.6±8.70	2.83±0.47	1.05±0.09	-24.1±0.34	41

All values are presented as the Mean ± Standard deviation. n/a= not available. Q represents the average discharge 10 days before sampling obtained from www.waterdata.usgs.gov.

Table 8. Seasonal variations in a^*_{375} and *S* in Bald Head Creek.

Month	**Season**		**a^*_{375} (m^2 g^{-1} C)**	***S* (μm^{-1})**
March		Min.	1.26	14.2
		Mean	2.14±0.48	15.1±0.48
	Spring	Max.	3.15	15.7
May		Min.	0.69	15.3
		Mean	1.39±0.21	16.3±0.51
		Max.	1.83	18.1
June		Min.	0.56	15.5
		Mean	1.04±0.24	16.4±0.40
	Summer	Max.	1.45	17.5
August		Min	0.69	15.6
		Mean	1.09±0.20	16.4±0.39
		Max.	1.44	17.6

(March: *N*=18; May-August: *N*=21)

Table 9. Coefficients resulting from regression analysis between a_{254}, DOC concentration and salinity. Linear equations were fitted to all variables ($y = ax + b$). In the CDOM-salinity and DOC-salinity relationship, y=CDOM and DOC and x=salinity, while in the CDOM-DOC relationship, y=CDOM and x=DOC.

Parameter	Month	Season	Slope (a)	Intercept (b)	R^2	N	P-value
a_{254} vs. salinity	*March*		-3.17	115.82	0.88	18	P<0.0001
	May	Spring	-2.58	105.67	0.40	21	P>0.0001
	June		-6.87	243.81	0.92	21	P<0.0001
	August	Summer	-1.81	71.56	0.92	21	P<0.0001
DOC vs. salinity	*March*		-0.20	8.28	0.95	18	P<0.0001
	May	Spring	-0.18	9.11	0.20	21	P>0.0001
	June		-0.67	25.00	0.85	21	P<0.0001
	August	Summer	-0.19	8.36	0.92	21	P<0.0001
DOC vs. a_{254}	*March*		15.10	-11.84	0.86	18	P<0.0001
	May	Spring	9.58	-3.90	0.90	21	P<0.0001
	June		9.44	-9.06	0.91	21	P<0.0001
	August	Summer	9.49	-8.78	0.95	21	P<0.0001

Table 10. Daily DOC fluxes and annual DOC export values from Bald Head Creek resulting from model simulations.

Month	**DOC flux (g C day^{-1})**	**DOC export (g C m^{-2} day^{-1})**	**Mean daily DOC export (g C m^{-2} d^{-1})**	**Net annual DOC export (g C m^{-2} y^{-1})**
March	-9.01×10^{4}	-0.02		
May	-2.99×10^{5}	-0.08	-0.15	-54
June	-3.81×10^{5}	-0.10		
August	-1.53×10^{6}	-0.40		

Negative values mean export out of the marsh to the Cape Fear River.

Table 11. Comparison of the annual DOC export from Bald Head Creek to other reported studies.

Creek/River name	Location	Annual DOC export ($g\ C\ m^{-2}\ y^{-1}$)	Source
Bald Head Creek	North Carolina, US	54	This study
Ware Creek	Virginia, US	80	Axelrad *et al.*, 1976
Carter Creek	Virginia, US	25	Axelrad *et al.*, 1976
Rhode River Estuary	Maryland, US	43	Jordan *et al.*, 1983
Bly Creek	South Carolina, US	250	Dame *et al.*, 1991
Kariega Estuary	South Africa	13	Taylor and Allanson, 1995
Swartkops Estuary	South Africa	103	Winter *et al.*, 1996
Slufter Estuary	The Netherlands	20	Asjes and Dankers, 1994
Broome‘s Branch	North Carolina, US	135	Osburn *et al.*, 2015
Duplin River	Georgia, US	128	Chalmers *et al.*, 1985
Upper Texas Coast	Texas, US	20	Borey *et al*, 1983
Apalachicola Bay	Louisiana, US	97	Joshi *et al.*, 2017
Canary Creek	Delaware, US	104	Roman and Daiber, 1989
North Inlet Estuary	South Carolina, US	328	Dame *et al.*, 1984
Brown’s Island	San Francisco, US	235	Downing *et al.*, 2009
Rhode River Estuary	Maryland, US	32	Tzortziou *et al.*, 2008
15 major US rivers	Across US	0.2-7.7	Spencer *et al.*, 2013

FIGURES

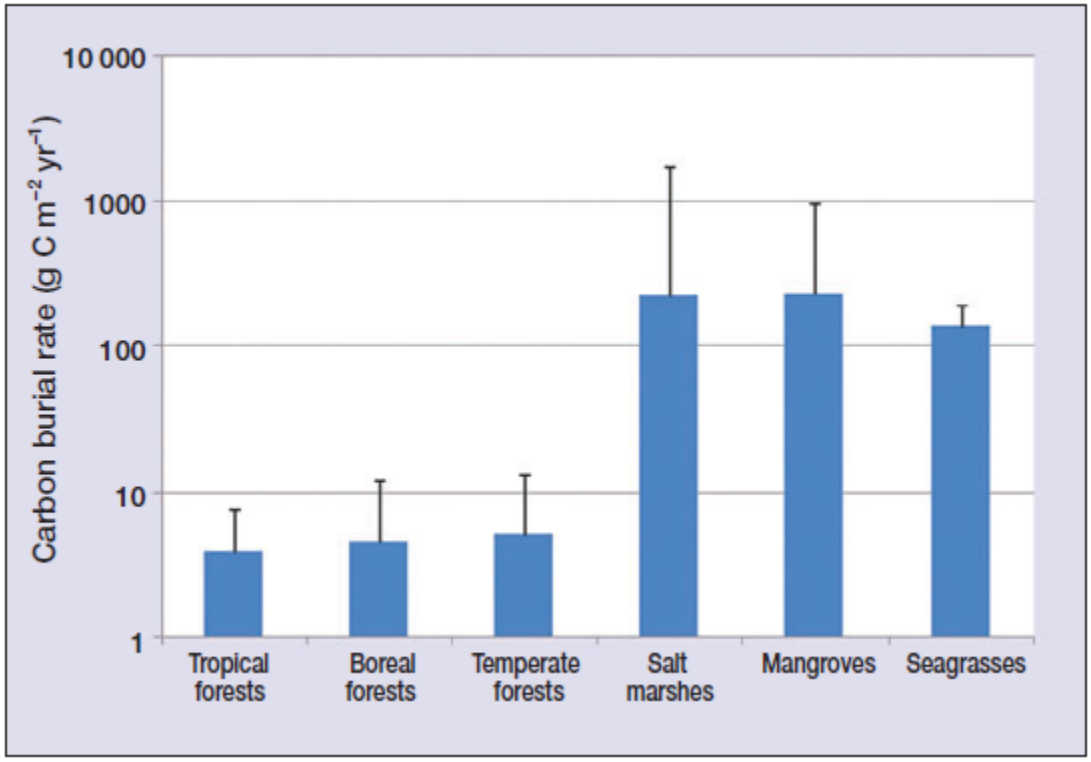

Figure 1. Mean long-term rates of C burial (g C m^{-2} yr^{-1}) in soils of terrestrial forests and sediments of coastal vegetated ecosystems. Error bars indicate maximum rates of accumulation (from Mcleod *et al*., 2011).

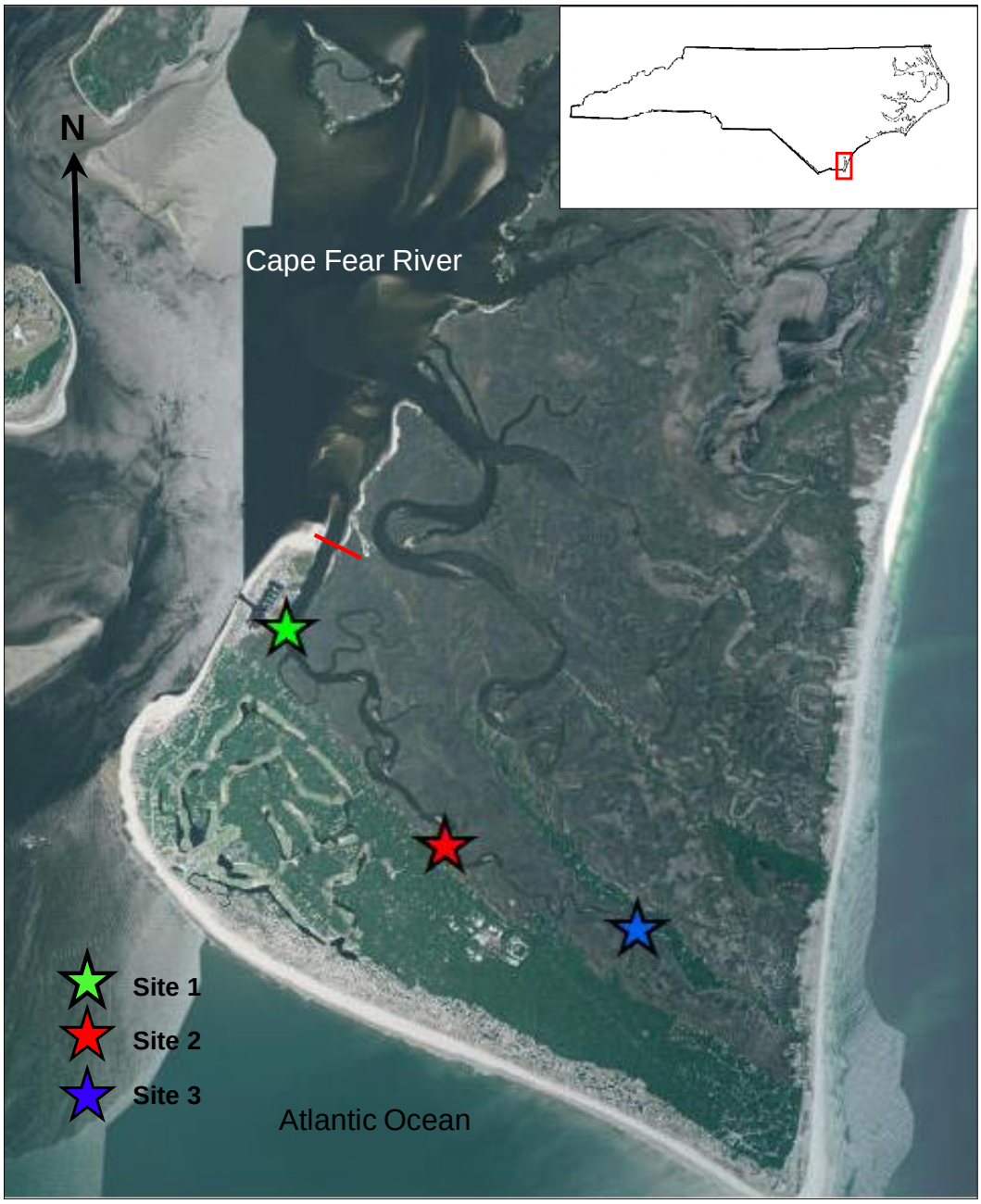

Figure 2. Satellite basemap of study site at Bald Head Creek showing locations of the three sampling sites. The red line close to the mouth of the creek represents the cross-section drawn for DOC flux and export calculations.

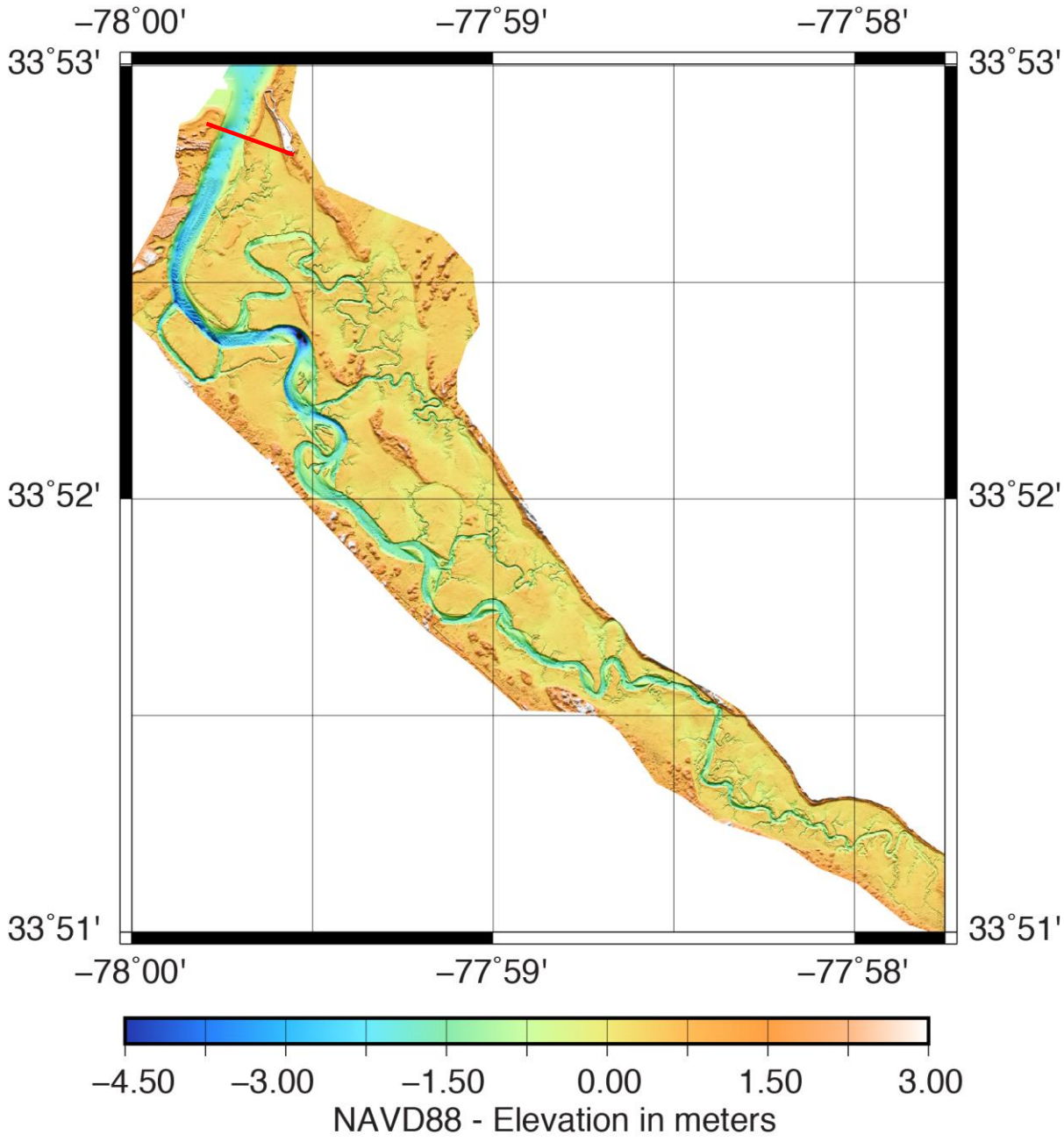

Figure 3. The digital elevation model (DEM) generated from the USV and NOAA LIDAR data (www4.ncsu.edu/~drbohnen/usv/baldhead). The red line close to the mouth of the creek represents the cross-section drawn for DOC flux and export calculations.

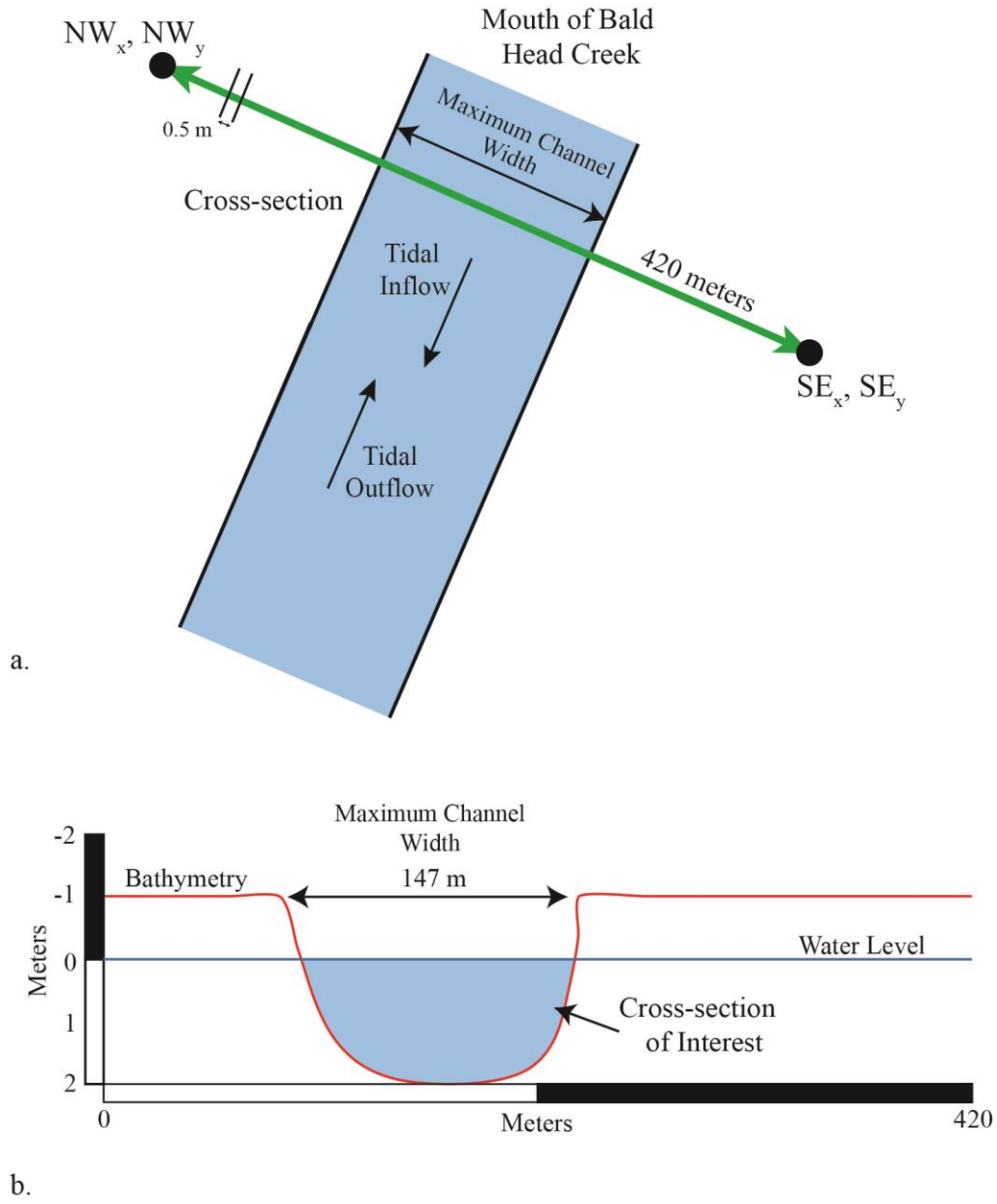

Figure 4. Diagram of the cross-section used in DOC flux and export calculations. (a) shows the cross-sectional line, 420 m long, and (b) shows the maximum channel width of 147 m and the cross-section of interest, where the channel depth was calculated as the difference between the bathymetry and water level. This channel depth at each time step multiplied by the 0.5 m spacing between each point was used to compute the cross-sectional area.

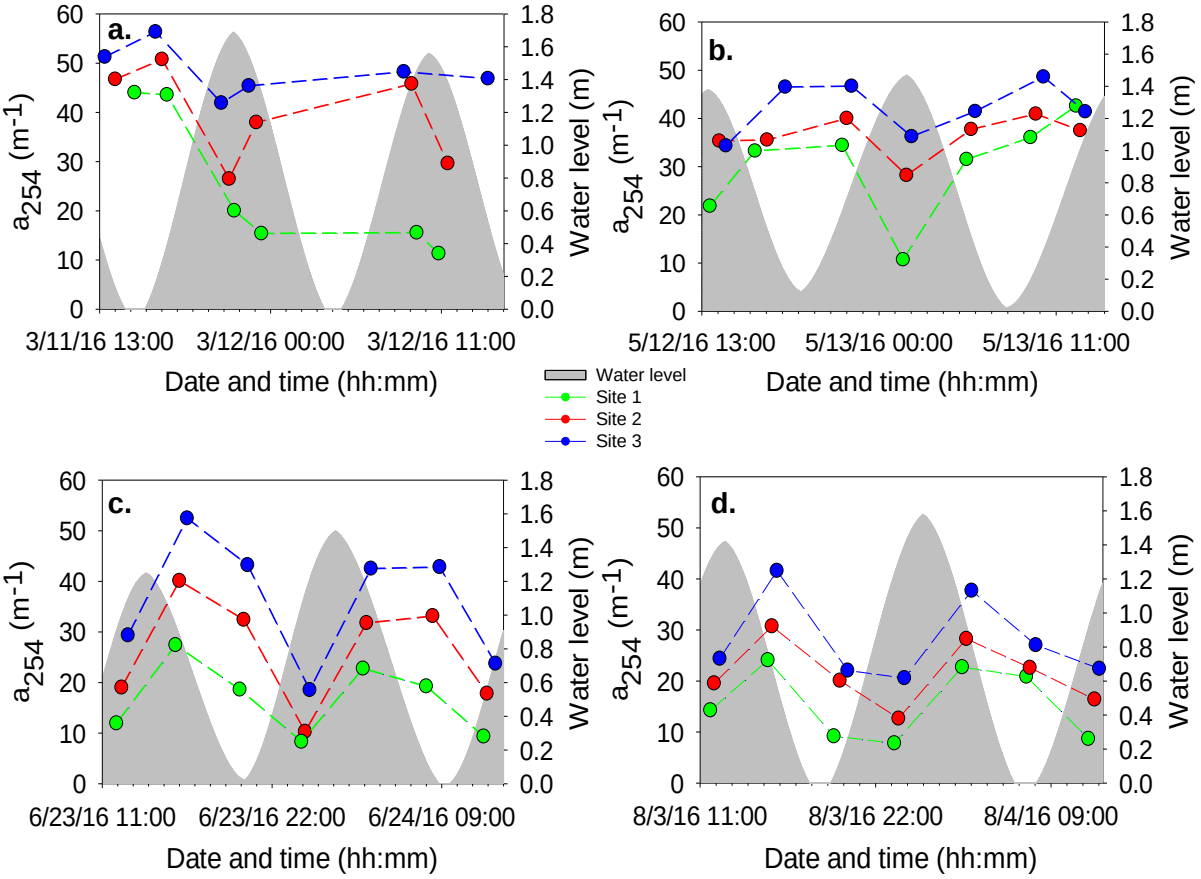

Figure 5. Tidal variability in CDOM a_{254} at the three locations along Bald Head Creek in (a) March, (b) May, (c) June, and (d) August, referenced to water levels from NOAA station 8658901 in MLLW datum. Time is shown in GMT.

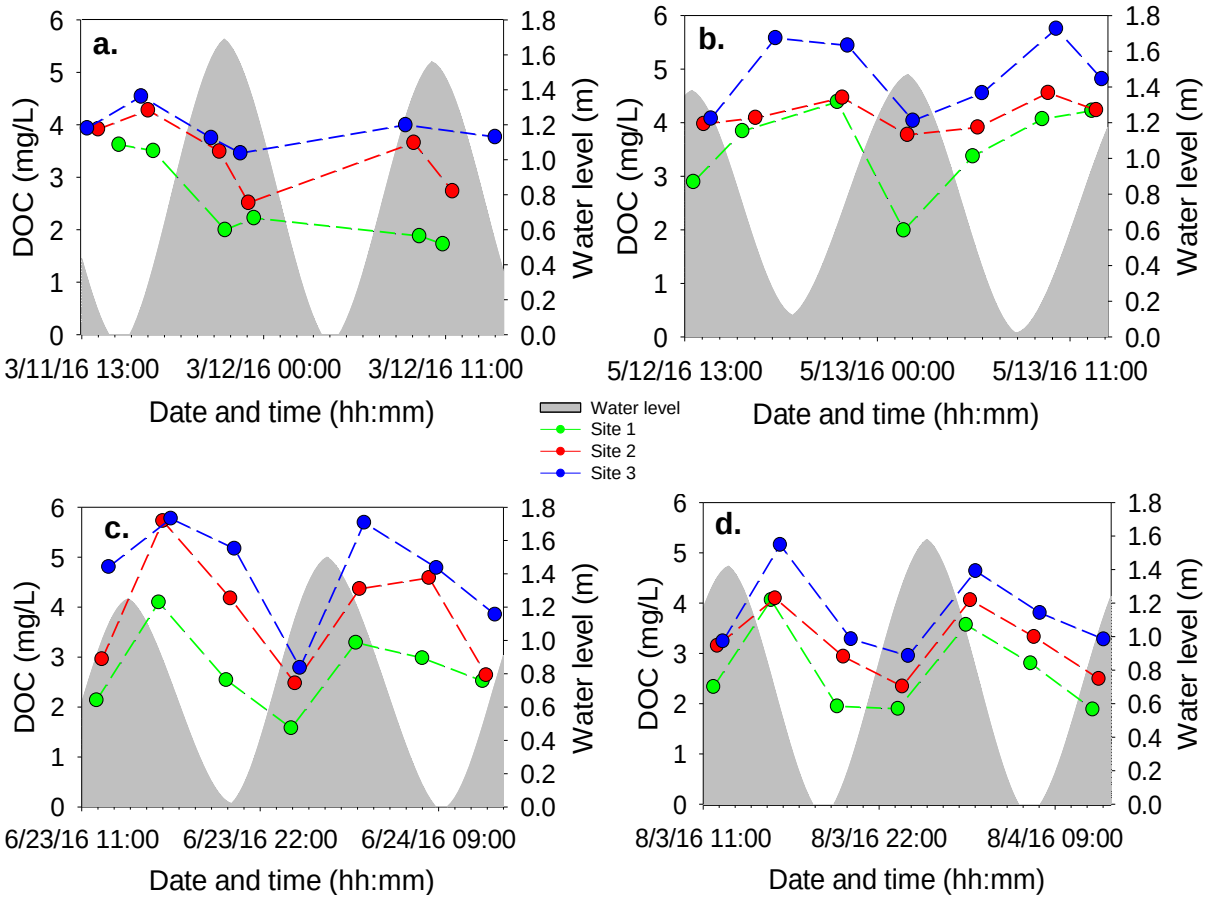

Figure 6. Tidal variability in DOC concentration at the three locations along Bald Head Creek in (a) March, (b) May, (c) June, and (d) August, referenced to water levels from NOAA station 8658901 in MLLW datum. Time is shown in GMT.

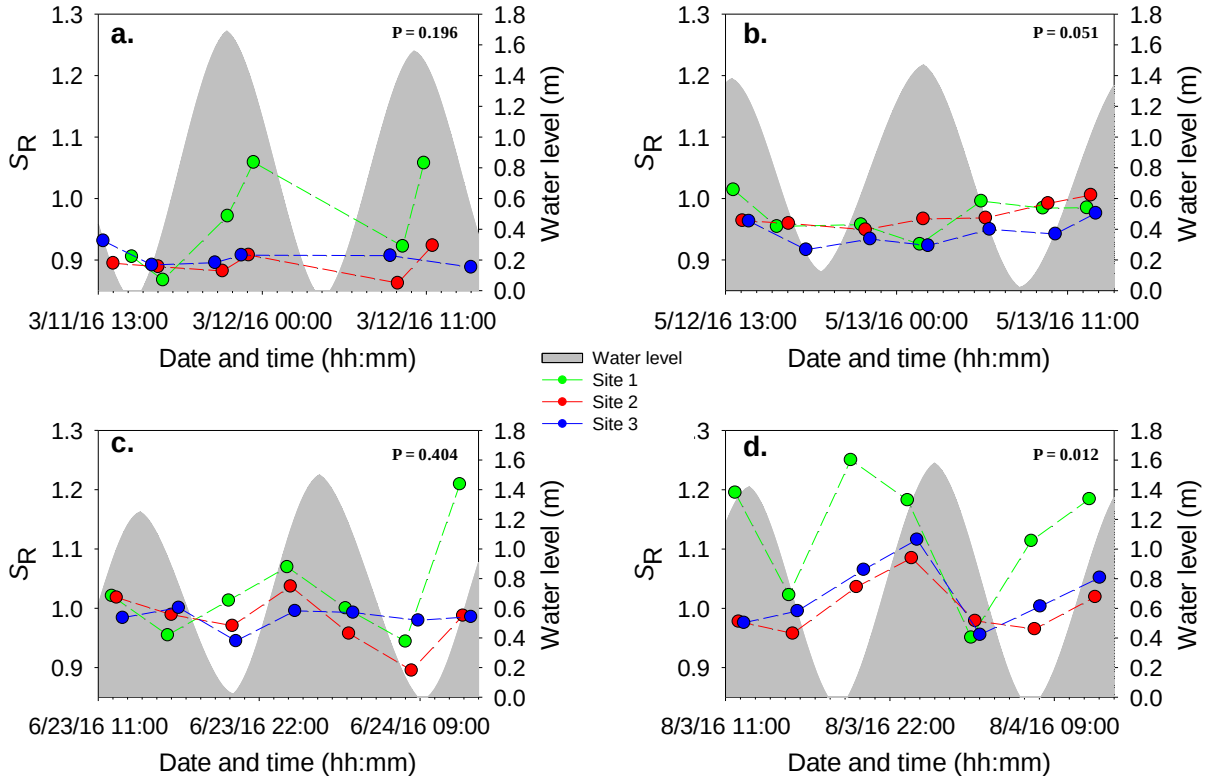

Figure 7. Tidal variability in spectral slope ratio (S_R) at the three locations along Bald Head Creek in (a) March, (b) May, (c) June, and (d) August referenced to water levels from NOAA station 8658901 in MLLW datum. Time is shown in GMT.

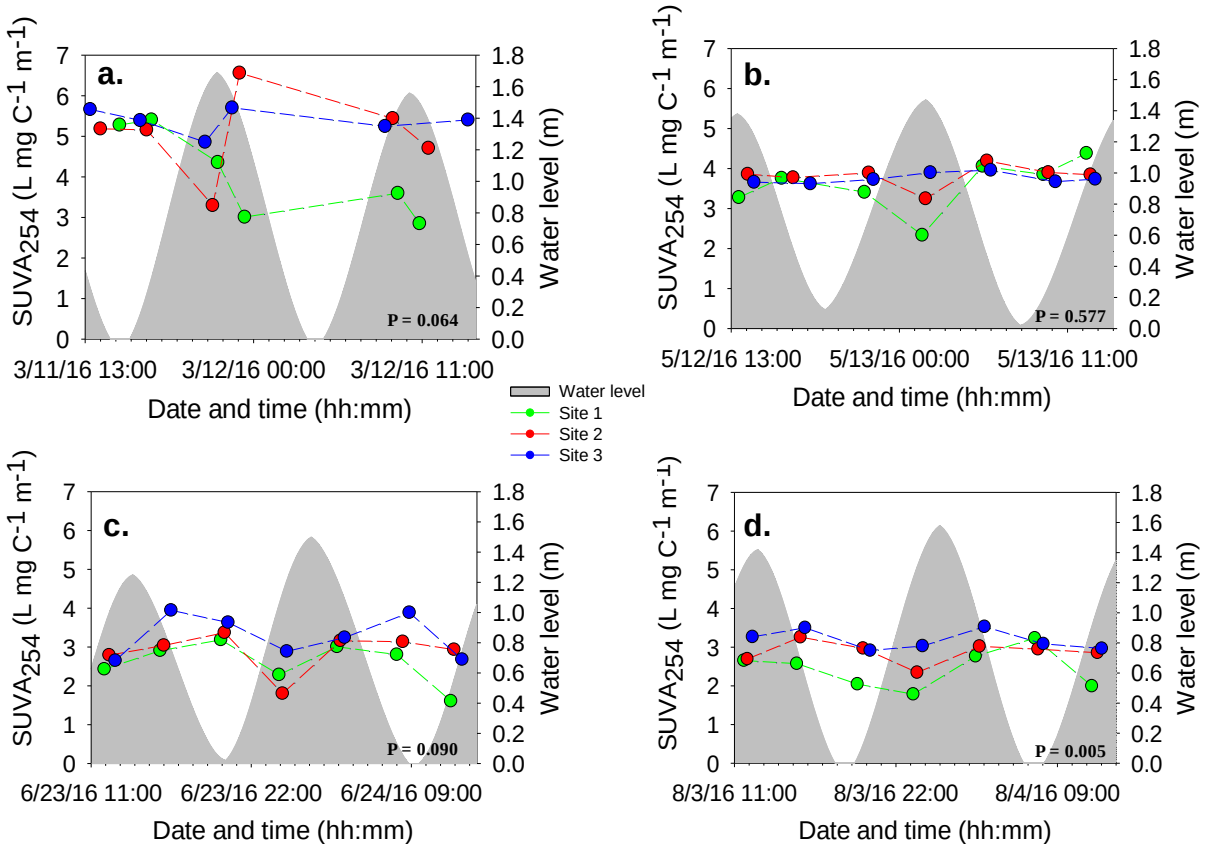

Figure 8. Tidal variability in specific UV absorbance at 254 nm ($SUVA_{254}$) at the three locations along Bald Head Creek in (a) March, (b) May, (c) June, and (d) August, referenced to water levels from NOAA station 8658901 in MLLW datum. Time is shown in GMT.

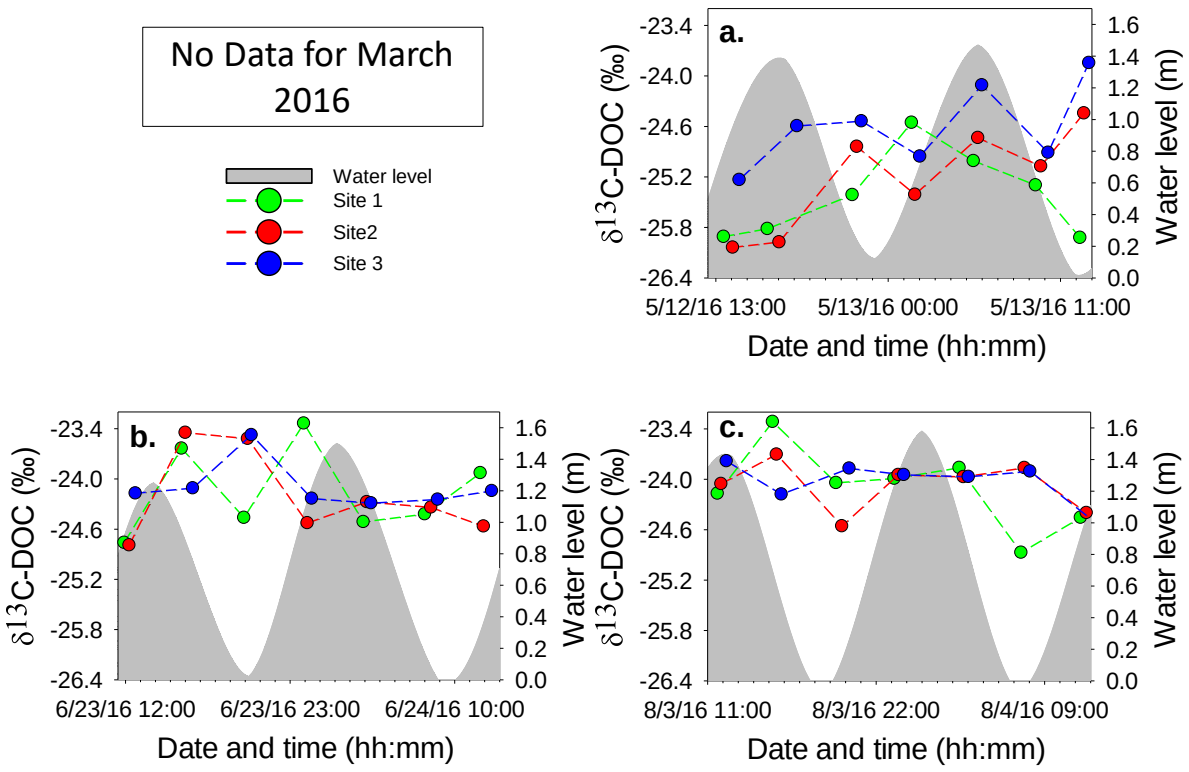

Figure 9. Tidal variability in δ^{13}C-DOC at the three locations along Bald Head Creek in (a) May, (b) June, and (c) August, referenced to NOAA station 8658901 in MLLW datum. Time is shown in GMT.

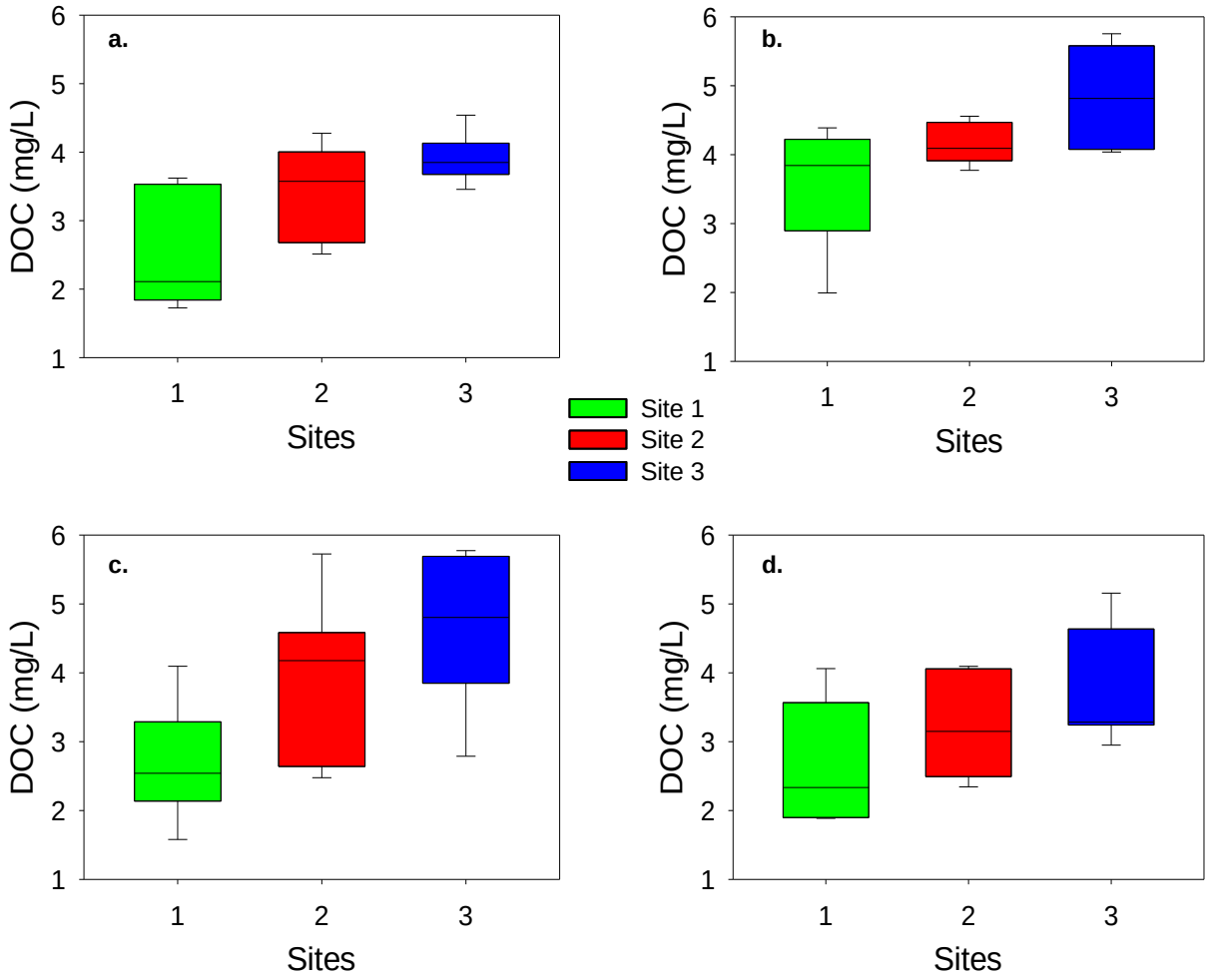

Figure 10. Spatial trend in DOC concentration along Bald Head Creek in (a) March, (b) May, (c) June, and (c) August.

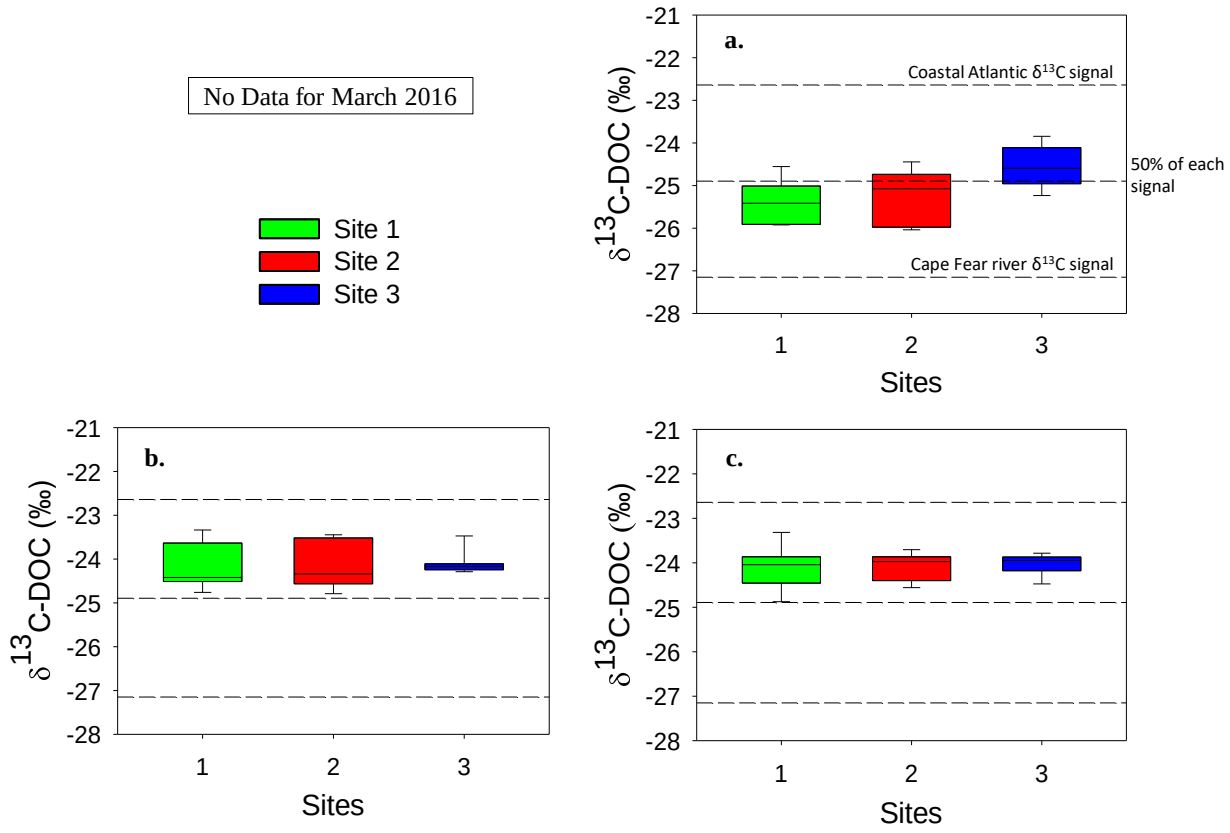

Figure 11. Spatial trend in δ^{13}C-DOC along Bald Head Creek in (a) May, (b) June, and (c) August, based on a two end-member mixing model in which a more enriched isotopic signal from the coastal Atlantic Ocean (δ^{13}C = -22.64‰) is used along with a more depleted Cape Fear River signal (δ^{13}C = -27.15‰) to establish their abundance throughout the estuary.

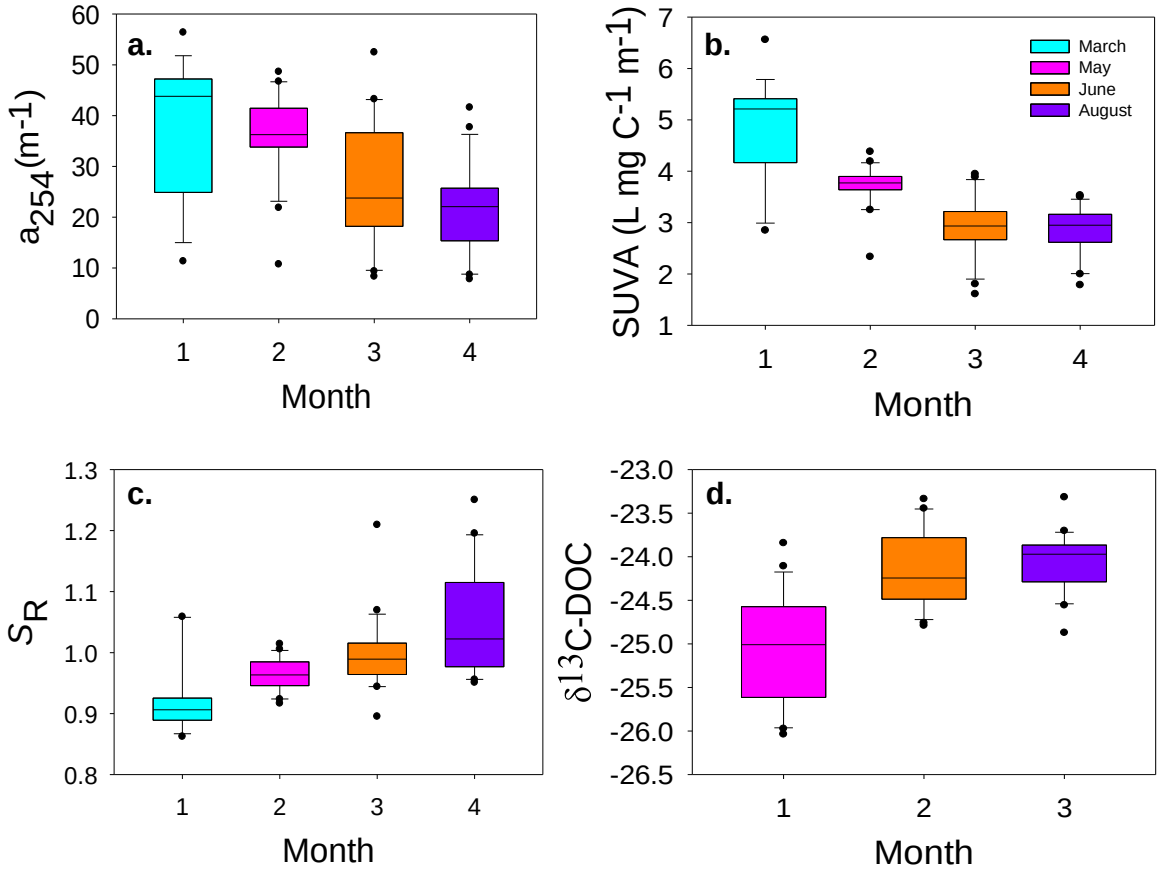

Figure 12. Temporal variability in (a) a_{254}, (b) $SUVA_{254}$, (c) S_R and (d) δ^{13}C-DOC during the spring and summer of 2016.

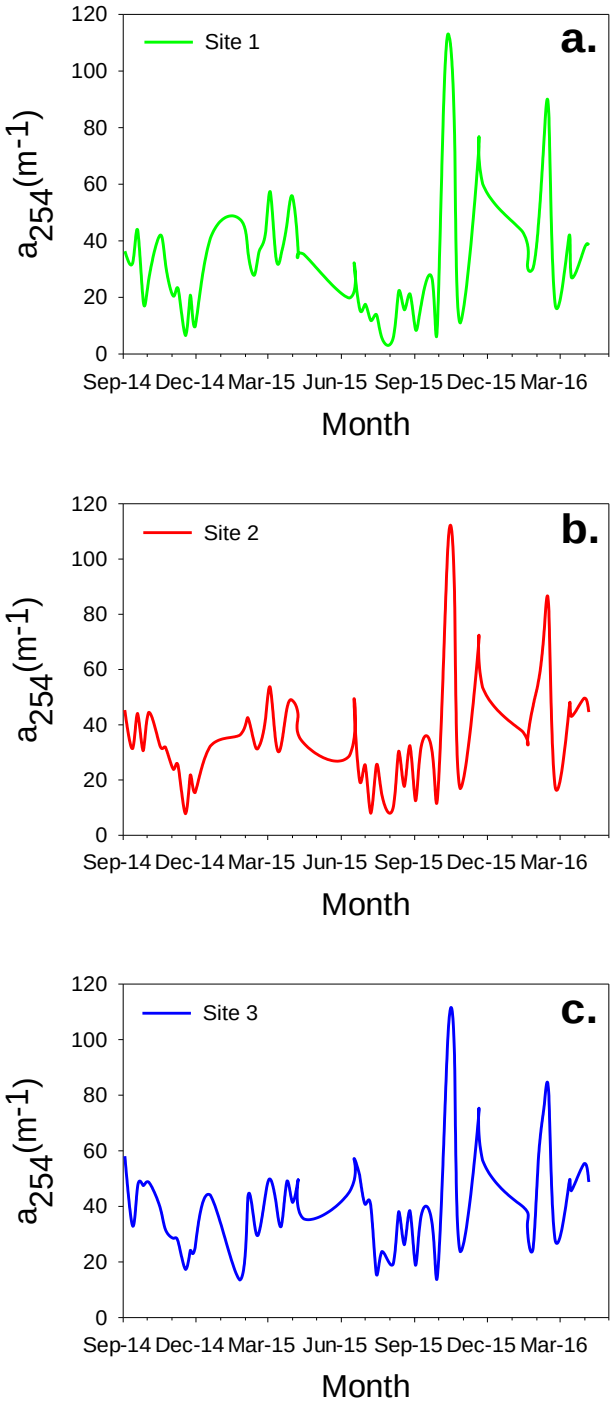

Figure 13. Time series analysis of a_{254} at (a) Site 1, (b)Site 2, and (c) Site 3 in Bald Head Creek from 2014 to 2016.

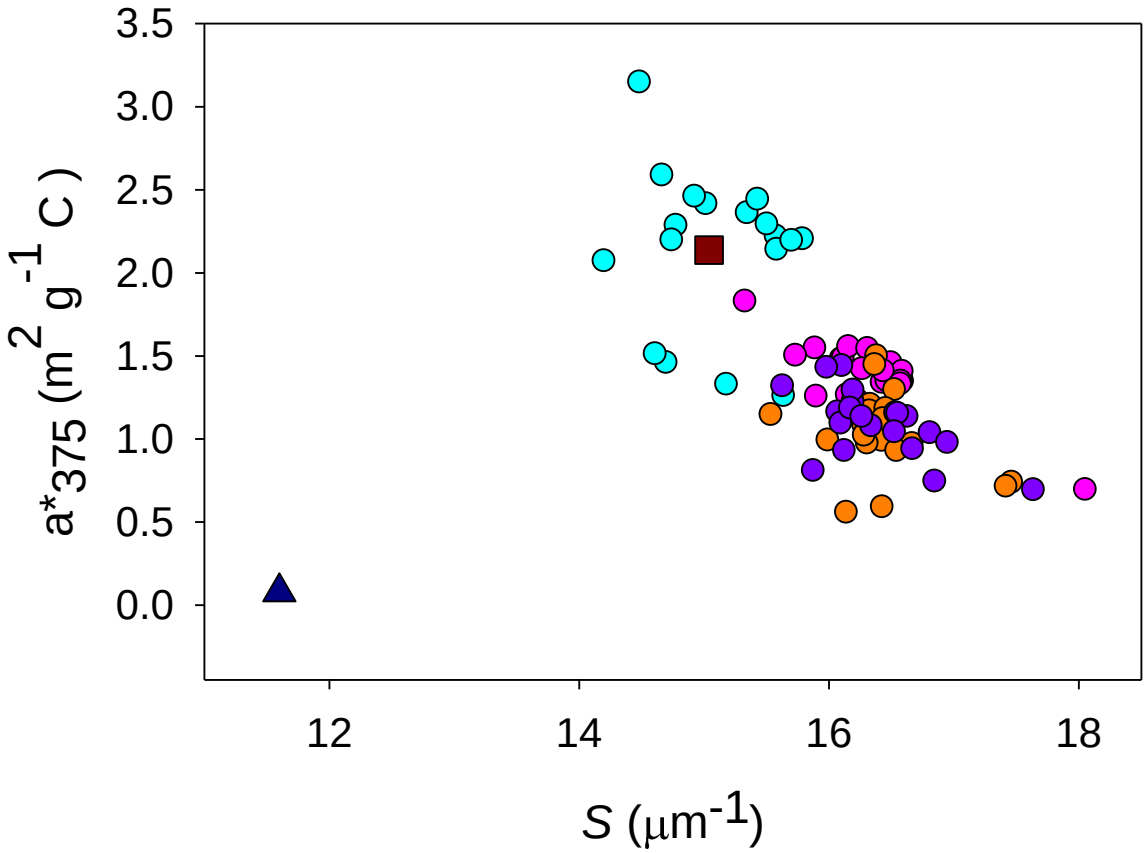

Figure 14. Specific absorption coefficient (a^*_{375}) as a function of spectral slope in Bald Head Creek during the spring and summer of 2016. Values are referenced to the CFR (S= 15.0 µm^{-1}, a^*_{375}= 2.14 m^2 g^{-1} C) and Onslow Bay, coastal Atlantic Ocean (S= 11.6 µm^{-1}, a^*_{375}= 0.08 m^2 g^{-1} C).

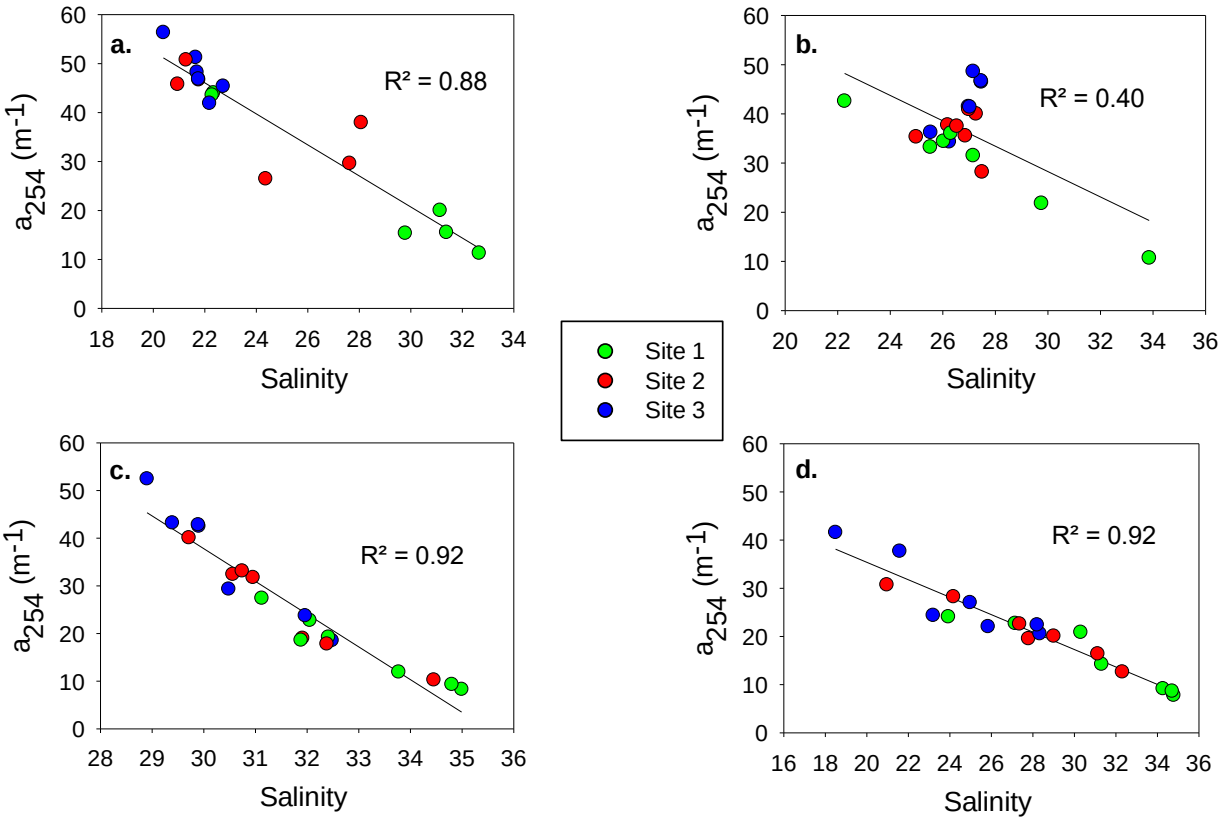

Figure 15. Linear regressions between a_{254} and salinity in Bald Head Creek in (a) March, (b) May, (c) June and (d) August (Coefficients resulting from the regression analyses are shown in Table 9).

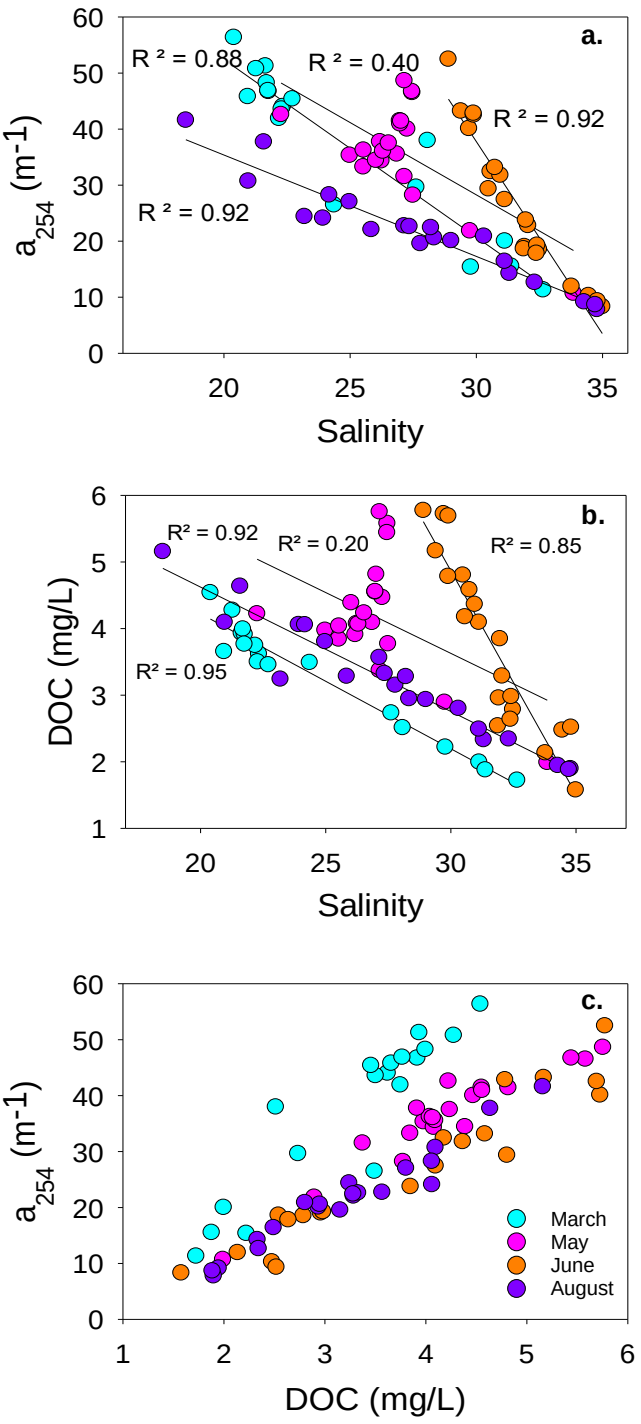

Figure 16. Correlation between (a) a_{254} and salinity, (b) DOC concentration and salinity and (c) a_{254} and DOC concentration in Bald Head Creek during the spring and summer of 2016.

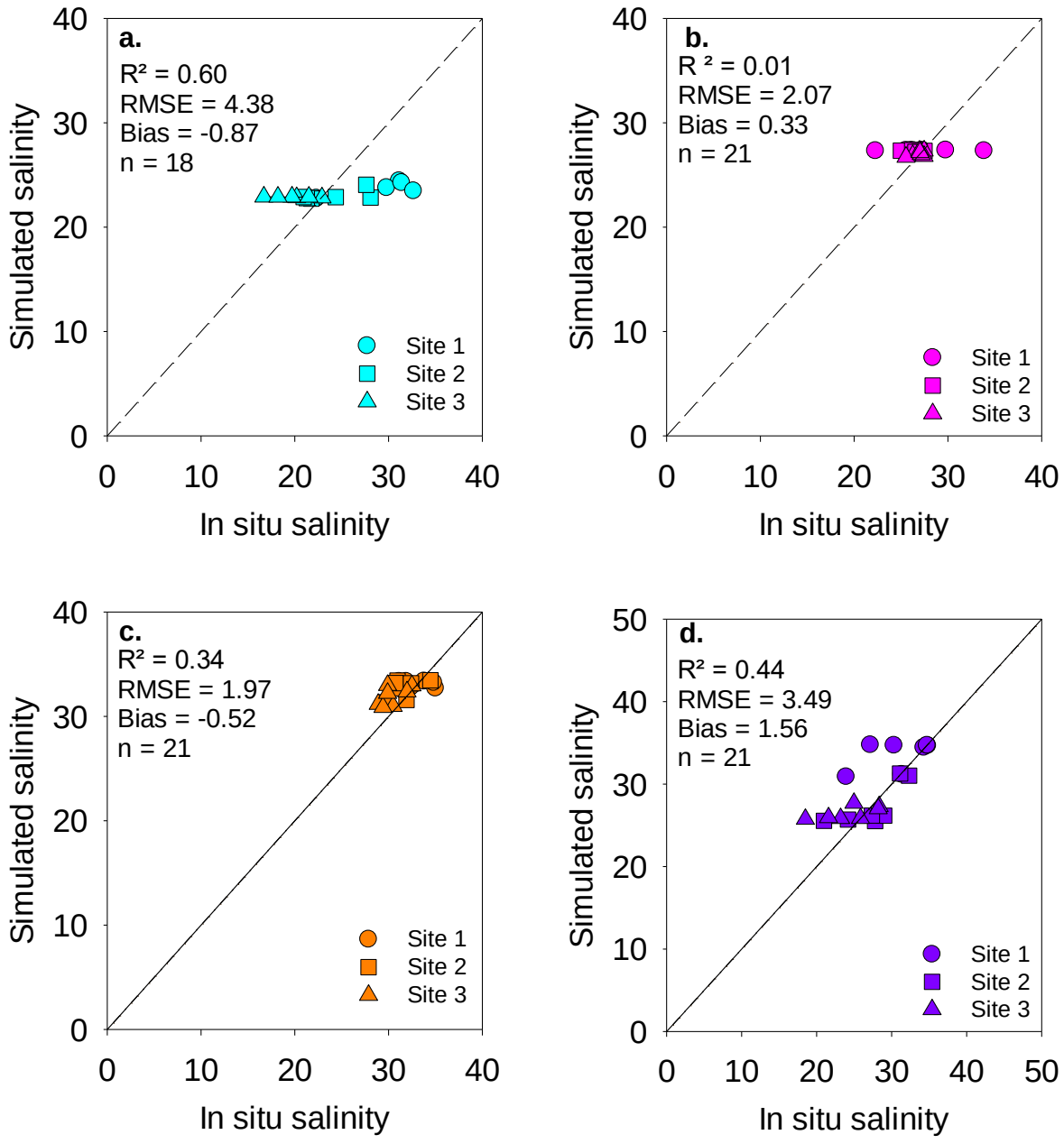

Figure 17. Match-up comparisons between in situ salinity and model-simulated salinity along the 1:1 line for (a) March, (b) May, (c) June and (d) August at the three different sites along Bald Head Creek.

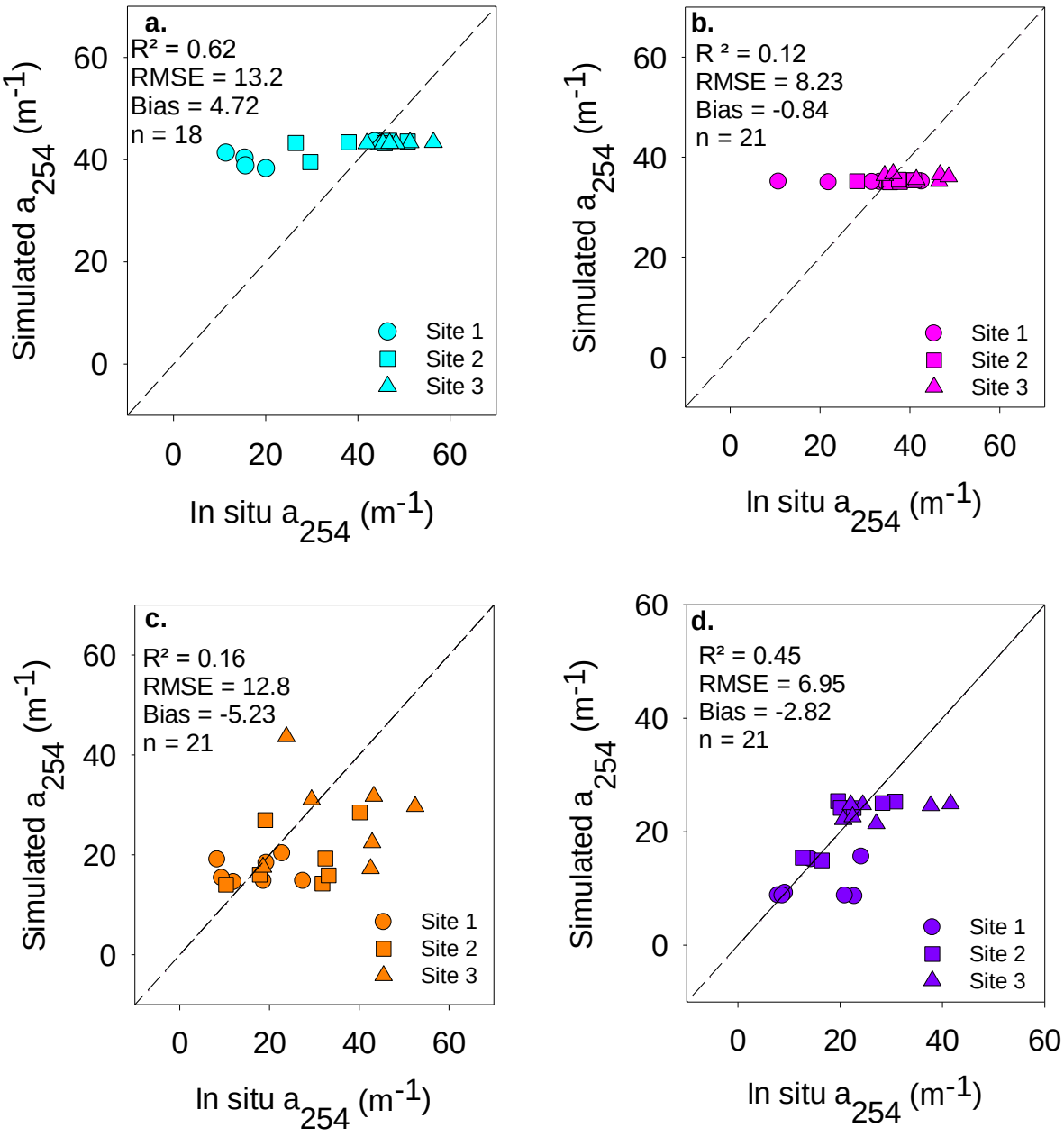

Figure 18. Match-up comparisons between in situ a_{254} and model-simulated a_{254} along the 1:1 line for (a) March, (b) May, (c) June and (d) August at the three different sites along Bald Head Creek.

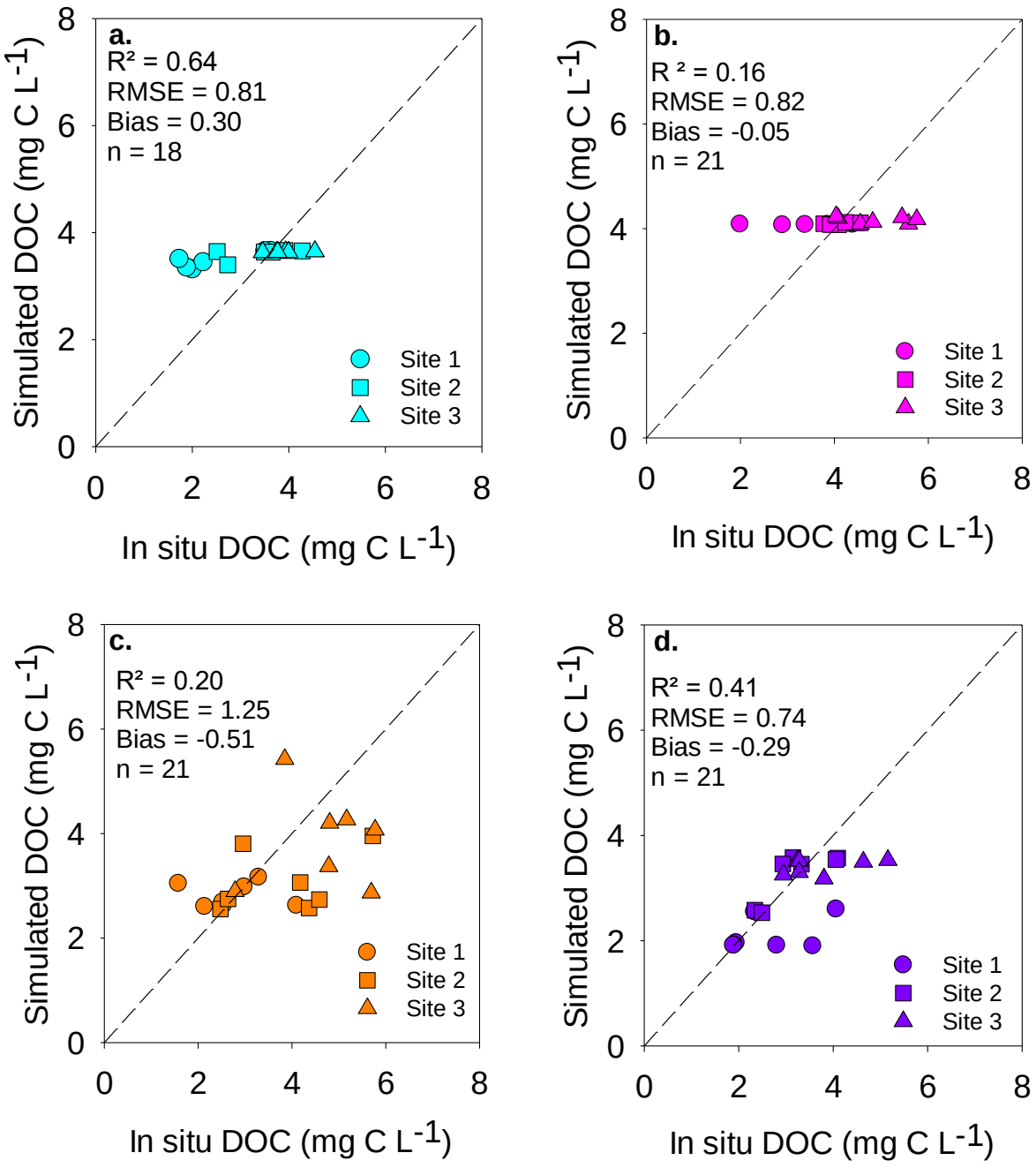

Figure 19. Match-up comparisons between in situ DOC concentration and model-simulated DOC concentration along the 1:1 line for (a) March, (b) May, (c) June and (d) August at the three different sites along Bald Head Creek.

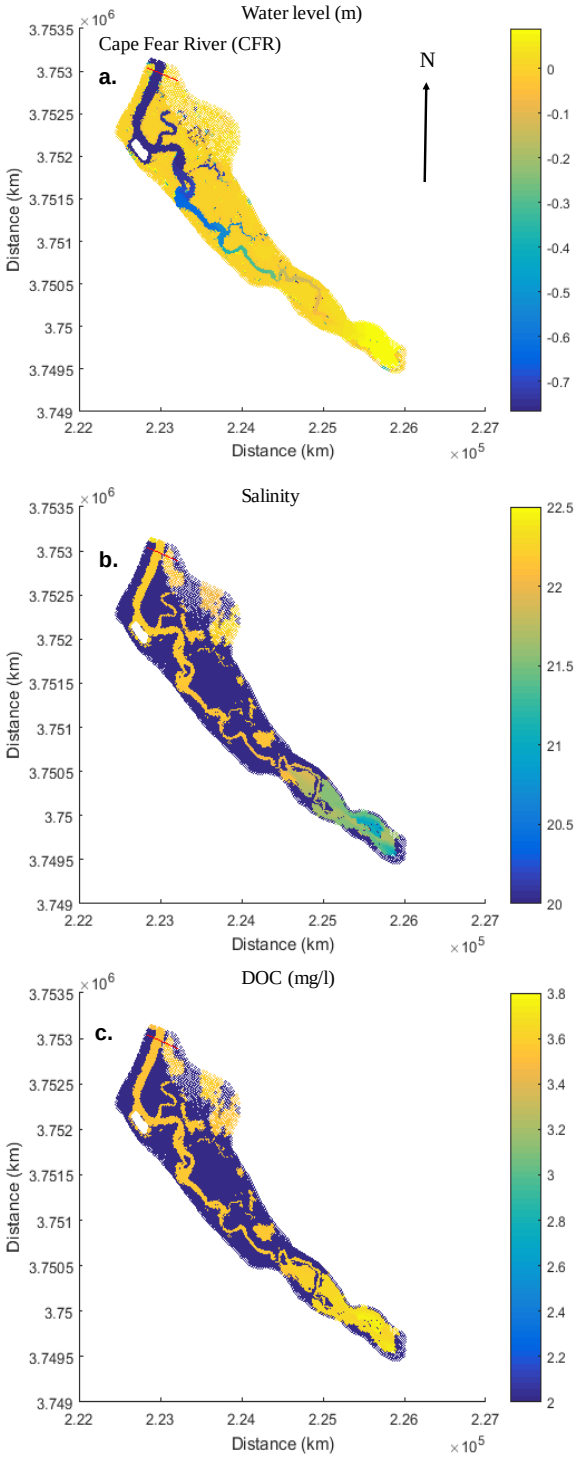

Figure 20. Model-derived (a) water level, (b) salinity, and (c) DOC concentration in Bald Head Creek at low tide in March (time, t=55).

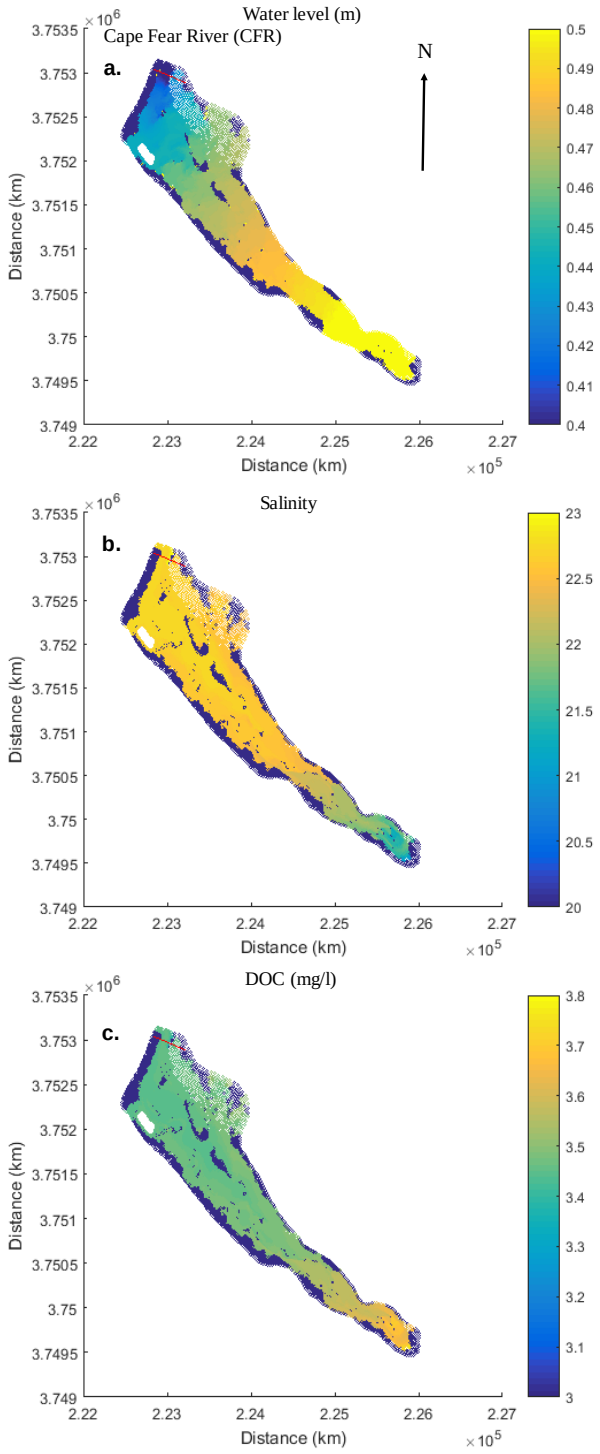

Figure 21. Model-derived (a) water level, (b) salinity, and (c) DOC concentration in Bald Head Creek at high tide in March (time, t=64).

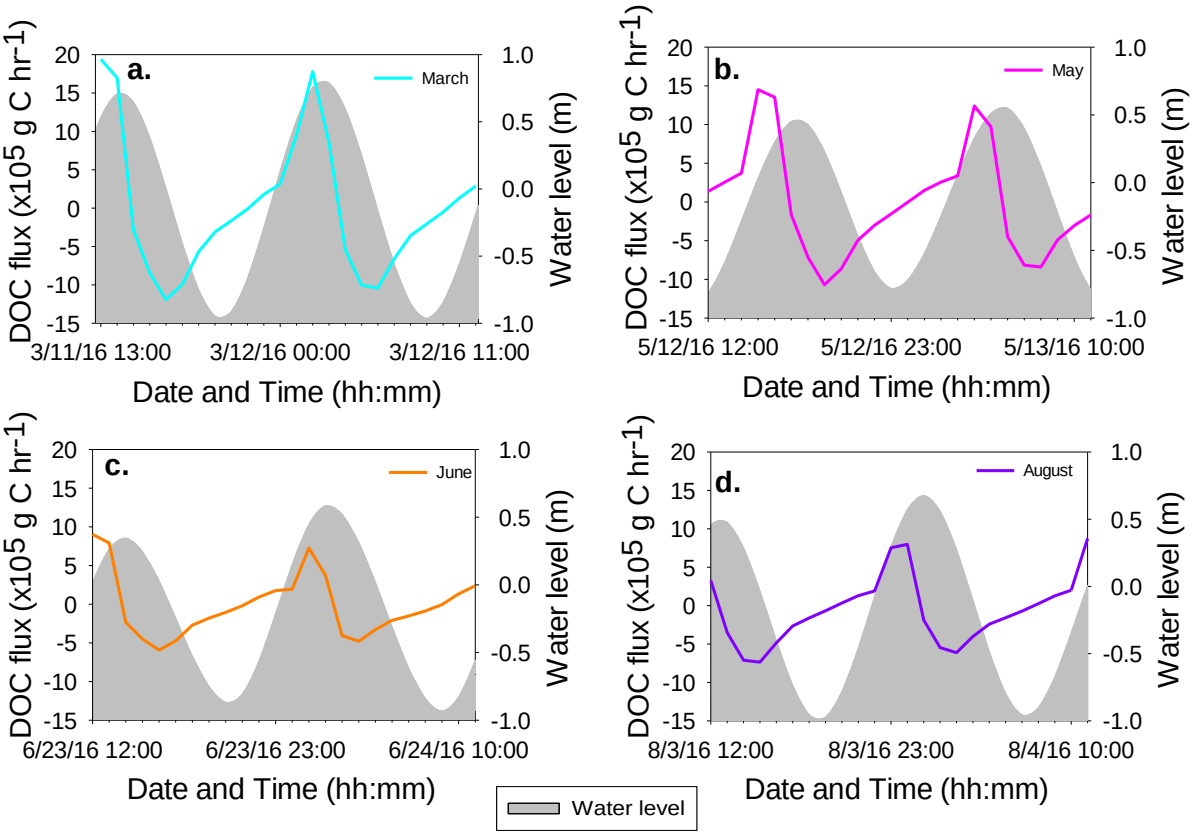

Figure 22. Tidal variability in hourly DOC flux in Bald Head Creek for (a) March, (b) May, (c) June and (d) August, referenced to water levels from NOAA station 8658901 in MSL datum. Time is shown in GMT.

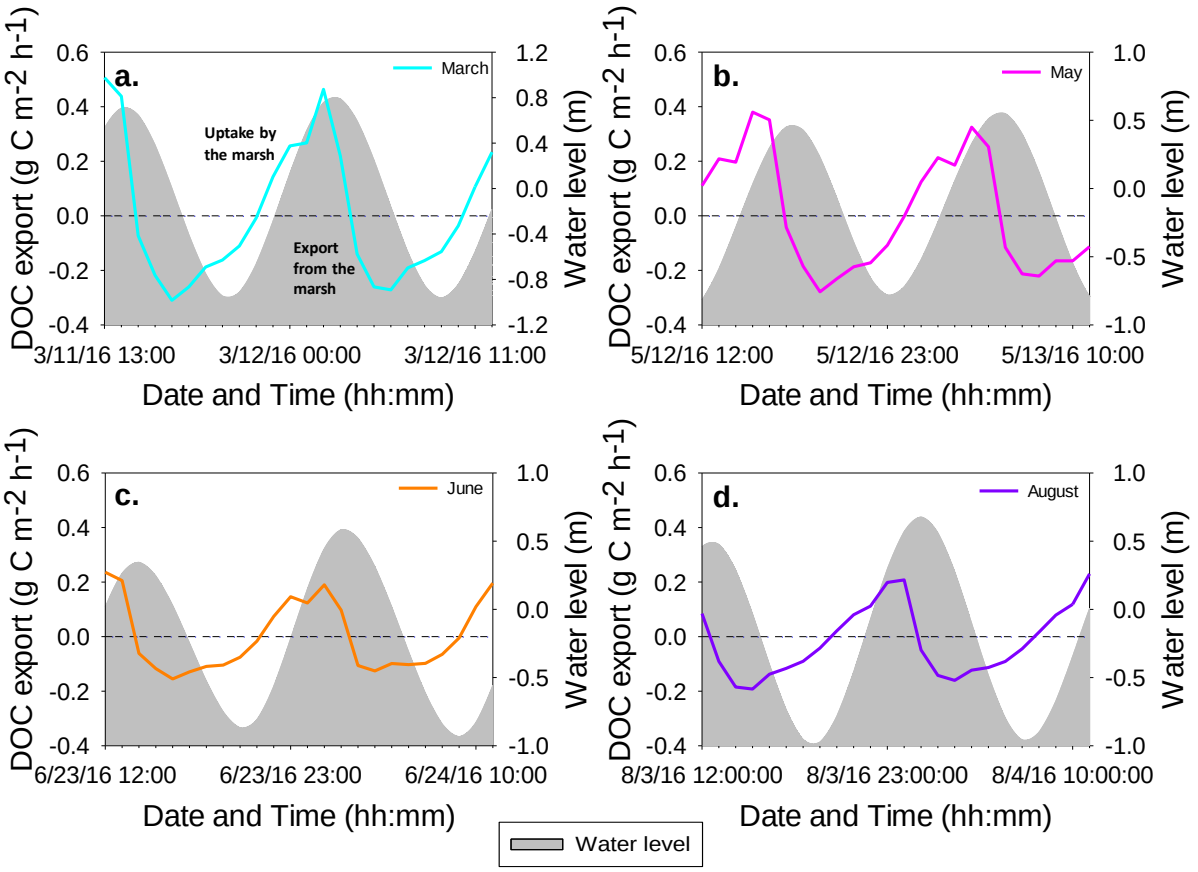

Figure 23. Tidal variability in hourly DOC export in Bald Head Creek for (a) March, (b) May, (c) June and (d) August, referenced to water levels from NOAA station 8658901 in MSL datum. Time is shown in GMT. The dashed line is a reference line at 0 where no net import or export occurs. Above the dashed line represents import/uptake by the marsh while below the dashed line represents export from the marsh, where negative values mean export out of the marsh to the Cape Fear River.

REFERENCES

Aiken G.R. (2014). Dissolved organic matter in aquatic systems. Comprehensive Water Quality and Purification. *Elsevier*. 205-220.

Anderson, N., & Stedmon, C. A. (2007). The effect of evapoconcentration on dissolved organic carbon concentration and quality in lakes of SW Greenland. *Freshwater Biology*, *52*(2), 280-289.

Asjes, J., & Dankers, N. M. J. A. (1995). Variations in tidal exchange processes between a Dutch salt marsh, the Slufter, and the North Sea. *Oceanographic Literature Review*, *9*(42), 734.

Aquaveo, LLC. (2016). SMS: Mesh Generation. Retrieved from http://www.xmswiki.com/wiki/SMS:Mesh_Generation.

Axelrad, D. M., Moore, K. A., & Bender, M. E. (1976). Nitrogen, phosphorus, and carbon flux in Chesapeake Bay marshes. Blacksburg: Virginia Water Resources Research Center, Virginia Polytechnic Institute and State University.

Bald Head Island Conservancy (BHIC). (2016) Retrieved from https://www.bhic.org/salt-marsh/.

Battin, T. J., Kaplan, L. A., Findlay, S., Hopkinson, C. S., Marti, E., Packman, A. I., Newbold, J.D., & Sabater, F. (2008). Biophysical controls on organic carbon fluxes in fluvial networks. *Nature Geoscience*, *1*(2), 95-100.

Bauer, J. E., & Bianchi, T. S. (2011). Dissolved organic carbon cycling and transformation. In *Treatise on Estuarine and Coastal Science* (pp 7-67). Waltham: Academic Press.

Bauer, J. E., Cai, W. J., Raymond, P. A., Bianchi, T. S., Hopkinson, C. S., & Regnier, P. A. (2013). The changing carbon cycle of the coastal ocean. *Nature*, *504*(7478), 61-70.

Becker, M. L., Luettich, R. A., & Mallin, M. A. (2010). Hydrodynamic behavior of the Cape Fear River and estuarine system: A synthesis and observational investigation of discharge–salinity intrusion relationships. *Estuarine, Coastal and Shelf Science*, *88*(3), 407-418.

Bianchi, T. S. (2011). *Biogeochemistry of Estuaries*. Oxford University Press.

Binding, C. E., & Bowers, D. G. (2003). Measuring the salinity of the Clyde Sea from remotely sensed ocean colour. *Estuarine, Coastal and Shelf Science*, *57*(4), 605-611.

Bittar, T. B., Berger, S. A., Birsa, L. M., Walters, T. L., Thompson, M. E., Spencer, R. G. M., Mann, E. L., Stubbins, A., Frischer, M. E., & Brandes, J. A. (2016). Seasonal dynamics of dissolved, particulate and microbial components of a tidal saltmarsh-dominated estuary under contrasting levels of freshwater discharge. *Estuarine, Coastal and Shelf Science*, *182*, 72-85.

Blough, N. V., & Del Vecchio, R. (2002). Chromophoric DOM in the Coastal Environment. In *Biogeochemistry of Marine Dissolved Organic Matter* (pp 509-532). Elsevier Science.

Borey, R. B., Harcombe, P. A., & Fisher, F. M. (1983). Water and organic carbon fluxes from an irregularly flooded brackish marsh on the upper Texas coast, USA. *Estuarine, Coastal and Shelf Science, 16*(4), 379-402.

Bouillon, S., Connolly, R. M., & Gillikin, D. P. (2011). Use of Stable Isotopes to Understand Food Webs and Ecosystem Functioning in Estuaries. In *Treatise on Estuarine and Coastal Science* (pp 143-173). Waltham: Academic Press.

Bowers, D. G., Evans, D., Thomas, D. N., Ellis, K., & Williams, P. L. B. (2004). Interpreting the colour of an estuary. *Estuarine, Coastal and Shelf Science, 59*(1), 13-20.

Boyd, T. J., & Osburn, C. L. (2004). Changes in CDOM fluorescence from allochthonous and autochthonous sources during tidal mixing and bacterial degradation in two coastal estuaries. *Marine Chemistry, 89*(1), 189-210.

Bricaud, A., Morel, A., & Prieur, L. (1981). Absorption by dissolved organic matter of the sea (yellow substance) in the UV and visible domains. *Limnology and Oceanography, 26*(1), 43-53.

Burla, M., Baptista, A. M., Zhang, Y., & Frolov, S. (2010). Seasonal and interannual variability of the Columbia River plume: A perspective enabled by multiyear simulation databases. *Journal of Geophysical Research: Oceans, 115*, C00B16, doi:10.1029/2008JC004964

Cai, W. J., & Wang, Y. (1998). The chemistry, fluxes, and sources of carbon dioxide in the estuarine waters of the Satilla and Altamaha Rivers, Georgia. *Limnology and Oceanography, 43*(4), 657-668.

Cai, W. J. (2011). Estuarine and coastal ocean carbon paradox: CO_2 sinks or sites of terrestrial carbon incineration? *Annual Review of Marine Science, 3*, 123-145.

Caress, D., & Chayes, D. N. (2010). MB-System Version 5.2, Open source software distributed from the MBARI and L-DEO. Retrieved from http://www.mbari.org/data/mbsystems.

Cawley, K. M., Yamashita, Y., Maie, N., & Jaffé, R. (2014). Using optical properties to quantify fringe mangrove inputs to the dissolved organic matter (DOM) pool in a subtropical estuary. *Estuaries and Coasts, 37*(2), 399-410.

Chaichitehrani, N., D'sa, E. J., Ko, D. S., Walker, N. D., Osburn, C. L., & Chen, R. F. (2014). Colored dissolved organic matter dynamics in the Northern Gulf of Mexico from ocean color and numerical model results. *Journal of Coastal Research, 30*(4), 800-814.

Chalmers, A. G., Wiegert, R. G., & Wolf, P. L. (1985). Carbon balance in a salt marsh: Interactions of diffusive export, tidal deposition and rainfall-caused erosion. *Estuarine, Coastal and Shelf Science*, *21*(6), 757-771.

Chen, R. F., & Gardner, G. B. (2004). High-resolution measurements of chromophoric dissolved organic matter in the Mississippi and Atchafalaya River plume regions. *Marine Chemistry*, *89*(1), 103-125.

Chen, Z., Li, Y., & Pan, J. (2004). Distributions of colored dissolved organic matter and dissolved organic carbon in the Pearl River Estuary, China. *Continental Shelf Research*, *24*(16), 1845-1856.

Chen, S., Huang, W., Wang, H., & Li, D. (2009). Remote sensing assessment of sediment re-suspension during Hurricane Frances in Apalachicola Bay, USA. *Remote Sensing of Environment*, *113*(12), 2670-2681.

Chen, S., Huang, W., Chen, W., & Chen, X. (2011). An enhanced MODIS remote sensing model for detecting rainfall effects on sediment plume in the coastal waters of Apalachicola Bay. *Marine Environmental Research*, *72*(5), 265-272.

Chen, M., Maie, N., Parish, K., & Jaffé, R. (2013). Spatial and temporal variability of dissolved organic matter quantity and composition in an oligotrophic subtropical coastal wetland. *Biogeochemistry*, *115*(1-3), 167-183.

Chmura, G. L., & Aharon, P. (1995). Stable carbon isotope signatures of sedimentary carbon in coastal wetlands as indicators of salinity regime. *Journal of Coastal Research*, *11*(1), 124-135.

Chmura, G. L., Anisfeld, S. C., Cahoon, D. R., & Lynch, J. C. (2003). Global carbon sequestration in tidal, saline wetland soils. *Global Biogeochemical Cycles*, *17*(4), 1111, doi:10.1029/2002GB001917

Chmura, G. L. (2009). Tidal salt marshes. In *The Management of Natural Coastal Carbon Sinks* (pp 5-12). IUCN, Gland, Switzerland.

Cifuentes, L. A., & Eldridge, P. M. (1998). A mass-and isotope-balance model of DOC mixing in estuaries. *Limnology and Oceanography*, *43*(8), 1872-1882.

Clark, C. D., Litz, L. P., & Grant, S. B. (2008). Salt marshes as a source of chromophoric dissolved organic matter (CDOM) to Southern California coastal waters. *Limnology and Oceanography*, 53(5), 1923-1933.

Coble, P. G. (2007). Marine optical biogeochemistry: the chemistry of ocean color. *Chemical Reviews*, *107*(2), 402-418.

Coffin, R. B., Fry, B., Peterson, B. J., & Wright, R. T. (1989). Carbon isotopic compositions of estuarine bacteria. *Limnology and Oceanography*, *34*(7), 1305-1310.

Cooper, A. W., & Satterthwaite, S. (1964). Smith Island and the Cape Fear Peninsula: a comprehensive report on an outstanding natural area. Wildlife Preserves. Inc, Raleigh, NC.

Craft, C. (2007). Freshwater input structures soil properties, vertical accretion, and nutrient accumulation of Georgia and US tidal marshes. *Limnology and Oceanography*, *52*(3), 1220-1230.

D'Sa, E. J., & Miller, R. L. (2003). Bio-optical properties in waters influenced by the Mississippi River during low flow conditions. *Remote Sensing of Environment*, *84*(4), 538-549.

Dame, R., Chrzanowski, T., Bildstein, K., Kjerfve, B., McKellar, H., Nelson, D., Spurrier, J. D., Stancyk, S., Stevenson, H., Vernberg, J., & Zingmark, R. (1986). The outwelling hypothesis and North inlet, South Carolina. *Marine Ecology Progress Series*, *33*(2), 7-229.

Dame, R. F., Spurrier, J. D., Williams, T. M., Kjerfve, B., Zingmark, R. G., Wolaver, T. G., Chrzanowski, T. H., McKellar, H. N., & Vernberg, F. J. (1991). Annual material processing by a salt marsh-estuarine basin in South Carolina, USA. *Marine Ecology Progress Series*, *72*(1/2), 153-166.

Deines, P. (1980). The carbon isotopic composition of diamonds: relationship to diamond shape, color, occurrence and vapor composition. *Geochimica et Cosmochimica Acta*, *44*(7), 943-961.

Del Castillo, C. E., Coble, P. G., Morell, J. M., López, J. M., & Corredor, J. E. (1999). Analysis of the optical properties of the Orinoco River plume by absorption and fluorescence spectroscopy. *Marine Chemistry*, *66*(1), 35-51.

Del Vecchio, R., & Blough, N. V. (2004). Spatial and seasonal distribution of chromophoric dissolved organic matter and dissolved organic carbon in the Middle Atlantic Bight. *Marine Chemistry*, *89*(1), 169-187.

Dittmar, T., & Stubbins, A. (2014). Dissolved organic matter in aquatic systems. *Treatise of Geochemistry*, *12*, 125-156.

Dixon, J. L., Osburn, C. L., Paerl, H. W., & Peierls, B. L. (2014). Seasonal changes in estuarine dissolved organic matter due to variable flushing time and wind-driven mixing events. *Estuarine, Coastal and Shelf Science*, *151*, 210-220.

Downing, B. D., Boss, E., Bergamaschi, B. A., Fleck, J. A., Lionberger, M. A., Ganju, N. K., & Fujii, R. (2009). Quantifying fluxes and characterizing compositional changes of dissolved organic matter in aquatic systems in situ using combined acoustic and optical measurements. *Limnology and Oceanography: Methods*, *7*(1), 119-131.

Duarte, C. M., Middelburg, J. J., & Caraco, N. (2005). Major role of marine vegetation on the oceanic carbon cycle. *Biogeosciences*, *2*(1), 1-8.

Duarte, C. M., Dennison, W. C., Orth, R. J., & Carruthers, T. J. (2008). The charisma of coastal ecosystems: addressing the imbalance. *Estuaries and Coasts*, *31*(2), 233-238.

Fagherazzi, S., Wiberg, P. L., Temmerman, S., Struyf, E., Zhao, Y., & Raymond, P. A. (2013). Fluxes of water, sediments, and biogeochemical compounds in salt marshes. *Ecological Processes*, *2*(1), 1-16.

Ferrari, G. M., Dowell, M. D., Grossi, S., & Targa, C. (1996). Relationship between the optical properties of chromophoric dissolved organic matter and total concentration of dissolved organic carbon in the southern Baltic Sea region. *Marine Chemistry*, *55*(3-4), 299-316.

Fichot, C. G., & Benner, R. (2011). A novel method to estimate DOC concentrations from CDOM absorption coefficients in coastal waters. *Geophysical Research Letters*, *38*, L03610, doi:10.1029/2010GL046152

Frankignoulle, M., Bourge, I., & Wollast, R. (1996). Atmospheric CO2 fluxes in a highly polluted estuary (the Scheldt). *Limnology and Oceanography*, *41*(2), 365-369.

Fry B., & Sherr E.B. (1989). $\delta^{13}C$ measurements as Iindicators of carbon flow in marine and freshwater ecosystems. In *Stable Isotopes in Ecological Research* (pp 196-229). Springer, New York.

Gardner, G. B., Chen, R. F., & Berry, A. (2005). High-resolution measurements of chromophoric dissolved organic matter (CDOM) in the Neponset River Estuary, Boston Harbor, MA. *Marine Chemistry*, *96*(1), 137-154.

Gordon, E. S., & Goñi, M. A. (2003). Sources and distribution of terrigenous organic matter delivered by the Atchafalaya River to sediments in the northern Gulf of Mexico. *Geochimica et Cosmochimica Acta*, *67*(13), 2359-2375.

Granskog, M. A. (2012). Changes in spectral slopes of colored dissolved organic matter absorption with mixing and removal in a terrestrially dominated marine system (Hudson Bay, Canada). *Marine Chemistry*, *134*, 10-17.

Green, S. A., & Blough, N. V. (1994). Optical absorption and fluorescence properties of chromophoric dissolved organic matter in natural waters. *Limnology and Oceanography*, *39*(8), 1903-1916.

Guo, H., Noormets, A., Zhao, B., Chen, J., Sun, G., Gu, Y., & Chen, J. (2009). Tidal effects on net ecosystem exchange of carbon in an estuarine wetland. *Agricultural and Forest Meteorology*, *149*(11), 1820-1828.

Guo, W., Yang, L., Hong, H., Stedmon, C. A., Wang, F., Xu, J., & Xie, Y. (2011). Assessing the dynamics of chromophoric dissolved organic matter in a subtropical estuary using parallel factor analysis. *Marine Chemistry*, *124*(1), 125-133.

Hansell, D. A., & Carlson, C. A. (Eds.). (2014). *Biogeochemistry of Marine Dissolved Organic Matter*. Academic Press, Cambridge, Massachusetts.

Harvey, E. T., Kratzer, S., & Andersson, A. (2015). Relationships between colored dissolved organic matter and dissolved organic carbon in different coastal gradients of the Baltic Sea. Ambio, *44*(3), 392-401.

Hedges, J. I., & Keil, R. G. (1999). Organic geochemical perspectives on estuarine processes: sorption reactions and consequences. *Marine Chemistry*, *65*(1), 55-65.

Hedges, J. I. (2002). Why dissolved organics matter. In *Biogeochemistry of Marine Dissolved Organic Matter* (pp 1-33). Elsevier Science.

Helms, J. R., Stubbins, A., Ritchie, J. D., Minor, E. C., Kieber, D. J., & Mopper, K. (2008). Absorption spectral slopes and slope ratios as indicators of molecular weight, source, and photobleaching of chromophoric dissolved organic matter. *Limnology and Oceanography*, *53*(3), 955-969.

Hemminga, M. A., Klap, V. A., Van Soelen, J., & Boon, J. J. (1993). Effect of salt marsh inundation on estuarine particulate organic matter characteristics. *Marine Ecology Progress Series*, *99*, 153-161.

Hopkinson, C. S. (1988). Patterns of organic carbon exchange between coastal ecosystems the mass balance approach in salt marsh ecosystems. In *Coastal-Offshore Ecosystem Interactions* (pp 122-154), Springer-Verlag, Berlin Heidelberg.

Hopkinson, C. S., Cai, W. J., & Hu, X. (2012). Carbon sequestration in wetland dominated coastal systems-a global sink of rapidly diminishing magnitude. *Current Opinion in Environmental Sustainability*, *4*(2), 186-194.

Jaffé, R., Boyer, J. N., Lu, X., Maie, N., Yang, C., Scully, N. M., & Mock, S. (2004). Source characterization of dissolved organic matter in a subtropical mangrove-dominated estuary by fluorescence analysis. *Marine Chemistry, 84*(3), 195-210.

Jaffé, R., McKnight, D., Maie, N., Cory, R., McDowell, W. H., & Campbell, J. L. (2008). Spatial and temporal variations in DOM composition in ecosystems: The importance of long-term monitoring of optical properties. *Journal of Geophysical Research: Biogeosciences*, *113*, G04032, doi:10.1029/2008JG000683.

Jordan, T. E., Correll, D. L., & Whigham, D. F. (1983). Nutrient flux in the Rhode River: tidal exchange of nutrients by brackish marshes. *Estuarine, Coastal and Shelf Science*, *17*(6), 651-667.

Joshi, I. D., D'Sa, E. J., Osburn, C. L., Bianchi, T. S., Ko, D. S., Oviedo-Vargas, D., Arellano, A.R., & Ward, N. D. (2017). Assessing chromophoric dissolved organic matter (CDOM) distribution, stocks, and fluxes in Apalachicola Bay using combined field, VIIRS ocean color, and model observations. *Remote Sensing of Environment*, *191*, 359-372.

Keith, D. J., Yoder, J. A., & Freeman, S. A. (2002). Spatial and temporal distribution of coloured dissolved organic matter (CDOM) in Narragansett Bay, Rhode Island: implications for phytoplankton in coastal waters. *Estuarine, Coastal and Shelf Science*, *55*(5), 705-717.

Kowalczuk, P., Cooper, W. J., Whitehead, R. F., Durako, M. J., & Sheldon, W. (2003). Characterization of CDOM in an organic-rich river and surrounding coastal ocean in the South Atlantic Bight. *Aquatic Sciences*, *65*(4), 384-401.

Kowalczuk, P., Stedmon, C. A., & Markager, S. (2006). Modeling absorption by CDOM in the Baltic Sea from season, salinity and chlorophyll. *Marine Chemistry*, *101*(1), 1-11.

Kowalczuk, P., Durako, M. J., Young, H., Kahn, A. E., Cooper, W. J., & Gonsior, M. (2009). Characterization of dissolved organic matter fluorescence in the South Atlantic Bight with use of PARAFAC model: Interannual variability. *Marine Chemistry*, *113*(3), 182-196.

Lalonde, K., Middlestead, P., & Gélinas, Y. (2014). Automation of 13C/12C ratio measurement for freshwater and seawater DOC using high temperature combustion. *Limnology and Oceanography: Methods*, *12*(12), 816-829.

Lamb, A. L., Wilson, G. P., & Leng, M. J. (2006). A review of coastal palaeoclimate and relative sea-level reconstructions using $\delta^{13}C$ and C/N ratios in organic material. *Earth-Science Reviews*, *75*(1), 29-57.

Lawaetz, A. J., & Stedmon, C. A. (2009). Fluorescence intensity calibration using the Raman scatter peak of water. *Applied Spectroscopy*, *63*(8), 936-940.

Leonard, L. A., & Luther, M. E. (1995). Flow hydrodynamics in tidal marsh canopies. *Limnology and Oceanography*, *40*(8), 1474-1484.

Loomis, M. J., & Craft, C. B. (2010). Carbon sequestration and nutrient (nitrogen, phosphorus) accumulation in river-dominated tidal marshes, Georgia, USA. *Soil Science Society of America Journal*, *74*(3), 1028-1036.

Macreadie, P. I., Hughes, A. R., & Kimbro, D. L. (2013). Loss of 'blue carbon' from coastal salt marshes following habitat disturbance. PloS ONE, 8(7): e69244. doi: 10.1371/journal.pone.0069244.

Maie, N., Sekiguchi, S., Watanabe, A., Tsutsuki, K., Yamashita, Y., Melling, L., Cawley, K. M., Shima, E., & Jaffé, R. (2014). Dissolved organic matter dynamics in the oligo/meso-haline zone of wetland-influenced coastal rivers. *Journal of Sea Research*, *91*, 58-69.

Markager, S., & Vincent, W. F. (2000). Spectral light attenuation and the absorption of UV and blue light in natural waters. *Limnology and Oceanography*, *45*(3), 642-650.

McCallister, S. L., Bauer, J. E., Cherrier, J. E., & Ducklow, H. W. (2004). Assessing sources and ages of organic matter supporting river and estuarine bacterial production: A multiple-isotope ($\Delta^{14}C$, $\delta^{13}C$, and $\delta^{15}N$) approach. *Limnology and Oceanography*, *49*(5), 1687-1702.

Mcleod, E., Chmura, G. L., Bouillon, S., Salm, R., Björk, M., Duarte, C. M., Lovelock, C. E., Schlesinger, W. H., & Silliman, B. R. (2011). A blueprint for blue carbon: toward an improved understanding of the role of vegetated coastal habitats in sequestering CO_2. *Frontiers in Ecology and the Environment*, *9*(10), 552-560.

Megonigal, J. P., & Neubauer, S. C. (2009). Biogeochemistry of tidal freshwater wetlands. In *Coastal Wetlands: An Integrated Ecosystem* (pp 535-564). Elsevier, Amsterdam.

Middelburg, J.J., & Herman, P. M. (2007). Organic matter processing in tidal estuaries. *Marine Chemistry*, *106*(1), 127-147.

National Oceanic and Atmospheric Administration (NOAA) (2000). Fisheries of the United States. Fisheries Statistics & Economics, National Marine Fisheries Service. Retrieved from http://www.st.nmfs.gov/st1/fus/fus99/index.html

Nelson, N. B., Siegel, D. A., & Michaels, A. F. (1998). Seasonal dynamics of colored dissolved material in the Sargasso Sea. *Deep Sea Research Part I: Oceanographic Research Papers*, *45*(6), 931-957.

Nelson, N. B., & Siegel, D. A. (2013). The global distribution and dynamics of chromophoric dissolved organic matter. *Annual Review of Marine Science*, *5*, 447-476.

Nellemann, C., Corcoran, E., Duarte, C. M., Valdés, L., De Young, C., Fonseca, L., Grimsditch, G. (2009). *Blue Carbon. A Rapid Response Assessment.* United Nations Environment Programme, GRID-Arendal: www.grida.no.

Neubauer, S. C., Miller, W. D., & Anderson, I. C. (2000). Carbon cycling in a tidal freshwater marsh ecosystem: a carbon gas flux study. *Marine Ecology Progress Series*, *199*, 13-30.

Neubauer, S. C., & Anderson, I. C. (2003). Transport of dissolved inorganic carbon from a tidal freshwater marsh to the York River estuary. *Limnology and Oceanography*, *48*(1), 299-307.

Nicholls, R. J., Hoozemans, F. M., & Marchand, M. (1999). Increasing flood risk and wetland losses due to global sea-level rise: regional and global analyses. *Global Environmental Change*, *9*, S69-S87.

Nieke, B., Reuter, R., Heuermann, R., Wang, H., Babin, M., & Therriault, J. C. (1997). Light absorption and fluorescence properties of chromophoric dissolved organic matter (CDOM), in the St. Lawrence Estuary (Case 2 waters). *Continental Shelf Research*, *17*(3), 235-252.

Osburn, C. L., & Morris, D. P. (2003). Photochemistry of chromophoric dissolved organic matter in natural waters. *UV Effects in Aquatic Organisms and Ecosystems*, *1*, 185-217.

Osburn, C. L., & St-Jean, G. (2007). The use of wet chemical oxidation with high-amplification isotope ratio mass spectrometry (WCO-IRMS) to measure stable isotope values of dissolved organic carbon in seawater. *Limnology and Oceanography: Methods*, 5, 296-308.

Osburn, C. L., Mikan, M. P., Etheridge, J. R., Burchell, M. R., & Birgand, F. (2015). Seasonal variation in the quality of dissolved and particulate organic matter exchanged between a salt marsh and its adjacent estuary. *Journal of Geophysical Research: Biogeosciences*, *120*(7), 1430-1449.

Paerl, H. W., Pinckney, J. L., Fear, J. M., & Peierls, B. L. (1998). Ecosystem responses to internal and watershed organic matter loading: consequences for hypoxia in the eutrophying Neuse River Estuary, North Carolina, USA. *Marine Ecology Progress Series*, *166*, 17.

Peierls, B. L., & Paerl, H. W. (2010). Temperature, organic matter, and the control of bacterioplankton in the Neuse River and Pamlico Sound estuarine system. *Aquatic Microbial Ecology*, *60*(2), 139-149.

Peterson, B., Fry, B., Hullar, M., Saupe, S., & Wright, R. (1994). The distribution and stable carbon isotopic composition of dissolved organic carbon in estuaries. *Estuaries and Coasts*, *17*(1), 111-121.

Phong, D. D., Lee, Y., Shin, K. H., & Hur, J. (2014). Spatial variability in chromophoric dissolved organic matter for an artificial coastal lake (Shiwha) and the upstream catchments at two different seasons. *Environmental Science and Pollution Research*, *21*(12), 7678-7688.

Poulin, B. A., Ryan, J. N., & Aiken, G. R. (2014). Effects of iron on optical properties of dissolved organic matter. *Environmental Science and Technology*, *48*(17), 10098-10106.

Pugach, S. P., Pipko, I. I., Semiletov, I. P., & Sergienko, V. I. (2015). Optical characteristics of the colored dissolved organic matter on the East Siberian shelf. *Doklady Earth Sciences*, *465*(2), 1293-1296, doi:10.1134/S1028334X15120120.

Raymond, P. A., & Bauer, J. E. (2001a). Use of ^{14}C and ^{13}C natural abundances for evaluating riverine, estuarine, and coastal DOC and POC sources and cycling: a review and synthesis. *Organic Geochemistry*, *32*(4), 469-485.

Raymond, P. A., & Bauer, J. E. (2001b). DOC cycling in a temperate estuary: a mass balance approach using natural ^{14}C and ^{13}C isotopes. *Limnology and Oceanography*, *46*(3), 655-667.

Rodrigues, M., Oliveira, A., Queiroga, H., Fortunato, A. B., & Zhang, Y. J. (2009). Three-dimensional modeling of the lower trophic levels in the Ria de Aveiro (Portugal). *Ecological Modelling*, *220*(9), 1274-1290.

Roman, C. T., & Daiber, F. C. (1989). Organic carbon flux through a Delaware Bay salt marsh: Tidal exchange, particle size distribution, and storms. *Marine Ecology Progress Series*,*54*(1), 149-156.

Sherrill, B. L., Snider, A. G., & DePerno, C. S. (2010). White-tailed deer on a barrier island: implications for preserving an ecologically important maritime forest. *In Proceedings of the Annual Conference of the Southeastern Association of Fish and Wildlife Agencies*, *64*, 38-43.

Sholkovitz, E. R. (1976). Flocculation of dissolved organic and inorganic matter during the mixing of river water and seawater. *Geochimica et Cosmochimica Acta*, *40*(7), 831-845.

Søndergaard, M., & Thomas, D. N. (2004). Dissolved organic matter (DOM) in aquatic ecosystems: A Study of European Catchments and Coastal Waters. *The DOMAINE project*. Retrieved from http://www.domaine.ku.dk/.

Spencer, R. G., Aiken, G. R., Dornblaser, M. M., Butler, K. D., Holmes, R. M., Fiske, G., Mann, P. J., & Stubbins, A. (2013). Chromophoric dissolved organic matter export from US rivers. *Geophysical Research Letters*, *40*(8), 1575-1579.

Stedmon, C. A., Markager, S., & Kaas, H. (2000). Optical properties and signatures of chromophoric dissolved organic matter (CDOM) in Danish coastal waters. *Estuarine, Coastal and Shelf Science*, *51*(2), 267-278.

Stedmon, C. A., & Markager, S. (2001). The optics of chromophoric dissolved organic matter (CDOM) in the Greenland Sea: An algorithm for differentiation between marine and terrestrially derived organic matter. *Limnology and Oceanography*, *46*(8), 2087-2093.

Stedmon, C. A., Markager, S., & Bro, R. (2003). Tracing dissolved organic matter in aquatic environments using a new approach to fluorescence spectroscopy. *Marine Chemistry*, *82*(3), 239-254.

Stedmon, C., & Nelson, N. B. (2014). The optical properties of DOM in the ocean. In *Biogeochemistry of Marine Dissolved Organic Matter* (pp 481-508). Elsevier Science.

Taylor, D. I., & Allanson, B. R. (1995). Organic carbon fluxes between a high marsh and estuary, and the inapplicability of the outwelling hypothesis. *Marine Ecology Progress Series*, *120*(1), 263-270.

Teal, J. M. (1962). Energy flow in the salt marsh ecosystem of Georgia. *Ecology*, *43*(4), 614-624.

Tehrani, N.C, D'Sa, E. J., Osburn, C. L., Bianchi, T. S., & Schaeffer, B. A. (2013). Chromophoric dissolved organic matter and dissolved organic carbon from sea-viewing wide field-of-view sensor (SeaWiFS), Moderate Resolution Imaging Spectroradiometer (MODIS) and MERIS Sensors: Case study for the Northern Gulf of Mexico. *Remote Sensing*, *5*(3), 1439-1464.

Tobias, C., & Neubauer, S. C. (2009). Salt marsh biogeochemistry: An overview. *Coastal Wetlands: An Integrated Ecosystem Approach*, *1*, 445-492.

Tzortziou, M., Neale, P. J., Osburn, C. L., Megonigal, J. P., Maie, N., & Jaffé, R. (2008). Tidal marshes as a source of optically and chemically distinctive colored dissolved organic matter in the Chesapeake Bay. *Limnology and Oceanography*, *53*(1), 148.

Tzortziou, M., Neale, P. J., Megonigal, J. P., Pow, C. L., & Butterworth, M. (2011). Spatial gradients in dissolved carbon due to tidal marsh outwelling into a Chesapeake Bay estuary. Marine Ecology Progress Series, *426*, 41-56.

Vodacek, A., Blough, N. V., DeGrandpre, M. D., Peltzer, E. T., & Nelson, R. K. (1997). Seasonal variation of CDOM and DOC in the Middle Atlantic Bight: Terrestrial inputs and photooxidation. *Limnology and Oceanography*, *42*(4), 674-686.

Wang, Z. A., & Cai, W. J. (2004). Carbon dioxide degassing and inorganic carbon export from a marsh-dominated estuary (the Duplin River): A marsh CO2 pump. *Limnology and Oceanography*, *49*(2), 341-354.

Wang, Z. A., Kroeger, K. D., Ganju, N. K., Gonneea, M. E., & Chu, S. N. (2016). Intertidal salt marshes as an important source of inorganic carbon to the coastal ocean. *Limnology and Oceanography*, *61*(5), 1916-1931.

Ward, N. D., Richey, J. E., & Keil, R. G. (2012). Temporal variation in river nutrient and dissolved lignin phenol concentrations and the impact of storm events on nutrient loading to Hood Canal, Washington, USA. *Biogeochemistry*, *111*(1-3), 629-645.

Weishaar, J. L., Aiken, G. R., Bergamaschi, B. A., Fram, M. S., Fujii, R., & Mopper, K. (2003). Evaluation of specific ultraviolet absorbance as an indicator of the chemical composition and reactivity of dissolved organic carbon. *Environmental Science & Technology*, 37(20), 4702-4708, doi:10.1021/es030360x.

Winter, P. E., Schlacherl, T. A., & Baird, D. (1996). Carbon flux between an estuary and the ocean: a case for outwelling. *Hydrobiologia*, *337*(1), 123-132.

Yoon, B., & Raymond, P. A. (2012). Dissolved organic matter export from a forested watershed during Hurricane Irene. *Geophysical Research Letters*, *39*(18), L18402, doi:10.1029/2012GL052785.

Zepp, R. G., Erickson Iii, D. J., Paul, N. D., & Sulzberger, B. (2007). Interactive effects of solar UV radiation and climate change on biogeochemical cycling. *Photochemical & Photobiological Sciences*, *6*(3), 286-300.

Zhang, Y., & Baptista, A. M. (2008). SELFE: a semi-implicit Eulerian–Lagrangian finite-element model for cross-scale ocean circulation. *Ocean modelling*, *21*(3), 71-96.

Zhang, Y. J., Ateljevich, E., Yu, H. C., Wu, C. H., & Jason, C. S. (2015). A new vertical coordinate system for a 3D unstructured-grid model. *Ocean Modelling*, *85*, 16-31.

Zhang, Y. J., Stanev, E. V., & Grashorn, S. (2016). Unstructured-grid model for the North Sea and Baltic Sea: validation against observations. *Ocean Modelling*, *97*, 91-108.

APPENDICES

Appendix A

Description of input files for SCHISM

To run a model on SCHISM, several mandatory input files are required:

- The horizontal grid, **hgrid.gr3**, which contains node-centered spatial data and mesh connectivity;
- The vertical grid, **vgrid.in,** which contains the depths**;**
- The parameter input file, **param.in**, where the model configuration parameters are defined such as the pre-processing option, useful for checking grid violations, and the number of tracers;
- The boundary conditions file, **bctides.in**, which contains boundary conditions such as tidal information;
- The bottom friction input file, **manning.gr3;** which contains bottom roughness
- A submission script containing information about run time (-W), number of nodes to run the job on (-n), the queue (-q) and the executable (mpiexec) (Fig. 22).

Other optional input files (driven by param.in) include:

- Initial conditions for salinity and temperature (**salt.ic, temp.ic**)
- Initial conditions for elevation and tracers (**elev.ic, ts.ic**)

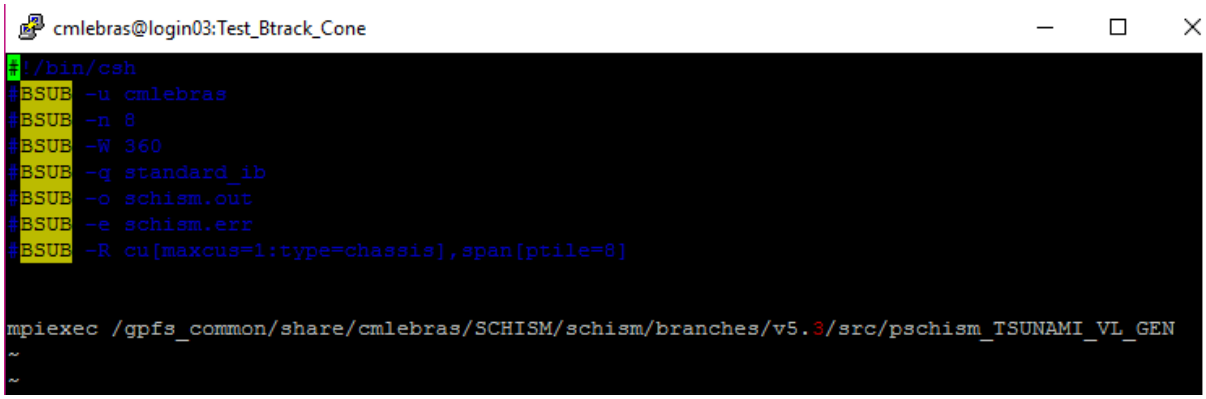

Figure 24. bsub_pschism script for job submission on HPC

Description of output files for SCHISM

The SCHISM outputs can be found in the **outputs** directory as run info output (mirror.out) and global output. For this study, the following standard outputs (i.e., node centered) from SCHISM were used:

- salt.63: 3D scalar - salinity
- hvel.64: 3D vector – horizontal velocity

These standard outputs were converted to netcdf format for ease of processing.

Appendix B

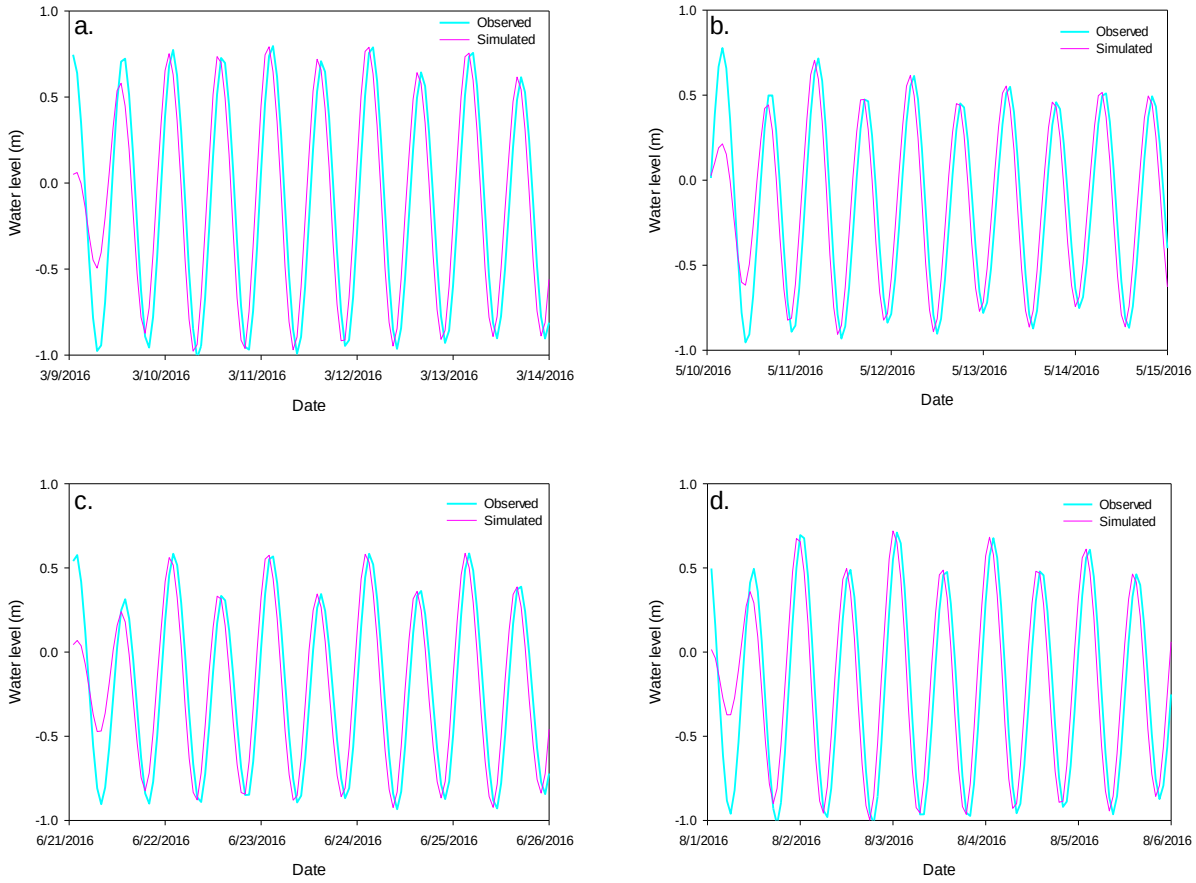

Figure 25. Observed versus model-simulated water levels at Site 1 in (a) March, (b) May, (c) June and (d) August in Bald Head Creek during spring and summer 2016, relative to mean sea level (MSL).

Appendix C

Error and uncertainty propagation in the estimated DOC export values for each month was calculated as follows:

$$\delta R = |R| \cdot \sqrt{\left(\frac{\delta x}{x}\right)^2 + \left(\frac{\delta y}{y}\right)^2 + \left(\frac{\delta z}{z}\right)^2}$$

Where,

δR is the uncertainty in DOC export in g C day^{-1}

R is the estimated DOC export in g C day^{-1}

δx is the RMSE for DOC calculations in g m^{-3}

x is the mean DOC in g m^{-3}

$\delta y/y$ is the percentage uncertainty in the area, which here was 0.05

$\delta z/z$ is the percentage uncertainty in the water flux, which here was 0.05